

UNIVERSIDADE DE LISBOA  
FACULDADE DE CIÊNCIAS  
DEPARTAMENTO DE BIOLOGIA ANIMAL



**Studying laminins in skeletal muscle development:  
Regulators of muscle stem cells and synaptic organizers**

Inês Curado Batista Antunes

**Mestrado em Biologia Evolutiva e do Desenvolvimento**

Dissertação orientada por:  
Professora Doutora Sólveig Thorsteindóttir  
Doutora Andreia Marcelino Nunes

2017



***“Destiny is a funny thing. You never know how things are going to work out. But if you keep an open mind and open heart, I promise you will find your own destiny someday.”***

Avatar, The Last Airbender



## Agradecimentos/ Acknowledgments

Estes agradecimentos são a última peça deste puzzle quebra-cabeças que foi esta tese! Foram mais complicados de escrever do que pensei, não porque não tenha a quem agradecer, mas porque tenho uma quantidade brutal de pessoas sempre dispostas a ajudar-me, e para as quais não estava a conseguir escrever palavras à altura dos agradecimentos merecidos (e nem sei se estão à altura, depois dizem-me ☺ )

Começo por agradecer à professora Solveig que me deixou entrar neste projecto fantástico, que desde o momento inicial eu disse que ia ser meu! Agradecer a coragem que teve em colocar o seu laboratório nas mãos da pessoa mais desastrada e despistada que há registo. Por ter acreditado em mim, pela motivação e incentivo constante, e pela paciência para as minhas crises existenciais constantes. Trabalhar neste laboratório foi sempre um prazer, mesmo nos dias mais negros (e se tais dias houve!), aqui encontrei um óptimo ambiente para se trabalhar e não só ☺ Obrigada pela oportunidade que me deu de passar de uma novata a brincar aos laboratórios e poder ter evoluído até onde evolui. Mais experiências estão à nossa espera, com tanto ou mais sucesso!

Agradecer (e muito!) à Andreia! Sem ti esta tese não teria sido possível. E não, não é um clichê! Estiveste, e estás, lá sempre para mim, nas dúvidas mais parvas, nos momentos de nervosismo e ansiedade, sempre ali a manter a minha sanidade mental, quando eu já não achava possível que ela existisse. Um ombro para quando os meus olhos insistiam em derramar lágrimas :p Todas as maratonas de longas horas no laboratório, e as prolongadas sessões no confocal, onde passamos toda a discografia pop dos anos 90! És uma pessoa extraordinária, e ter-te conhecido já faz valer este ano e todas as suas peripécias. És a melhor companheira de bancada que alguém pode pedir, sempre atenta e disponível, e com uma paciência que desafia os limites do universo. De tudo o que esta tese me deu, e muitas coisas estão nessa lista, a tua amizade é das mais valiosas! Obrigada por me teres adoptado ☺ Ah e o Danny claro, o cão mais fofinho do mundo!!! (Sabias que eu ia ter que falar dele não é verdade?) Este agradecimento parece-me pouquinho, mas são tantas e tantas e tantas e tantas coisas pelas quais te tenho que agradecer, que não havia palavras suficientes. Fica só um **obrigada** com reticências que acumulam tudo!

À Ana agradeço a sua presença sempre incondicional, não só neste ano, mas especialmente este ano. Por todas as vezes que abandonaste o teu trabalho para me apoiar. Por todas as vezes que correste para o comboio porque ficaste à espera que me despachasse. Por todos os sábados, domingos e feriados que vieste comigo para a fcul, não porque tivesses que o fazer, mas para me fazeres companhia. Oficialmente a minha tech support girl, sempre lá para me ajudar com os desafios da formatação! Pela paciência que tiveste em ouvir-me deambular sobre laminina, embriões, ratinhos...etc...etc... Por seres uma amiga para todas as ocasiões!

Aos meus companheiros, colegas e amigos que o mestrado me ofereceu: Ritinha por teres sido o meu apoio incondicional durante o primeiro ano de tese, mas não só. Por teres oferecido a tua casa vezes e vezes sem conta, pelas vezes em que me levavas o computador porque as minhas costas já estavam a desistir, por todo o tempo que passamos quando ainda eramos proto-cientistas. Depois fugiste para o Algarve, achas bem!!!? Se eu pudesse agradecia-te com um jantar de sushi, mas sabes que isso não consigo comer, por mais que tentes :p Agradecer ao André Mesquita por ser a personificação de um velhinho rabugento, mas com o sentido de humor que como se costuma dizer, é um gosto adquirido, só para os fortes. Obrigada por todo o companheirismo destes dois anos, por estares sempre a dizer que eu constato o óbvio, mas também por me ajudares sempre que tinha que ir ao IGC e nunca fazia ideia de onde eram os edifícios naquele labirinto! À Mariana Ferreira, a minha primeira amiga BEDiana, já desde as aulas de excel na licenciatura, onde percebeste rapidamente a minha inimizade com as tecnologias :p

e que gosta imenso de me pregar sustos quando estava concentrada a abrir ovos... Actualmente a minha guia turística do IMM!

Agradecer também à Teresa e ao Rodrigo que insistem sempre em sugerir sushi cada vez que combinamos um jantar, e só depois se lembram que eu sou a ovelha negra que não gosta de comida não cozinhada!

Não menos importante, agradecer aos elementos do grupo BD que me receberam muito bem. Ao Luís pela imensa ajuda que me deu na microscopia e tratamento, pelas horas gastas no confocal todo XPTO, essencialmente pelo espírito de entre-ajuda que sempre demonstrou. Ao André pela sua boa disposição, pelas piadas à hora de almoço, e pela ajuda que me deu a tratar dos meus ratinhos, quando eu não podia! À Marta pela sua disponibilidade e eficiência a ajudar-me sempre que precisei, um obrigada! À Prof. Gabriela pela sua boa disposição, e por fim, à Patricia, que apesar de só a ver de tempos a tempos no lab, traz sempre uma alegria nova ao ambiente!

Agradeço também aos meus amigos fculianos, Patricia, Luís Dias, Célia, Manel, Filipa, Mariana, começamos jovens e inocentes a licenciatura e hoje estamos todos em áreas diferentes mas com a pipoca queimada em comum ☺

À Rita Graça, uma amiga de longa data, que vive a 20 minutos de mim, mas co-habitamos em fusos horários diferentes, e apesar de só nos vermos quase que sazonalmente, eu sei que estás sempre a um telefonema de distância e não hesitas para me ajudar. Temos que melhorar a nossa resolução de ano novo de nos vermos mais frequentemente!

E por fim, mas que foram os primeiros sempre desde a idade das fraldas, à minha família que me apoiou sempre nesta aventura louca do curso superior. Aos tios e primos do coração. À minha avó Lurdes, que é um pilar daquilo que sou hoje, parte integrante e essencial do caminho que construí até aqui.

E claro, aos meus **Pais** que me aturaram até hoje, que me apoiaram sempre incondicionalmente. Por terem sempre acreditado em mim, e por permitirem que continuasse a estudar até querer, sem nunca pedir nada em troca, e quase irem à bancarrota à minha custa. Eu sei que trabalharam e investiram muito nisso, e por tal sou imensamente grata! Espero que esta tese seja um orgulho para vocês!

## Abstract

MDC1A is a crippling neuromuscular disease caused by the absence of the  $\alpha 2$ -chain of laminins 211/221, major components of basement membranes. The onset of this disease during development *in utero* is marked by impaired muscle growth which correlates with a reduction in the number of mononucleated muscle cells in the fetal muscle masses (Nunes et al., 2017). Skeletal muscle development starts during early embryogenesis, when the dermomyotomal Pax3- and/or Pax7-positive muscle precursors cells are induced to enter the myogenic program and subsequently delaminate from the dermomyotome to form the myotome. Later on, when the dermomyotome dissociates, Pax3- and/or Pax7-positive muscle stem cells are released, some of which differentiate into myoblasts and fuse with myotomal cells or with each other, forming the primary myofibers during primary myogenesis that occurs between E11.5 and E14.5. The primary myofibers later serve as a scaffold for the formation of secondary myofibers and secondary myoblasts fuse with both primary and secondary myofibers to increase their size. Motor axons enter the muscle masses in parallel with primary myogenesis, but it is during secondary myogenesis (between E14.5 until birth) that the nerve contacts the muscle, and proper innervation is essential for normal fetal muscle development. During mid-secondary myogenesis, the Pax7-positive muscle stem cells become closely associated with the myofibers and their basement membrane. Laminin 211 and 221 are assembled around the adult myofiber and synaptic endplate, respectively, and are known to play important roles both in myofiber and neuromuscular junction development.

In this thesis we aimed to contribute to the study of the fetal myogenesis defect in *dy<sup>W</sup>* mice in two ways:

First, we asked what cell types produce laminins during fetal myogenesis. We performed a detailed analysis of laminin production and assembly in fetal muscles at stages preceding the onset of MDC1A. We found that mononucleated cells, including Pax7-positive cells, are a major source of laminins at the beginning of secondary myogenesis, but during later stages of secondary myogenesis, myofibers also express laminin genes. This suggests that Pax7-positive muscle stem cells play a major role in constructing the laminin microenvironment in the fetal muscles. We then used the *Myf5<sup>cre</sup>*-NICD mouse model (Mourikis et al., 2012) where Pax7-positive cells are unable to differentiate and thus do not form muscle fibers. We found that Pax7-positive cells at E14.5 produce and assemble laminins 211, 411 and 511, but at E17.5, the capacity to produce laminins is greatly diminished as they only produce laminin 511. These results indicate that Pax7-positive cells at E17.5 require the presence of myofibers to produce and assemble laminins 211 and 411.

Second, since it is known that fetal myogenesis depends on innervation, we used the *dy<sup>W</sup>* mouse model, which has a mutation in the *Lama2* gene, to assess the role of laminin 211/221 during neuromuscular junction development. We found that laminin 521 is closely assembled around the synapse, while laminins 421 is present, but does not seem to be in direct contact with the synapse. In the wildtype, laminin 221 has a distribution like laminin 421. However, our spatial analysis showed that  $\alpha 2$ -laminin deficient synapses tend to have a less clustered organization compared to wildtype ones and display a deficient AChR patterning. Based on these results, we hypothesize that laminin 221 might play a crucial role in NMJ development and that this may contribute to the onset of the fetal myogenesis defect in *dy<sup>W</sup>* mice.

Together, our results provide new insights into laminin production and assembly during fetal muscle development and provide new indications into the mechanism underlying disease onset during development *in utero* in a mouse model for MDC1A.

**Keywords:** Skeletal muscle; Laminins; Pax7-positive muscle stem cells; neuromuscular junction; Merosin-deficient congenital dystrophy type 1A



## Resumo alargado

O desenvolvimento do músculo, ou miogénese, é um processo bastante conservado entre os vertebrados. Todos os músculos-esqueléticos do tronco e dos membros são provenientes dos sómitos, estruturas epiteliais que se formam em ambos os lados do tubo neural. Os sómitos são posteriormente padronizados em diferentes compartimentos que darão origem a diferentes linhagens celulares. A porção mais ventral do sómito perde a sua estrutura epitelial e forma o esclerótomo, fonte de células precursoras do esqueleto axial. A porção mais dorsal, o dermamiótomo, permanece epitelial e é constituído pelos precursores miogénicos (MPCs) e os precursores da derme, entre outros.

Os músculos-esqueléticos iniciam o seu desenvolvimento quando os progenitores no dermamiótomo, que expressam os factores de transcrição Pax3 e/ou Pax7 são induzidos a activar o programa de diferenciação miogénica, controlado pelos factores regulatórios da miogénese (MRF), nomeadamente Myf5, MyoD, Mrf4 e Miogenina.

O dermomiótomo encontra-se dividido em três compartimentos distintos: (1) dermomiótomo dorsomediano (2) dermomiótomo central e (3) dermomiótomo ventrolateral. O desenvolvimento dos músculos epaxiais inicia-se no ratinho por volta de E8.5 com a formação do miótomo através da adição das células do dermamiótomo quando estas delaminam do dermomiótomo e povoam a zona ventral ao dermamiótomo para constituir o miótomo. As células precursoras musculares no dermamiótomo, ou células musculares estaminais, que passam a expressar os MRFs, entram no miótomo como mioblastos, mas no miótomo acabam por diferenciar-se em miócitos. O miótomo cresce nos estádios subsequentes com a adição progressiva de células estaminais musculares que diferenciam. Com o início da dissociação do dermamiótomo a E10.5, os progenitores que não se diferenciam acabam por migrar para as massas constituídas por miócitos. Entre E11.5 e E14.5, alguns destes progenitores diferenciam-se em mioblastos primários que fundem com os miócitos para formar as fibras primárias- miogénese primária. Durante os estádios subsequentes até ao nascimento, outra porção de células estaminais que se diferencia em mioblastos, desta vez secundários, que se fundem entre si para formar as fibras secundárias, mas também fundem com as fibras primárias. Esta fase é responsável pelo aumento do tamanho das massas musculares, quer em número de fibras quer no tamanho das mesmas. O sistema de inervação do músculo, mais especificamente a formação das junções neuromusculares (NMJs), sinapses especializadas que se formam entre o músculo e o nervo, desenvolve-se em paralelo com a miogénese. O primeiro contacto entre músculo e nervo antecede o início da miogénese secundária. Por esta altura, já existe uma pré-padronização da distribuição dos receptores de acetilcolina (AChR) no músculo, que será posteriormente remodelada. Dado que a miogénese e a inervação são processos interdependentes para o correcto funcionamento do músculo, estes processos requerem uma comunicação estruturada entre o músculo e o nervo.

Durante a miogénese secundária (por volta de E16.5) as células musculares estaminais, positivas para Pax7, migram para o espaço existente entre a fibra muscular e a membrana basal. Esta localização é mantida pelas células estaminais musculares que não se diferenciam durante a miogénese *in utero* e que constituem a população de células satélite, as células estaminais musculares adultas. Dado que estas se encontram em contacto directo com a membrana basal, a matriz extracelular adquire um papel crucial na regulação do comportamento destas células. Os diferentes elementos que constituem a membrana basal, tais como colagénio, perlecano e laminina permitem que as células estaminais musculares reconheçam o microambiente que as envolve. Além do microambiente que providencia à fibra e às células estaminais musculares durante o desenvolvimento do músculo esquelético, a membrana basal é um componente essencial no desenvolvimento das NMJs.

De entre os vários componentes da membrana basal, as lamininas são dos componentes mais bem estudados. As lamininas são trímeros, que apresentam uma estrutura cruciforme ou em T com três

cadeias: alpha ( $\alpha$ ), beta ( $\beta$ ) e gamma ( $\gamma$ ). Actualmente são conhecidas 16 isoformas diferentes denominadas com base na sua constituição. Por exemplo, a laminina 211 é constituída pelas cadeias  $\alpha 2$ ,  $\beta 1$  e  $\gamma 1$ . As lamininas ligam-se principalmente a dois tipos de receptores no músculo: (1) integrinas, receptores transmembranar compostos por duas sub-unidades alpha ( $\alpha$ ) e beta ( $\beta$ ); (2) distroglicano, que se liga intracelularmente à distrofina. Durante a miogénese secundária, as principais isoformas presentes no músculo e nas NMJ são, respectivamente, 211, 411, 511 e 221, 421 e 521. Porém, no músculo adulto, a isoforma que permanece a volta das miofibras é a 211, enquanto nas NMJs adultas continuam presentes as isoformas 221, 421, 521, todas elas cruciais para o desenvolvimento e correcto funcionamento do sistema neuromuscular. As lamininas são determinantes desde cedo no desenvolvimento do músculo-esquelético durante a formação do miótomo através do controlo do balanço entre proliferação e diferenciação das células do dermamiótomo. Em estádios mais tardios do desenvolvimento fetal, as lamininas são parte integrante do microambiente das fibras e das células estaminais musculares que parece ser determinante para o crescimento normal das massas musculares. Em paralelo, as lamininas desempenham papel igualmente preponderante durante o desenvolvimento das junções neuromusculares

As células estaminais musculares localizadas entre a membrana basal e a fibra representam no músculo adulto a principal fonte da capacidade regenerativa. Para que a reserva de células estaminais musculares não se esgote é necessário garantir que exista um equilíbrio entre a proporção de células que se mantêm quiescentes, as células que são activadas e as células que se diferenciam no momento da regeneração. A membrana basal que hospeda estas células representa um elemento determinante em distintas vias de sinalização que operam no sentido de instruir as células a manterem-se quiescentes, a activar, a proliferar ou diferenciar. A sinalização Notch destaca-se como reguladora deste processo. Quando abolida, as células estaminais musculares diferenciam-se precocemente sem a necessária proliferação que permite manter a população e desta forma a população acaba por esgotar-se. A Distrofia muscular congénita merosina negativa (MDC1A) é um tipo de distrofia causado por mutações no gene *LAMA2* que levam à perda das lamininas 211 e 221 da membrana basal das fibras e junções neuromusculares, respectivamente. Esta doença é caracterizada por fraqueza muscular, neuropatia, dificuldades respiratórias, entre outros sintomas. Neste estudo, usámos o modelo de ratinho *dy<sup>w</sup>* como modelo de estudo para a MDC1A. Estudos recentes do nosso laboratório demonstraram que no ratinho, o desenvolvimento da MDC1A inicia-se *in utero* entre E17.5 e E18.5. O início desta distrofia é demarcado por uma diminuição significativa no número de células positivas para Pax7, em paralelo com uma diminuição do crescimento do músculo fetal.

O trabalho realizado nesta tese teve como objectivo compreender melhor como é que as células musculares constroem o seu microambiente e de que forma alterações no microambiente tanto das células musculares como das junções neuromusculares influencia o crescimento do músculo fetal.

Numa primeira abordagem, avalíamos a capacidade das células musculares, tanto as células estaminais musculares como as fibras, de produzirem e montarem as matrizes de laminina. Os nossos resultados demonstram que numa fase inicial da miogénese secundária, as células estaminais musculares são as principais produtoras de laminina no músculo e montam as suas matrizes de laminina mesmo na ausência das fibras. Durante fases mais tardias da miogénese secundária, as fibras passam a expressar os diferentes genes de laminina e a sua presença parece ser importante para que as matrizes de laminina sejam mantidas no microambiente das células estaminais musculares. Desta forma, este trabalho revela que as células musculares desempenham papéis diferentes na construção das matrizes de laminina em fases distintas da miogénese secundária e que as células estaminais e as fibras são interdependentes na construção das matrizes de laminina.

Numa segunda abordagem, esta tese teve como objectivo compreender em maior detalhe o papel da laminina 221 durante a formação das NMJs e compreender a sua influência no início/progressão da

MDC1A. Para tal, estudámos o desenvolvimento das NMJs durante a miogénese secundária em ratinhos *dy<sup>w</sup>*. Os nossos resultados revelam que enquanto as lamininas  $\alpha 2$  e  $\alpha 4$  não aparentam ter um contacto directo com sinapse a E15.5, as lamininas  $\alpha 5$  apresentam uma proximidade com a sinapse. Esta dinâmica não parece estar alterada na ausência da laminina  $\alpha 2$  (211/221). Contudo, a nossa análise do desenvolvimento das NMJ na ausência de laminina 221, ainda que preliminar, sugere que a distribuição dos receptores de acetilcolina está alterada e que há uma tendência para que os receptores se encontrem mais dispersos ao longo do músculo na ausência de lamininas  $\alpha 2$ . Estes resultados apontam para um papel das lamininas na agregação dos receptores junto da fenda sináptica.

Em suma, o trabalho desenvolvido ao longo desta tese realça a complexidade das dinâmicas de produção e construção das matrizes de laminina durante a miogénese secundária. Os dados desta tese exemplificam igualmente a diversidade de microambientes aos quais as células estaminais estão sujeitas durante diferentes fases da miogénese secundária. Esta tese analisa em particular o papel das lamininas  $\alpha 2$  durante o desenvolvimento das NMJs e fornece novas evidências acerca da influência da inervação do músculo no início da MDC1A.

**Palavra-chave:** Músculo-esquelético; Lamininas, Células estaminais Pax7+; Junção neuromuscular, MDC1A.



## Table of contents

Agradecimientos/ Acknowledgments	I
Abstract	III
Resumo alargado	V
List of figures and tables	XI
List of abbreviations and acronyms	XII
Chapter 1 - Introduction	1
Myotome formation	2
Primary and Secondary Myogenesis	4
Extracellular Matrix	5
Laminins	6
Laminins in Skeletal Muscle	8
Laminins in Neuromuscular Junctions	8
Satellite Cells	10
Merosin-deficient congenital muscular dystrophy type 1A (MDC1A)	12
Aims of this thesis	12
Chapter 2 – Materials and Methods	15
Embryo collection	16
Genotyping	16
Cryosectioning	16
<i>In situ</i> probe production	16
a. Transformation	16
b. Primary culture	16
c. Linearization	17
d. Transcription	17
<i>In situ</i> hybridization	17
a. RNA whole-mount in situ hybridization	17
b. In situ hybridization on sections	18
c. Immunohistochemistry over in situ hybridization	18
Immunohistochemistry	18
a. Whole-Mount immunohistochemistry DMSO/Methanol Method	18
b. Whole-Mount immunohistochemistry – thick sections	19
c. Immunohistochemistry on 30 and 100µm sections	19
Immunohistochemistry on Myf5Cre-NICD fetuses	19
Real time quantitative RT-qPCR	19
Image analysis and quantifications	20

Statistical analysis	20
Data analysis of $dy^w$ muscle masses	20
a. Coordinate acquisition	20
b. Data visualization	21
c. Quadrat analysis and Variance-to-Mean Ratio	21
d. G function	23
e. Ripley's K function	24
Chapter 3 - Results	27
Both myofibers and mononucleated cells contribute to the production of <i>Lama2</i> , <i>Lama4</i> and <i>Lama5</i> mRNA	28
A stage-dependent role for mononucleated cells in the synthesis of laminin	30
Number of synapses increases in neuromuscular junctions lacking laminin 211 and 221	32
The absence of $\alpha 2$ laminin does not interfere with the distribution of $\alpha 4$ and $\alpha 5$ laminin in the synapse	36
Chapter 4 - Discussion	39
Laminin assembly dynamics in fetal muscles: mononucleated cells and myofibers working together	40
The muscle stem cell population: a diverse population with different niches	42
Absence of $\alpha 2$ -laminins appears to lead to alterations in acetylcholine receptor clustering	43
Does innervation influence muscle stem cell dynamics?	43
Final considerations	44
Chapter 5 - References	47
Annexes	55
Annex I – Protocols	56
Annex II – Solutions and Reagents	58
Annex III – Antibodies	64
Annex IV – R Script	65

## List of figures and tables

**Figure 1** - The main phases of skeletal muscle development throughout time, terminology used to designate cells and their major markers.

**Figure 2** - Myotomal myogenesis.

**Figure 3** - Primary and secondary myogenesis.

**Figure 4** - Laminin trimer structure and laminin isoforms. Laminins are cruciform or T-shaped heterotrimers.

**Figure 5** - The neuromuscular junction & the laminin distribution within the synaptic cleft.

**Figure 6** - Neuromuscular synapse formation in the mouse.

**Figure 7** - Satellite cell fate decisions.

**Figure 8** - The Notch signaling pathway.

**Figure 9** - Schematic representation of Ripley's K function results.

**Figure 10** - Both myofibers and mononucleated cells express *Lama2*, *Lama4* and *Lama5* genes at E15.5, but expression in mononucleated cells appears stronger.

**Figure 11** - Both myofibers and mononucleated cells still express *Lama2*, *Lama4* and *Lama5* genes at E17.5.

**Figure 12** - Characterization of laminin assembly in the presumptive epaxial muscle area in the absence of myofibers at E14.5.

**Figure 13** - Laminin assembly in the presumptive epaxial muscle area decreases as development proceeds.

**Figure 14** - E15.5 *dy*<sup>W/-</sup> fetuses display differences concerning the synaptic number and size.

**Figure 15** - Spatial analysis of the distribution of synapses in wildtype E15.5 longissimus muscle.

**Figure 16** - Spatial analysis of the distribution of synapses in *dy*<sup>W/-</sup> E15.5 longissimus muscle.

**Figure 17** - Laminin distribution in the NMJ at E15.5.

**Figure 18** - Schematic representation depicting the main alteration in neuromuscular junction development in  $\alpha 2$ -laminin-deficient muscles at E15.5.

**Figure 19** - Schematic representation of Pax7-positive cells possible laminin niches at E14.5 and E17.5.

**Figure 20** - The diversity of laminin niches in the heterogeneous population of Pax7-positive cell.

## Tables:

**Table 1** - Laminin nomenclature and composition.

**Table S1** - Laminin probes

**Table S2** - Variance to mean ratio analysis.

**Table S3** - Nearest-neighbour distance analyses - G Function - R score and statistical significance, Z-test - associated.

## **List of abbreviations and acronyms**

**AChR** – Acetylcholine Receptor

**BM** – Basement Membrane

**DGC**- Dystrophin-associated Glycoprotein Complex

**DML** – Dorsomedial Lip

**DNA**- Deoxyribonucleic Acid

**ECM** – Extracellular Matrix

**FACS** - Fluorescence-Activated Cell Sorting

**FGF** – Fibroblast Growth Factors

**JAK-STAT** - Janus Kinase/Signal Transducers and Activators of Transcription

**LAMA2-CMD** – Laminin  $\alpha$ 2 Congenital Muscular Dystrophy

**MDC1A** – Merosin-deficient Congenital Muscular Dystrophy Type 1A

**MHC** – Myosin Heavy Chain

**MPC** – Myogenic Precursors Cells

**MRF** – Myogenic Regulatory Factor

**mRNA** – messenger Ribonucleic Acid

**NICD** – Notch Intracellular Domain

**NMJ** – Neuromeuscular Junction

**RNA** - Ribonucleic Acid

**Shh** – Sonic hedgehog

**VLL** – Ventrolateral Lip

**VMR** – Variance-to-Mean Ratio

**WNT** - Wingless/Integrated Family Members



# **Chapter 1**

## **Introduction**

## Introduction

Muscle development occurs through a process conserved among amniotes (Picard 2002). In the vertebrate embryo, all trunk and limb muscles arise from the somites, transient embryonic structures originated from the paraxial mesoderm (Brent & Tabin 2002; Pu et al., 2015; Chal & Pourquié, 2017). The specification of somites results from a dynamic molecular process, involving a segmentation clock, which generates pulses of Notch, FGF and Wnt signalling (Andrade et al., 2005).

Once formed the somites are patterned into different compartments that will give rise to distinct cell lineages (Brent & Tabin, 2002). The most ventral part undergoes an epithelial to mesenchymal transition and will form the sclerotome, the source of the axial skeleton and tendons. On the other hand, the most dorsal part of the somite will remain epithelial forming the dermomyotome, which contains myogenic progenitors (MPCs) (Brent & Tabin 2002; Dumont et al., 2015b; Chal & Pourquié, 2017), as well as dermis progenitors (Cinnamon et al., 1999; Scaal & Christ, 2004; Chal & Pourquié, 2017), among others.

Skeletal muscle development is initiated with the specification and differentiation of myoblasts. In response to specific signals, dermomyotomal cells, expressing Pax3 and/or Pax7 and precursors of muscle stem cells (see **Figure 1** for terminology), activate the myogenic program which is controlled by specific transcription factors, the myogenic regulatory factors (MRFs), Myf5, MyoD, Mrf4 and Myogenin (Brent & Tabin, 2002; Buckingham & Rigby, 2014).

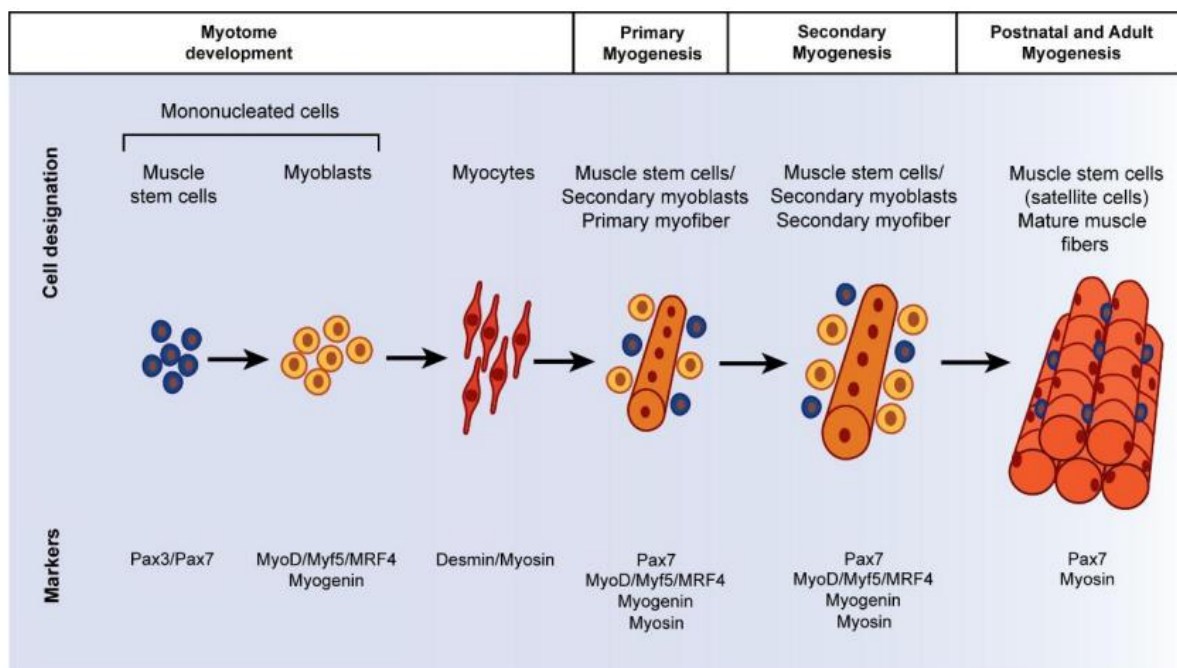


**Figure 1 - The main phases of skeletal muscle development throughout time, terminology used to designate cells and their major markers.** The muscle stem cells express one or both of the transcription factors Pax3 and Pax7. As they start expressing the myogenic regulatory factors (MRFs), Myf5, MyoD, Mrf4 and Myogenin, they first become committed myoblasts and then differentiate. The differentiated myoblasts – myocytes – express specific muscle fiber proteins, such as myosin, dystrophin and desmin. These myocytes fuse giving rise to multinucleated muscle cells – the myotubes. A second wave of differentiation gives rise to the secondary myotubes that contribute to muscle growth. Adapted from Deries and Thorsteinsdóttir, 2016; Nunes, 2017.

## Myotome formation

All epaxial and hypaxial skeletal muscle are derived from the dermomyotome (Brent & Tabin, 2002; Thorsteinsdóttir et al., 2011). The dermomyotome can be regionalized in three main domains. The

epaxial dorsomedial lip (DML) the central dermomyotome, and the hypaxial ventrolateral lip (VLL) (Eloy-Trinquet & Nicholas, 2002, Brent & Tabin, 2002).

The formation of the myotome (**Figure 2**) is a crucial step of skeletal muscle formation (Gros et al., 2004). In amniotes, it starts when the cells from the DML are induced to express Myf5 (Pownall & Emerson, 1992, Brent & Tabin, 2002) and downregulate Pax3 (Williams & Ordahl, 1994) (E8.5) (Biressi et al., 2007). Myf5 and MyoD are the first MRFs expressed in the myogenic program and are determination factors, i.e. they set the myogenic fate (Kablar et al., 2003). Mrf4 can also act as a determination factor (Kassar-Duchossoy et al., 2004), while Myogenin (and also Mrf4) act later in the myogenesis program, as differentiation factors (Kablar & Rudnicki, 2000; Tajbakhsh & Buckingham, 2000; Kablar et al., 2003; Buckingham & Rigby, 2014).

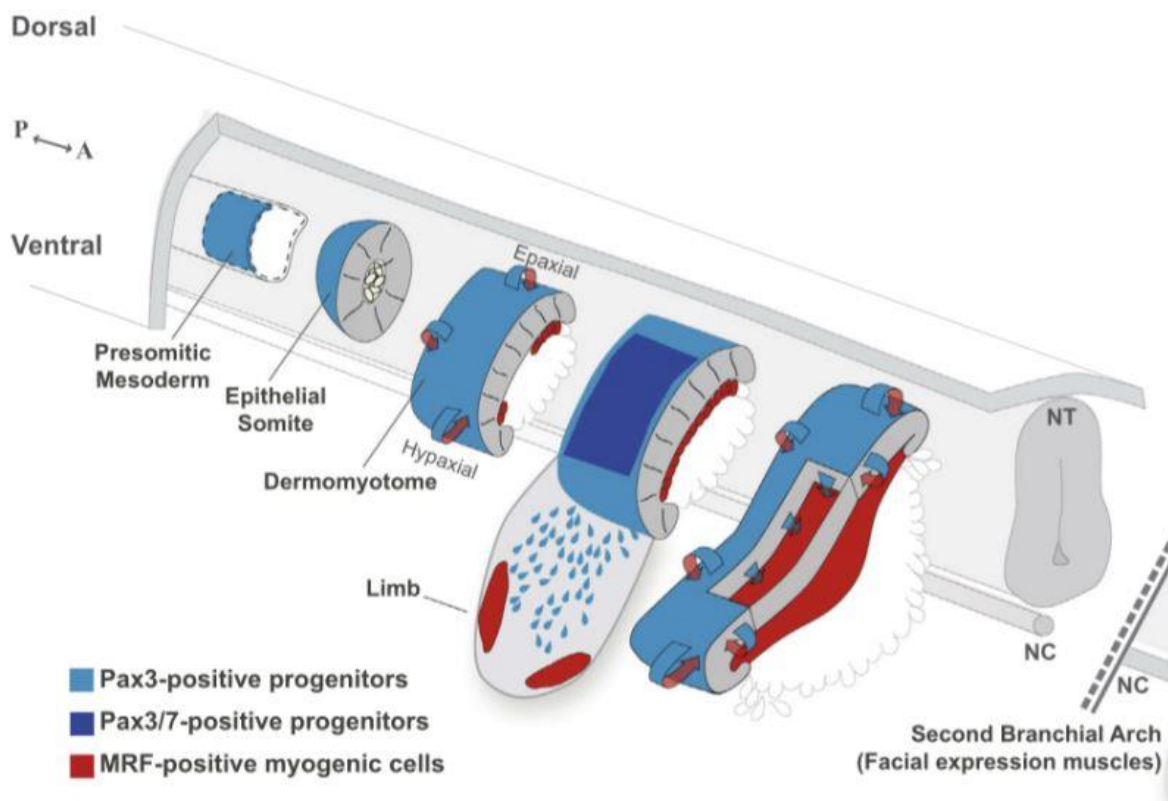


**Figure 2 - Myotomal myogenesis.** All epaxial and hypaxial skeletal muscles are derived from the dermomyotome. The dermomyotome can be compartmentalized into three domains, the epaxial dorsomedial lip (DML), the central dermomyotome and the hypaxial ventrolateral lip (VLL). The cells from the epaxial DML activate the expression of myogenic regulatory factors (MRF) Myf5 and MyoD. Those cells migrate to the underlying space giving rise to the myotome. The epaxial myotome gives rise to the epaxial muscles (transversospinalis, longissimus, iliocostalis and levatores costarum), while the hypaxial myotome originates the intercostal and abdominal muscles. More cells are progressively added to the myotome as myoblasts that either differentiate into myocytes or fuse with the existing ones. The myotome grows both dorso-ventrally and medio-laterally and myogenesis proceeds as a rostro-to-caudal wave of differentiation. From Buckingham and Rigby, 2014.

Myf5 and MyoD-positive myoblasts (see **Figure 1**) migrate to the underlying space giving rise to the third somitic compartment – the myotome - which continues to grow due to the ongoing entry of cells. The myotome is also a compartmentalized structure, as the epaxial myotome that originates from the cells migrating from the DML, and the hypaxial myotome develops from cells delaminating from the VLL. At certain axial levels, the hypaxial myotome does not form, but cells delaminate and migrate long distances to form the muscles of the limbs, tongue and diaphragm (Derries et al., 2016).

More and more cells are progressively added to the myotome as myoblasts where they either differentiate into new myocytes or fuse with the existing myocytes to form first bi- and then

multinucleated myotubes, thus contributing to myotome growth (Relaix et al., 2005; see **Figure 1** for terminology). Consequently, the myotome grows medio-laterally and myogenesis proceeds as a rostral-to-caudal wave of maturation (Gros et al., 2004).

Eventually, the central dermomyotome loses its epithelial structure and the Pax3- and/or Pax7-positive muscle stem cells enter the underlying, myotomal space. These cells can either activate Myf5 or MyoD and differentiate or keep proliferating, providing a reserve cell population for muscle growth during development (Buckingham & Rigby, 2014).

The myotome is a transient structure that transforms into the epaxial (deep back) muscles between E11.5 and E12.5 in the mouse (Deries et al., 2010, 2012) thus losing its segmented organization. This process includes translocation, re-orientation, elongation of existing myotomal myocytes (Deries et al., 2010). Concomitantly, the dissociation of the dermomyotome brings in MPCs of which some differentiate into myoblasts that drive primary myogenesis in the epaxial muscle masses (Deries et al., 2010).

Primary fibers of the epaxial muscle masses cleave into four muscle masses, corresponding to the transversospinalis, iliocostalis, longissimus and levatores costarum all clearly distinguishable at E15.5 (Vallois, 1922). Each newly formed muscle includes populations of Pax3- and Pax7-positive muscle stem cells intermingled with them, which contribute to their future growth and development (Deries et al., 2010).

### Primary and Secondary Myogenesis

Post-myotome myogenesis is marked by the formation of myofibers which occurs in two main phases: embryonic or primary myogenesis, from E11.5 to E14.5, and fetal or secondary myogenesis, spanning from E14.5 to postnatal development (Patton et al., 1997; Biressi et al., 2007; **Figure 3**).

Primary myogenesis provides the basic muscle pattern of the body. It involves the differentiation of a subset of Pax3- and/or Pax7-positive muscle stem cells into primary myoblasts that will contribute to formation of the primary myofibers (**Figure 1** and **Figure 3**), upon which the muscle grows during secondary myogenesis (Messina et al., 2010).

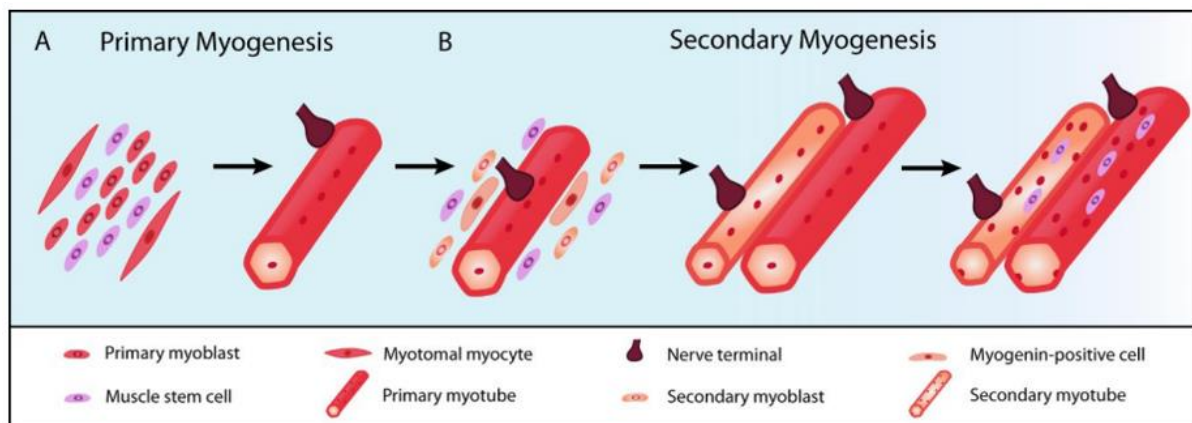


**Figure 3 - Primary and secondary myogenesis.** Post-myotome myogenesis is marked by the formation of myofibers. It is divided in two distinct phases: **(A)** Primary or embryonic myogenesis (from E11.5 to E14.5) and **(B)** Secondary or fetal myogenesis (from E14.5 to birth). Primary myogenesis occurs simultaneous with the entry of nerves into the muscle masses (Hurren et al., 2015), and is essential to form the basic muscle pattern of the body, upon which the muscle grows during secondary myogenesis. The increment in muscle mass occurs during secondary myogenesis, with a differentiation wave of secondary myoblasts that fuse with each other at the site of the innervation of the primary myofiber, giving rise to the secondary myofibers. From Nunes, 2017.

In the trunk, primary myofibers are generated by the fusion of primary myoblasts with the myotomal myocytes forming the primary myotubes, while in the limbs, diaphragm and tongue, differentiated myoblasts fuse with each other to form the primary myotubes. The primary myotubes will eventually attach to cartilaginous structures, such as the vertebrae of the trunk, and thus become the scaffold on which myogenesis will proceed (Deries et al., 2010).

Secondary myogenesis is responsible for the increment in muscle mass, both in the number of myofibers as well as their size (Biressi et al., 2007). Secondary myofibers form through a wave of differentiation of Pax7-positive cells into secondary myoblasts that will start to fuse with each other at the site of innervation of the primary myofiber, forming the secondary myofibers. In the absence of functional innervation, the formation of secondary muscle fibers is impaired. (Wigmore & Evans, 2002). Secondary myoblasts then also fuse with all existing myofibers, increasing their size (Biressi et al., 2007).

In early development, MPCs express either Pax3 or Pax7 or both. However, as development proceeds, Pax3-positive cells decline in frequency (Deries et al., 2010) and, at least in the case of epaxial muscles, become restricted to the ventrolateral edge of the differentiated muscle masses. From E14.5 onwards, Pax7-expressing muscle stem cells are found in large numbers, which shows a role of Pax7-positive cells in driving fetal stages of muscle growth including the freshly started secondary myogenesis (Biressi et al., 2007; Hutcheson et al., 2009). By this time, the fetal muscle stem cells only express Pax7 (Hutcheson et al., 2009) and become closely associated with differentiating muscle fibers at E15.5. Between E16.5 and E18.5 the basement membrane (or basal lamina) which has been assembled around the muscle fibers, comes to enclose the Pax7-positive cells underneath it. The location underneath the basement membrane is maintained during later stages of myogenesis and is a landmark of adult muscle stem cells, firstly termed satellite cells due to this characteristic location (Mauro, 1961; Zammit & Beauchamp, 2001). It is believed that satellite cells are direct descendants of the Pax3 and/or Pax7-positive cells of the dermomyotome (Kassar-Duchossoy et al., 2005; Relaix et al., 2005).

## **Extracellular Matrix**

Skeletal muscle development is understood today as a complex process that goes much beyond myoblast differentiation and fusion. The impact of transcription factors and signalling pathways in determining the course of events is now well recognized. However, there is a third element that adds complexity and tinkering to this developmental process, namely the extracellular matrix (ECM). Soon after somites develop, a basement membrane is laid down around it (Duband et al., 1987, Ostrovsky et al., 1988), playing a key role in maintaining the undifferentiated epithelial state of the dermomyotome (Bajanca et al., 2006).

The importance of the ECM is illustrated by the wide range of syndromes that arise from genetic abnormalities regarding several of its components (Frantz et al., 2010). Mutations affecting the expression of ECM components and receptors are associated with developmental arrest affecting several different tissues, and in some cases embryonic lethality (Poschl et al., 2004; Yurchenco et al., 2011).

The structural and scaffolding role of the ECM is undeniable. However, it is a highly dynamic network in constant remodelling. The ECM is composed of glycoproteins such as collagens, fibronectin, laminins, tenascins, and polysaccharides like glycosaminoglycans and proteoglycans (Frantz et al., 2010), and can be characterized as two biochemically and morphologically separate entities: the interstitial matrix as observed for example in connective tissue (Laurila & Leivo, 1993), and the pericellular matrix, which includes basement membranes, which is in close contact with cells and has a different molecular composition.

Interstitial collagens, often secreted by fibroblasts, are the most abundant fibrous proteins within the interstitial matrix, constituting the main structural element providing tensile strength, regulating cell adhesion, migration and therefore often directing tissue development (Rozario & DeSimone, 2010). Interstitial matrices also often contain fibronectin, another fibril-forming matrix protein, which plays a crucial role in mediating cell attachment, polarization and tissue compartmentalization (Rozario & DeSimone, 2010; Thorsteinsdóttir et al., 2011).

Basement membranes are evolutionarily ancient macromolecular structures first described in muscle as a “membranaceous sheath of the most exquisite delicacy” (Bowman, 1840), present in every tissue (LeBleu et al., 2007). BMs are a network of several large glycoproteins and proteoglycans which line epithelial and endothelial cells and surround muscle, nerve, and fat cells (Durbeej, 2010; Yurchenco et al., 2011). The main components of BMs are type IV collagen, laminin, nidogen/entactin, perlecan and agrin. (LeBleu et al., 2007; Yurchenco et al., 2011; Thorsteinsdóttir et al., 2011).

BMs are first assembled in the pre-implantation embryo and soon after in Reichert’s membrane (Wartiowaara et al., 1979; Leivo et al., 1980; Thorsteinsdóttir, 1992). They require the presence of laminin 111 and 511, which are already expressed at E4.5 (Miner, 2004). Both collagen type IV and laminins are able to self-assemble in a calcium dependent way and they constitute the basic networks of the BM, (Murray & Edgar, 2000). Components such as nidogen and perlecan play a decisive role in stabilization of the structure by bridging the two networks (LeBleu et al., 2007).

BMs have a structural role, whereby through direct cell-ECM interaction, they give cells an accurate understanding of their surroundings. In addition, BMs can also modulate cell behaviour by binding (or repelling) molecules, such as paracrine factors, thus creating areas of high (or low) concentrations of these factors. Thus BMs are not only providers of mechanical support but also play active roles in developmental and regenerative processes by modulating key cellular responses such as proliferation, polarization, migration, differentiation, survival and apoptosis (Frantz et al., 2010; Rozario & DeSimone, 2010; Thorsteinsdóttir et al., 2011).

In skeletal muscle, these roles are vividly illustrated through the processes of myogenesis and synaptogenesis (Patton et al., 1997; Sanes, 2003; Rogers & Nishimune, 2017).

## **Laminins**

Laminins are the major and best studied BM components (Aumailley, 2013). They are cruciform or T-shaped heterotrimers consisting of one  $\alpha$ , one  $\beta$  and one  $\gamma$  chain (Aumailley et al., 2005; Durbeej, 2010; Domogatskaya et al., 2012), forming at least 16 known isoforms (Durbeej, 2010). The current nomenclature is based on their chain composition, as for example, laminin 211 is composed of an  $\alpha 2$ ,  $\beta 1$  and  $\gamma 1$  chain (Aumailley et al., 2005; **Figure 4**, Table 1). The individual chains are joined through the long coiled-coil domains to produce a molecule with one long arm and up to three short arms (Lebleu et al., 2007; Durbeej, 2010; Aumailley, 2013).

Laminins can be classified according to their domain composition and fall into polymerizing and non-polymerizing groups (Yurchenco, 2015). Their polymerization is an important contributor to basement membrane assembly (Cheng et al., 1997; Hohenester & Yurchenco, 2013). The biological role of laminins is mediated mostly by their interaction with cell surface receptors that link laminin matrices to intracellular signalling pathways. The major receptors are integrins, and certain non-integrin receptors such as dystroglycan (Durbeej, 2010).

Integrins are transmembrane heterodimeric receptors composed of an  $\alpha$  and a  $\beta$  subunit, involved in a multitude of functions. The majority of integrins are involved in cell-ECM adhesion (Burkin & Kaufman, 1999; Barczyk et al., 2010). The predominant laminin-binding integrin receptors are  $\alpha 1\beta 1$ ,



$\alpha 2\beta 1$ ,  $\alpha 3\beta 1$ ,  $\alpha 6\beta 1$  and  $\alpha 7\beta 1$  (Nishiuchi et al., 2006; Scheele et al., 2007; Yurchenco et al., 2011). Integrin  $\alpha 7\beta 1$  binds strongly to laminins 211 and 221, while  $\alpha 6\beta 1$  has more affinity to laminins 511 and 521 (Nishiuchi et al., 2006).

Dystroglycan is a non-integrin laminin receptor, part of the dystrophin glycoprotein complex (DGC), which is composed of two subunits, encoded by a single gene (Dag1). Dystroglycan binds to laminin (extracellularly) and dystrophin (intracellularly) linking the muscle fiber cytoskeleton to the basement membrane (Durbeej, 2010; Domogatskaya et al., 2012). Laminins can also bind to two other non-integrin receptors, the heparin sulfates and sulfated glycolipids (Hohenester & Yurchenco, 2013).

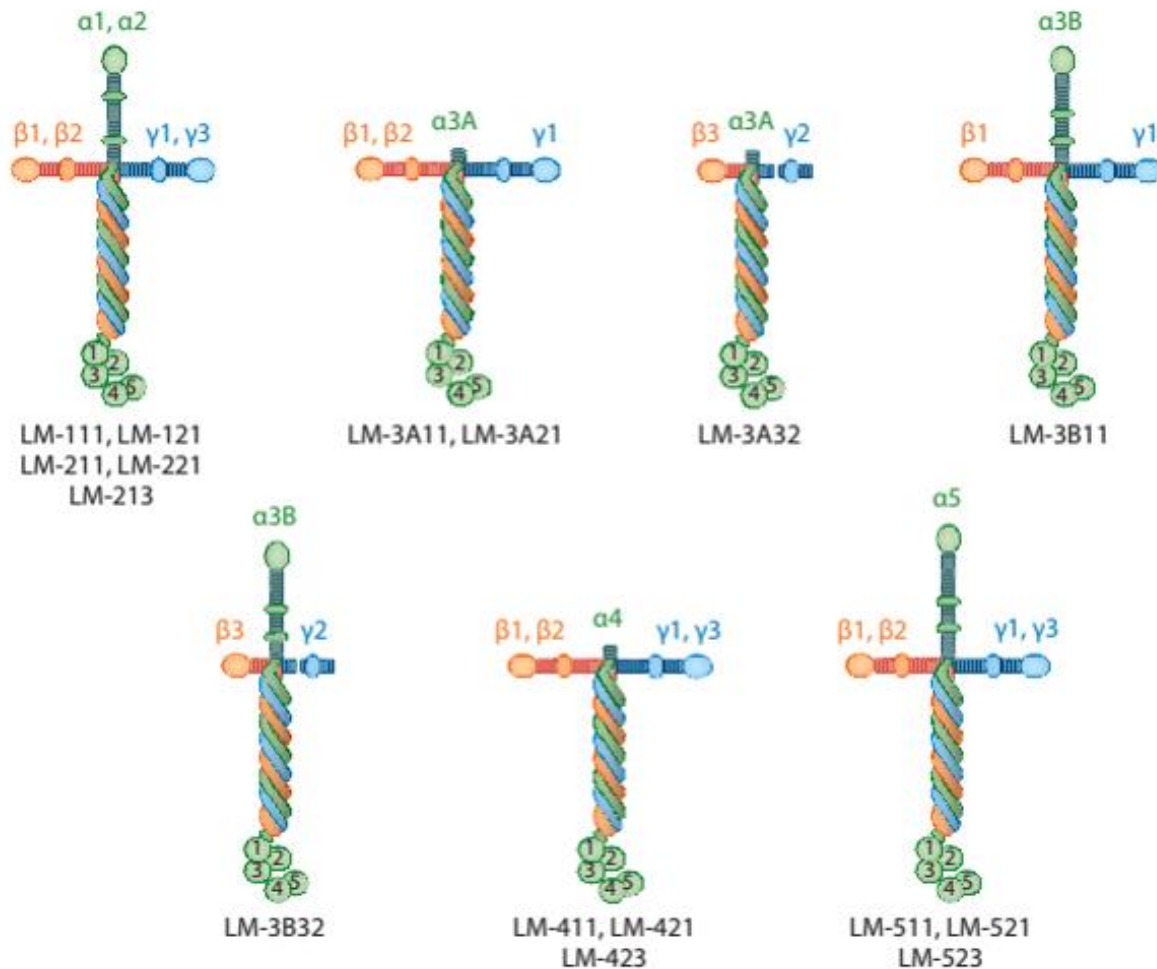


**Figure 4 - Laminin trimer structure and laminin isoforms.** Laminins are cruciform or T-shaped heterotrimers. They are constituted by one  $\alpha$ , one  $\beta$  and one  $\gamma$  chain that assemble to form at least 16 known isoforms, with one long arm and up to three short arms. Laminins are denominated based on their chain composition, as for example, laminin 211 is composed by  $\alpha 2$ ,  $\beta 1$  and  $\gamma 1$  chain. From Domogatskaya et al., 2012.

It has already been shown that laminins play a crucial role in tissue morphogenesis, beginning to be expressed in the preimplantation embryo in the mouse, during implantation and throughout organogenesis into the postnatal period (Miner, 2004; Durbeej, 2010). Laminins have often specific cell type-specific functions in processes such as adhesion, differentiation, migration and resistance to apoptosis (Domogatskaya et al., 2012), with vital roles in many physiological functions in all types of muscle, in the nervous system, as well as in skin, kidney, the digestive system and vasculature (Durbeej, 2010).

Table 1 - **Laminin nomenclature and chain composition.** From Thorsteinsdóttir et al., 2011

<b>Current laminin nomenclature</b>	<b>Old laminin nomenclature</b>	<b>Chain composition</b>	<b>Genes</b>
Laminin <b>111</b>	Laminin – 1	$\alpha 1\beta 1\gamma 1$	<i>Lama1 Lamb1 Lamc1</i>
Laminin <b>121</b>	Laminin – 3	$\alpha 1\beta 2\gamma 1$	<i>Lama1 Lamb2 Lamc1</i>
Laminin <b>211</b>	Laminin – 2	$\alpha 2\beta 1\gamma 1$	<i>Lama2 Lamb1 Lamc1</i>
Laminin <b>221</b>	Laminin – 4	$\alpha 2\beta 2\gamma 1$	<i>Lama2 Lamb2 Lamc1</i>
Laminin <b>213</b>	Laminin – 12	$\alpha 2\beta 1\gamma 3$	<i>Lama2 Lamb1 Lamc3</i>
Laminin <b>212</b> ( <i>existence proposed</i> )	-	$\alpha 2\beta 1\gamma 2$	<i>Lama2 Lamb1 Lamc2</i>
Laminin <b>222</b> ( <i>existence proposed</i> )	-	$\alpha 2\beta 2\gamma 2$	<i>Lama2 Lamb2 Lamc2</i>
Laminin <b>311</b>	Laminin - 6	$\alpha 3A\beta 1\gamma 1$	<i>Lama3A Lamb1 Lamc1</i>
Laminin <b>321</b>	Laminin – 7	$\alpha A3\beta 2\gamma 1$	<i>Lama3A Lamb2 Lamc1</i>
Laminin <b>332</b>	Laminin – 5	$\alpha 3A\beta 3\gamma 2$	<i>Lama3A Lamb3 Lamc2</i>
Laminin <b>3B32</b>	Laminin – 5B	$\alpha 3B\beta 3\gamma 2$	<i>Lama3B Lamb3 Lamc2</i>
Laminin <b>333</b>	-	$\alpha 3A\beta 3\gamma 3$	<i>Lama3A Lamb3 Lamc3</i>
Laminin <b>411</b>	Laminin – 8	$\alpha 4\beta 1\gamma 1$	<i>Lama4 Lamb1 Lamc1</i>
Laminin <b>421</b>	Laminin – 9	$\alpha 4\beta 2\gamma 1$	<i>Lama4 Lamb2 Lamc1</i>
Laminin <b>423</b>	Laminin – 14	$\alpha 4\beta 2\gamma 3$	<i>Lama4 Lamb2 Lamc3</i>
Laminin <b>511</b>	Laminin – 10	$\alpha 5\beta 1\gamma 1$	<i>Lama5 Lamb1 Lamc1</i>
Laminin <b>521</b>	Laminin – 11	$\alpha 5\beta 2\gamma 1$	<i>Lama5 Lamb2 Lamc1</i>
Laminin <b>522</b> ( <i>existence proposed</i> )	-	$\alpha 5\beta 2\gamma 2$	<i>Lama5 Lamb2 Lamc2</i>
Laminin <b>523</b>	Laminin - 15	$\alpha 5\beta 2\gamma 3$	<i>Lama5 Lamb2 Lamc3</i>

## Laminins in Skeletal Muscle

The influence of laminins on skeletal muscle begins early in embryo development during the assembly of the dermomyotome basement membrane which has a role in preventing precocious myogenesis (Bajanca et al, 2006). Another basement membrane is assembled soon after in the interface between the myotome and the sclerotome (Tosney et al., 1994; Bajanca et al., 2004).

The laminin isoform content in skeletal muscle changes throughout development, postnatal time and adulthood (Patton et al., 1997; Nunes et al., 2017). In the myotome, laminins 211 and 511 are found. During primary myogenesis, essentially no assembled laminins are present, but later on, at the onset of secondary myogenesis (E14.5), laminins 211, 411 and 511 are assembled around myotubes (Patton et al., 1997; Nunes et al., 2017). The adult expression of laminins is a subset of those made during development. The  $\alpha 2$ - and  $\gamma 1$ - laminin chains are expressed ubiquitously in the myofiber as well as in the synaptic basement membranes.  $\alpha 5$ - and  $\alpha 4$ -chain containing laminins initially have a widespread pattern, but become restricted to the neuromuscular junction perinatally, where  $\beta 2$  is also present.  $\beta 1$  is excluded from the NMJ, but is present in the myofiber basement membrane thus occupying 99% of the muscle basement membranes (Patton et al., 1997). In conclusion, laminin 211 is the major isoform surrounding the muscle fibers in the adult, while laminin 221, 421 and 521 becomes characteristic of the neuromuscular junction area (Patton et al., 1997; Patton, 2000; Yurchenco, 2015). Both of them are crucial for myofiber function and survival (Vachon et al., 1996; Holmberg & Durbeek, 2013).

## Laminins in Neuromuscular Junctions

The specialized junction that forms between the motor neuron and skeletal muscle fibers is known as the neuromuscular junction (NMJ) (Witzemann, 2006; Rogers & Nishimune, 2017). Synapse formation requires a complex interplay between the pre- and post-synaptic region (**Figure 5**). There is an interchange of information that assures the proper maturation of the neuromuscular junction (Noakes et al., 1995; Sanes & Lichtman, 1999).



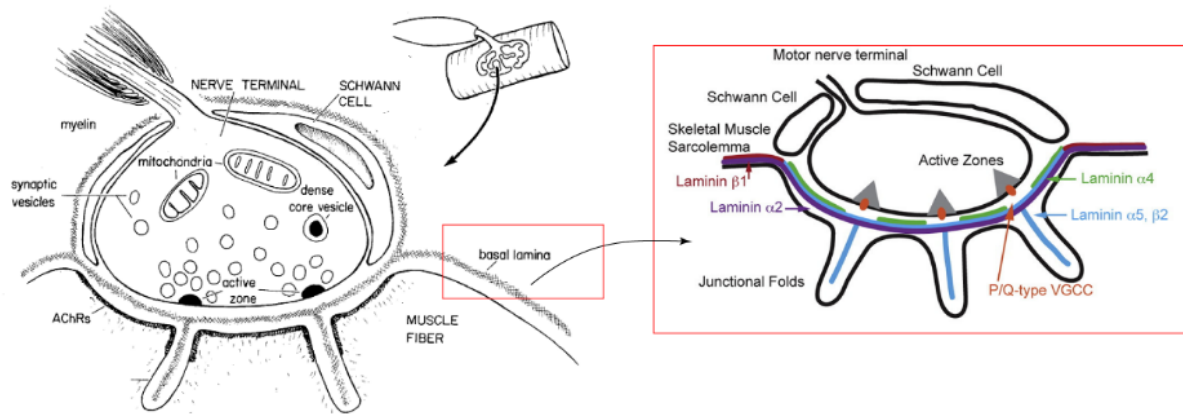


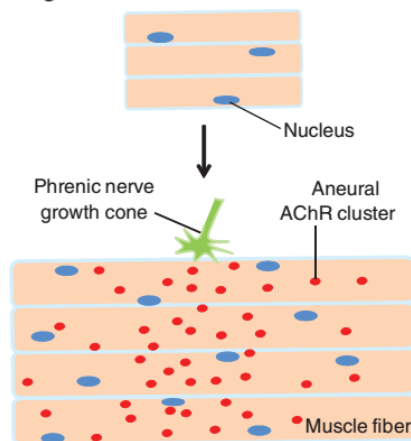
**Figure 5 - The neuromuscular junction & the laminin distribution within the synaptic cleft.** The neuromuscular junction is a specialized synapse between the motor neuron and myofiber. Acetylcholine receptors in the myofiber membrane distribute in a prepattern before innervation, however this initial distribution is remodeled after the nerve contacts the muscle. Laminins are muscle-derived synaptic organizers crucial for the development and maturation of the NMJ. The synaptic basal lamina is constituted by laminin 221, 421 and 521. Adapted from Hall & Sanes, 1993, and Patton, 2001.

The first contact between nerves and myogenic cells occurs before the beginning of secondary myogenesis, with acetylcholine and its receptor (AChR) being the main communication system of the neuromuscular system (Witzemann, 2006; Hurren et al., 2015).

The distribution of acetylcholine receptors on muscle fibers is prepatterned, even before the contact with a motor neuron and subsequent contact between the neuron and the myofiber reinforces this pattern (**Figure 6**; Grady et al., 2005). Multiple innervations are eliminated to form a single synaptic contact, and by E17.5 the synaptic site and endplate pattern is fully established (Grady et al., 2005). The process of innervation by motor neurons requires a guidance system allowing the communication between them and their target, the endplate. Laminins are known to play a role in this process (Patton, 2003; Sanes, 2003). As mentioned before, the basement membrane envelops the entire muscle fiber, as well as the synaptic cleft (Sanes, 2003).

#### A Mouse

##### a Early stage



##### b Late stage

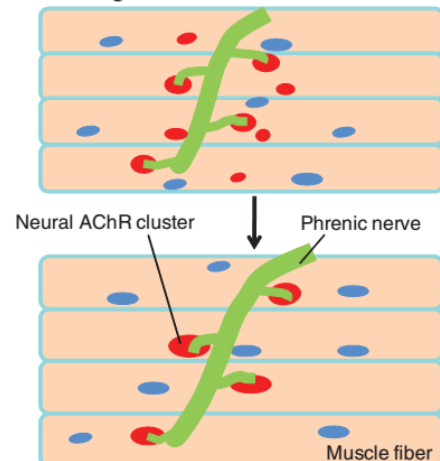


**Figure 6 - Neuromuscular synapse formation in the mouse.** The post-synaptic area of the neuromuscular junction is characterized by the presence of aneurial AChR clusters, i.e. which are clusters of AChR in the myofiber membrane that formed without nerve contact. When innervation occurs, there is a reorganization of the AChR clusters in the membrane of myofibers, with the receptors becoming concentrated in the synaptic region while primitive clusters in non-synaptic areas disappear. From Wu et al., 2010.

Laminins are muscle-derived synaptic organizer that promote pre- and post-synaptic differentiation by an autocrine mechanism (Nishimune et al., 2008). This process depends largely on the aggregation of dystroglycan in the post-synaptic membrane, known to bind to agrin, a nerve-derived synaptic organizer (Witzemann, 2006; Nishimune et al., 2008; Rogers & Nishimune, 2017). Laminins are crucial for the proper development and maturation of the NMJ and the synaptic basement membrane contains laminins 221, 421, 521 (Patton et al., 1997; Patton, 2000). Laminins 421 and 521 have a determinant role in organizing active zones and endplate structures in NMJs (Patton, 2000). These two laminins are responsible for the correct alignment of the pre- and post-synaptic structures, and the specific presence of the laminin  $\beta 2$  chain is crucial for motor neuron adhesion, inhibition of neurite outgrowth, ultimately acting as a stop signal (Noakes et al., 1995; Nishimune et al., 2008). Mouse models lacking laminin- $\alpha 2$  chain display partial detachment of motor neuron terminals from the endplate, have demyelination of motor axons and Schwann cell infiltration into the synaptic cleft (Patton, 2000). Furthermore disruption between laminins and their receptors (integrins and/or dystroglycan), due to aging or injury, results in defects at the NMJ. A fragmented distribution of AChR and the loss of precise apposition of the pre- and post-synaptic apparatus are the major phenotypes (Noakes et al., 1995; Patton et al., 2001). Ultimately, breaking this structural connection leads to a progressive degeneration of the neuromuscular system.

### Satellite Cells

Vertebrate skeletal muscle has an exquisite regenerative capacity that maintains the neuromuscular system healthy and functioning (Chargé & Rudnicki, 2004). Satellite cells, which are localized between the basement membrane and the muscle fiber, (Mauro, 1961) are muscle stem cells (Tajbakhsh, 2009). They are derived from the Pax3- and Pax7- expressing cells of the central dermomyotome, and represent the principal regenerative source of the skeletal muscle in postnatal life (Kassar-Duchossoy et al., 2005; Relaix et al., 2005).

Muscle regeneration is characterized by a degenerative phase triggered by the disruption of the myofibers allowing the entry of macrophages (Chargé & Rudnicki, 2004), and a regenerative phase which is accomplished by satellite cell activation, proliferation, differentiation into myoblasts and fusion of these myoblasts with each other or the pre-existing fibers (Chargé & Rudnicki, 2004; Kuang et al., 2007; Sambasivan et al., 2011).

Upon injury, satellite cells are activated in response to both intrinsic and extrinsic signals. They proliferate for a while after which some downregulate Pax7, upregulate Myf5 and MyoD, enter the myogenic program and differentiate into myoblasts which either fuse with each other giving rise to new multinucleated myofibers or fuse with existing ones. After that, satellite cells which did not enter the myogenic program, re-enter quiescence again and become nested underneath the basal lamina (Schultz & Jaryszak, 1985).

Recent studies have shown that the satellite cell population is heterogeneous, with 90% of Pax7+/Myf5+ cells, known to be more prone to differentiation, and about 10% of Pax7+/Myf5-. The latter is believed to be a more stem population crucial to restore and maintain the satellite cell pool after regeneration (Kuang et al., 2007).

The reservoir of muscle stem cells is maintained and expanded mainly through asymmetric and symmetric divisions, respectively (**Figure 7**). The ratio of these two types of divisions is extensively influenced by the satellite cell niche. The niche that is essentially asymmetric, with the cells contacting with two opposing environments, the basement membrane and the myofiber membrane, leads to an asymmetric distribution of proteins, for example integrin  $\alpha 7 \beta 1$  on the basal side, near the basement membrane, and  $\beta$ -catenin on the apical side, near the myofiber (Dumont et al., 2015a).

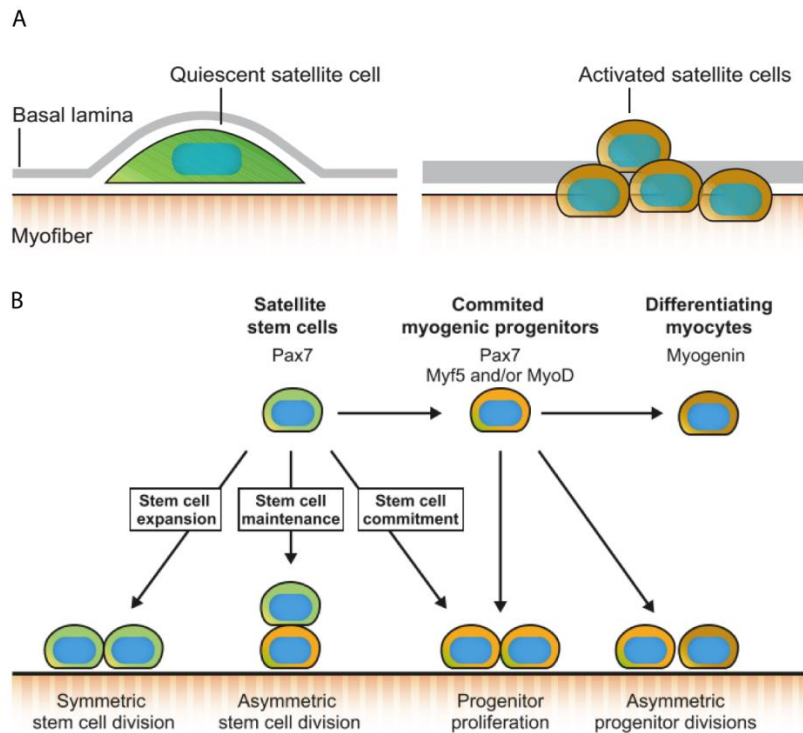


**Figure 7 - Satellite cell fate decisions.** (A) Satellite cells are located under the basement membrane, juxtaposed to the muscle fiber, in a quiescent state. Satellite cells are a heterogeneous population that in response to both intrinsic and extrinsic signals are activated and re-enter the cell cycle. Then they proliferate and some of them upregulate the MRFs Myf5 and MyoD. (B) When activated, the satellite stem cells can undergo two different types of divisions. The symmetric divisions allow for the expansion of the stem cell pool. The asymmetric divisions maintain the stem cell pool while generating committed myogenic progenitors. The committed cell proceeds in the myogenic program, giving rise to myoblasts that will fuse to form new myofibers. From Dumont et al., 2015a.

Several signalling pathways are known to play roles in the return to quiescence (e.g. Le Grand & Rudnicki, 2007; Shea et al., 2010; Chakkalakal et al., 2012). However, Notch signalling (**Figure 8**) has emerged as a master regulator of satellite cell state. Notch signalling occurs when Delta1-like ligand and the Notch receptor are present on adjacent cell surfaces (Conboy & Rando, 2002). Similarly with lateral inhibition, also controlled by Notch, when an asymmetric cell division occurs, the daughter cell committed to differentiate will express high levels of delta1, whereas the other one expresses Notch3 receptor. The cell expressing Notch will receive a notch signal from the Delta1-expressing cells and the subsequent release of the Notch intracellular domain (NICD) to the nucleus, promotes the expression of Pax7 (Bröhl et al., 2012) and the return to quiescence, (Kuang et al., 2007) maintaining their proliferative capacity. Depletion of Notch receptor will lead to spontaneous uncontrolled differentiation resulting in the satellite cell pool depletion (Vasyutina et al., 2007), while forced expression of notch intracellular domain (NICD) maintains Pax7-positive cells in an undifferentiated state

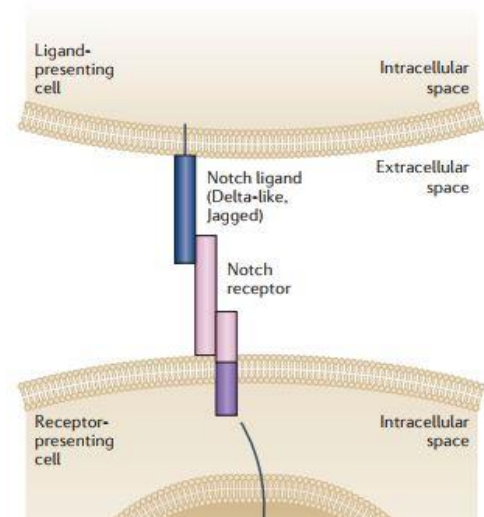


**Figure 8 - The Notch signaling pathway.** Notch signaling is activated when a notch-ligand (Delta-like, Jagged) in the neighbor cell contacts with the notch receptor in the receiving cell. This connection induces a proteolytic event and the notch receptor is cleaved. This cleavage releases the notch intracellular domain (NICD), which is translocated to the nucleus and functions as a transcription factor that, together with other cofactors, activates the transcription of Notch target genes. From Anderson et al., 2014

thus blocking myogenic differentiation (Mourikis et al., 2012).

The unequivocal necessity of Pax7-positive satellite cells in adult regenerative myogenesis, does not rule out the importance of the contribution of other cell types to the regeneration process. These other cell types can definitely modulate the behaviour and survival of the Pax7-positive satellite cells (Sambasivan et al., 2011). For example, the presence of nerves have been shown to influence satellite cells since after denervation, satellite cell numbers decline dramatically, impairing the regenerative capacity of muscles (Jejurikar et al., 2002).

### **Merosin-deficient congenital muscular dystrophy type 1A (MDC1A)**

Merosin-deficient congenital muscular dystrophy type 1A (MDC1A) is a type of congenital muscular dystrophy, also known as laminin- $\alpha$ 2 CMD (LAMA2-CMD). It is a neuromuscular disease resulting from a mutation in the laminin- $\alpha$ 2 gene (*LAMA2*) (Tomé et al., 1994). MDC1A is characterized by severe muscle weakness and neonatal hypotonia, as well as delayed motor milestones and neuropathies (Gawlik & Durbeej, 2011), representing about 40% of cases of CMD in Europe (Allamand & Guicheney, 2002).

As mentioned above, laminin 211 is the main isoform in the basement membrane surrounding muscle fibers, while 221 is mostly concentrated at the neuromuscular junction. (Patton et al., 1997; Nunes et al., 2017). The absence of the  $\alpha$ 2 chain and consequently the laminin 211 and 221 trimers, is thought to result in a disruption between the basement membrane and the muscle fiber cytoskeleton, leading to a structural instability and consequently increased muscle fiber degeneration (Vachon et al., 1996).

There are several mouse models for studying laminin- $\alpha$ 2 deficiency, the one recommended as a MDC1A model by Cure CMD ([www.curecmd.org](http://www.curecmd.org)) being the  $dy^w/dy^w$  mouse, which expresses a small amount of truncated  $\alpha$ 2 chain (Gawlik & Durbeej, 2011). Using the  $dy^w/dy^w$  model, Nunes et al. showed for the first time that the onset of the disease occurs prenatally and in the absence of any muscle fiber damage. Rather, they found that E18.5  $dy^w/dy^w$  muscles display significantly fewer Pax7-positive muscle cells and an overactivation of the JAK-STAT signalling compared to same stage wild-type muscles (Nunes et al., 2017). One way to explain these results is that the absence of laminin 211/221 somehow shifts the balance of muscle stem cell division to asymmetric divisions, which could lead to an early depletion of the stem cell pool.

It is imperative to gain a deeper and more detailed understanding of the functional mechanisms underlying the communication between muscle cells and their basement membrane and how mutation affecting this communication lead to disease, such as muscular dystrophies. It is important to comprehend the way in which the different players involved in skeletal muscle formation regulate each other's development. What are the key players coordinating the formation of a functional musculoskeletal system? In what way do these players communicate with each other? A better understanding of how this communication occurs, and how it goes wrong in disease, will allow us to envision new and precise therapies targeting the key events involved in the onset of diseases such as muscular dystrophies. Such an approach may be more effective since it targets the disease early, at an earlier stage of development.

### **Aims of this thesis**

As mentioned above, laminin matrices have been found to play crucial roles during skeletal muscle development. Here we aim to build on the results obtained in our group and characterize the fetal myogenesis defect in the  $dy^w/dy^w$  mouse in more detail. We propose to first analyse how normal fetal muscle stem cells establish their niche. This will be done by determining precisely which cells in the

fetal muscle masses express the *Lama2*, *Lama4* and *Lama5* genes, and studying the laminin assembly dynamics around the muscle stem cells and myofibers during secondary myogenesis. Knowing how this occurs in normal fetuses will contribute to understanding what goes wrong in  $dy^w/dy^w$  fetuses. Secondly, we know that the development of a functional musculoskeletal system depends on innervation. Thus we will study the development of NMJs in the absence of  $\alpha 2$ -laminin, aiming to determine if the NMJs are somehow altered in the  $dy^w/dy^w$  mouse model, and if so, in what way.



# **Chapter 2**

## **Materials and Methods**

## Materials and methods

### Embryo collection

- a. Wild-type fetuses (E15.5 - E18.5) obtained from crossing of outbred CD-1 mice (Jackson Laboratories), were used to assess the distribution of laminin variants during normal myogenesis. The pregnancies were dated through observation of the copulation plugs, with the morning of the plug staging the embryonic day 0.5 (E0.5). Pregnant females were anesthetized with an anaesthetic drug – isoflurane (2-chloro-2-(difluoromethoxy)-1,1,1-trifluoro-ethane) - and confirmed unconscious with loss of pinch toe and reflexes. They were sacrificed by cervical dislocation. Fetuses were removed from the uterus in cold phosphate buffered saline (PBS), then beheaded and processed for cryosectioning and immunohistochemistry.
- b. *dy<sup>W</sup>* mice have a *LacZ-neo* cassette inserted in the *Lama2* gene, and homozygous animals produce a small amount of a truncated laminin  $\alpha 2$  protein lacking the N-terminal LN domain (Engvall YEAR). To obtain homozygous *dy<sup>W/-</sup>* mutants and wildtype controls, heterozygous *dy<sup>W</sup>* were crossed.
- c. *Myf5<sup>Cre/+</sup>:R26R<sup>stop-NICD-nGFP/+</sup>* mice express the notch intracellular domain (NICD) under the control of the *Myf5* promotor, which enables the constitutive activation of NICD in muscle stem cells that have activated *Myf5* gene (Mourikis et al., 2012).

### Genotyping

The fetuses from heterozygous *dy<sup>W</sup>* crossings were genotyped with the following primers: 5' ACTGCCCTTTCTACCCACCCTT 3', 5' GTTGATGCGCTTGGGACTG 3' and 5' GTCGACGACGACAGTACTGGCCTCAG 3'. (**Annex I – P1**)

All procedures involving mice were performed under two approved protocols: (3/2016) from the Animal Welfare Body of the Faculty of Sciences, University of Lisbon.

### Cryosectioning

Fetuses staged between E15.5 and E18.5 were processed for cryosectioning, and fixed in 4% paraformaldehyde (PFA) in phosphate buffered saline (PBS) or 2% (fixative for *in situ* hybridization) FISH. They were washed and incubated for 48h in a sucrose gradient: solution 1 (0.12M phosphate buffer with 4% sucrose), solution 2 (0.12M phosphate buffer with 15%). Finally, the fetuses were washed and incubated in solution 3 (0.12M phosphate buffer with 15% sucrose and 7.5% gelatine) for 3h at 37°C and frozen in small aluminium boats on the surface of dry ice-chilled isopentane. Sections were made with a Leica CM1860 UV Cryostat.

### *In situ* probe production

#### a. Transformation

One microliter of *Lama2*, *Lama4* and *Lama5* plasmid (1-10ng) was added to 50μL of DH $\alpha$ 5 competent *E. coli* bacteria. The resulting solutions were incubated on ice for 30min, subjected to heat shock during 35s at 42°C without shaking and immediately transferred to ice for 2min. Nine hundred and fifty microliters of pre-warmed lysogeny broth (LB) medium without ampicillin were added to the bacteria tubes, which were incubated at 225rpm at 37°C for 1h. After that, 100μL of each tube was plated in the pre-warmed selective plates. The plates remained inverted overnight at 37°C.

#### b. Primary culture

Four tubes per plasmid with 4mL of LB medium treated with ampicillin (100μg/mL; selection plates) pre-warmed at 37°C were inoculated during 8h at 300rpm with isolated colonies picked up from



the plates. After that, 1mL of culture was used to perform a confirmation Mini-Prep (Annex I – P2), in order to choose the best colony and verify if the transformation was efficient.

Subsequently, we proceeded to a secondary culture, where 500µL of primary culture were incubated in 100mL of LB medium with ampicillin, at 37°C for 16h in autoclaved Erlenmeyer flasks. The plasmid of interest was then extracted using a JetStar - The Novel Plasmid Purification System (Annex I – P3), and diluted in 30µL of TE and stored at -20°C.

### ***c. Linearization***

Ten micrograms of the plasmid were digested for 2h30 at 37°C with 5 units of the proper restriction enzyme, see SI - Table A.

The plasmid linearization was confirmed through gel electrophoresis (1% agarose). DNA was precipitated with 300µL of DEPC water and 800µL of isopropanol at -20°C for 2h, followed by a 13000rpm centrifugation at 4°C during 45min. The pellet was washed in 1200µL of ethanol (EtOH) 100% followed by a 15min centrifugation in the previous conditions. The supernatant was discarded and a second EtOH wash for 5min was performed. The DNA pellet was resuspended in 30µL of TE buffer.

### ***d. Transcription***

One microgram of linearized DNA was incubated for 2h30 at 37°C with 2µL of transcription buffer 10x, 2µL of DIG labelling mix, 1µL of DTT, 0.5µL of RNasin, 1µL of RNA polymerase and the necessary amount of DEPC/nuclease free water to make up the 19.5µL volume. RNA presence was confirmed through gel electrophoresis (2% agarose), and the RNA proceeded to precipitation with 2.5µL of LiCl 4M, 75µL of EtOH 100% and 1µL of EDTA 0.5M pH = 8.0, leaving the solution at -20°C overnight. After centrifugation and removal of the supernatant, the pellet was washed by a gradient of ethanol. The pellet was resuspended in 30µL of DEPC water and measured in Nanodrop for concentration and purification ratios. The probe was diluted in hybridization solution (hybmix, see Annex II) at a concentration of 1µg/mL and stored at -20°C.

## ***In situ hybridization***

To determine mRNA expression pattern of *Lama2*, *Lama4* and *Lama5*, fetuses from E15.5 to E18.5 were fixed in 4% PFA for in situ hybridization as previously described (Bajanca et al., 2004).

### ***a. RNA whole-mount in situ hybridization***

We began by testing two possible approaches of the *in situ* hybridization protocol. Initially, we tested the efficiency of RNA whole-mount in situ hybridization adapted for mouse fetuses from Cepko/Tabin lab and based on Bajanca et al. 2004.

Fetuses were collected and dissected, leaving only the back musculature, in PBS DEPC 1x, and fixed in fresh 4% PFA/PBS DEPC at 4°C overnight. They were washed in PBT and dehydrated in a methanol gradient, to be stored at -20°C.

The *in situ* hybridization protocol begins by a methanol to PBT gradient rehydration. The fetuses were bleached with 6% H<sub>2</sub>O<sub>2</sub> and treated with proteinase K (10µg/mL). Then incubated in 2mg/mL glycine for 10min and fixed in a solution of 0.2% glutaraldehyde and 4% PFA in PBT. Finally they were washed in a gradient of PBT:Hybmix and incubated overnight at 70°C in the probe solution. In the next day, fetuses were washed in pre-warmed hybmix at 70°C.

From this step onwards, all washes were performed at room temperature, starting with long washes (2 x 30min) in TBST. For the blocking step, fetuses were left incubating for 1h in a solution of TBST +

2% blocking + 20% Sheep Serum at room temperature. The fetuses were incubated overnight at 4°C in a solution with anti-dioxygenin (1:2000).

Probe localization was detected with alkaline phosphatase conjugated anti-dioxygenin antibodies and NBT/BCIP (Roche) as a substrate in NTMT (4.5 µL NBT/1mL NTMT and 3.5µL BCIP/1mL NTM). The reaction is complete after 7 overnights of incubation and the colour development is stopped with PBS followed by post-fixation in 4% PFA + 0.2% glutaraldehyde in PBT 2h at RT or O/N at 4°C.

Unfortunately this protocol did not give consistent results because the penetration of the probe did not appear to be sufficient to give a positive signal, most likely due to the tissue density of a more advanced stage (E15.5). For these reasons, we modified the approach to detect the presence of mRNA in the epaxial muscles, for an *in situ* hybridization of sectioned samples.

### ***b. In situ hybridization on sections***

Every solution was DEPC treated to avoid mRNA degradation. We began by cryosectioning the fetus into 30µm-thick sections which were placed on SuperFrost Ultra Plus microscope slides and let dry for 1h30. Afterwards, we proceeded with PBS DEPC 1x washes, followed by proteinase K treatment (10µg/mL). Treatment with proteinase K has a major influence on tissue integrity so we tried several different times and found that 2min was optimum. Post-fixation time was also optimized, and best results were obtained with 45min in 4% PFA in PBS. Incubation in pre-hybmix solution at room temperature for 5min and then at 70°C for 30min. The tissue sections were with the probe solution overnight at 70°C (the optimal hybridization temperature).

The next day we started with 30min washes in post-hybmix previously heated to 70°C. Thereafter, the tissue sections were washed at room temperature in TBST by changing the solution every 30min. Then we proceeded to the blocking step with TBST + 2% Blocking + 20% sheep serum for 1h30 at room temperature. Probe localization was detected with alkaline phosphatase conjugated anti-dioxygenin antibodies (1:2000 in blocking solution) overnight at 4°C, followed by incubation in NBT/BCIP (Roche) in NTMT (4.5µL NBT/1mL NTMT and 3.5µL BCIP/1mL NTM) for two weeks. PBS was used to stop development, followed by post-fixation in 4% PFA in PBS and slides were finally mounted in Aquatex aqueous embedding medium.

### ***c. Immunohistochemistry over in situ hybridization***

SIGMAFASTA 3,3-Diaminobenzidine (DAB) tablets have been developed for use in immunohistology as a precipitating substrate for detection of peroxidase activity. DAB is the immunohistology substrate of choice as it produces an intense brown-black stain, which is resistant to alcohol. After the *in situ* hybridization protocol, but before mounting in Aquatex, sections were incubated with (3% H<sub>2</sub>O<sub>2</sub> in PBS) for about 5min, followed by the primary antibody incubation, at 4°C overnight. Detection was performed using a goat anti-mouse HRP secondary antibody for 1h at room temperature. Protein was visualized by DAB staining, where antibody-protein conjugates turn brown (SIGMAFAST, Sigma Aldrich Cat-D4418; St. Louis, MO). Colour development was carefully monitored during the reaction and stopped by washing in PBS. The tissue sections were submitted to post-fixation in 4% PFA in PBS and mounted in Aquatex.

## **Immunohistochemistry**

### ***a. Whole-Mount immunohistochemistry DMSO/Methanol Method***

Whole mount immunohistochemistry was performed as described in (Gonçalves et al., 2016), with minor changes.

Fetuses from E15.5 to E18.5 were beheaded and fixed in 2% PFA in PBS over 2 nights, at 4°C. After washed in PBS, they were incubated in a 0.1M glycine in PBS for 1h, at room temperature. Afterwards, we proceeded to the dehydration with methanol gradients (20%, 50%, 80% and 100%). Then, the fetuses were incubated in Dent's fixative solution for about of 2 weeks, at 4°C. After that, we continued to the immunostaining. All of the following incubations were done on a shaker, since good mixing is critical. We started with rehydration from 100% methanol into PBS 1x followed by several washes in PBS. After that, the fetuses were incubated overnight at 4°C in blocking solution. On the following day, we applied the primary antibodies diluted in the previous solution for over 2 nights at 4°C. All antibodies used are listed in Table C. The final washes were performed in 4x PBS to remove non-specific antibody bindings, we did another incubation with blocking overnight at 4°C, followed by the secondary antibodies incubation overnight. Fetuses were then intensively washed in 4x PBS for 2 days, being slowly dehydrated in methanol gradients and mounted in methylsalicylate on coverslips sealed with paraffin (Martins et al., 2009).

### ***b. Whole-Mount immunohistochemistry – thick sections***

This second approach to immunohistochemistry was performed essentially as described in Bajanca et al., 2004 with minor changes. Fetuses were fixed in 2% PFA in PBS and embedded in gelatine (see next section). A nearly one-centimetre-thick cross-section of the fetuses was cut with a scalpel. After the gelatine melts, the section of the fetuses was washed in PBS for 1h. Then, the section was incubated in ID solution for 4h at room temperature. Primary and secondary antibodies incubations were done for 2 overnights, at 4°C. The following days are essentially long washes in 4x PBS. To finalize, the sections were fixed in 0.2% PFA in PBS for 2h, followed by a treatment with 0.1M glycine in PBS for 1h. The section was dehydrated in methanol gradients, were mounted in methylsalicylate and sealed with paraffin between slide and coverslip (Martins et al., 2009).

### ***c. Immunohistochemistry on 30 and 100µm sections***

Fetuses were fixed in 2% PFA in PBS for 2 days at 4°C. Longitudinal cryosections were collected on Super Frost slides and processed for immunohistochemistry, performed as described by Nunes et al., (2017) with minor changes. The sections dried for 2h at room temperature. Sections were permeabilized in 0.2% Triton X-100 in PBS for 40min. Mouse-On-Mouse (MOM) Kit (Vector laboratories) was used. The primary antibodies were diluted in Protein Concentrate and placed on sections overnight at 4°C. Secondary antibodies were incubated for 1h at room temperature. For nuclear staining, it was used MethylGreen. The cryosections were post-fixed in 2% PFA in PBS for 30min. Afterwards, the slides were mounted in propyl gallate and sealed after. Antibodies and respective dilutions used are listed in Table (C).

## **Immunohistochemistry on Myf5Cre-NICD fetuses**

Transverse cryosections of E14.5 and E17.5 Myf5Cre-NICD fetuses were processed for immunohistochemistry, as in Nunes et al., (2017) with minor changes. Antigen retrieval was done in E14.5 and E17.5 tissue, to stain Pax7, by immersing sections in Tris-EDTA (10mM Tris base, 1mM EDTA, 0.05% Tween 20) buffer, pH = 9.0 at 95°C for 10 and 5min respectively. When staining with monoclonal mouse antibodies, the MOM kit was used.

## **Real time quantitative RT-qPCR**

We took a RT-qPCR approach to assess the expression of *Fgfr1*, and *Fgf2*, both known to have the ability to drive the break of quiescence and loss of self-renewal capacity by the cells, and the expression of *Sprouty1*, an inhibitor of FGF signaling. RNA was extracted from E17.5 back muscles with Trizol Reagent Kit (Ambion, Life Technologies). First-strand cDNA synthesis was performed

using the SuperScript III First-Strand Synthesis System for RT-qPCR kit (Ambion, Life Technologies). Real time qPCR reactions were performed in triplicates with SYBR Green Master Mix 2x and 500ng RNA. The cDNA production followed protocol P4 in supplementary information. Transcripts levels were normalized against *Gapdh* expression and the fold change was calculated using  $\Delta\Delta C_t$  method. *Fgfr1*, *Fgf2* and *Sprouty1* transcript RNA sequences were obtained from the NCBI database (<https://www.ncbi.nlm.nih.gov/>). Forward and reverse primers were designed in ApE Plasmid Editor (<http://biologylabs.utah.edu/jorgensen/wayned/ape/>).

## **Image analysis and quantifications**

*In situ* hybridizations were photographed with an Olympus DP50 camera coupled to an Olympus BX51 microscope. Images for the immunohistochemistry preparations were obtained with Leica SPE/SP8 confocal microscope system. The acquired images were analysed in Fiji version 1.49. Longitudinal sections processed for immunohistochemistry were used for quantification of the total number of synapses per muscle, using 6 sections per fetus. Overlapping confocal images of longissimus muscle were obtained with a 10x lens and individual stacks were stitched together into a large composite image using the Fiji Plugin Pairwise Stitching (Preibisch et al., 2009). Quantifications were performed using Fiji Plugin Cell Counter ([http://fiji.sc/Cell\\_Counter](http://fiji.sc/Cell_Counter)). Confocal images of individual synapses were obtained with a 63x oil immersion lenses and 3D-reconstructed with Amira V.5.3.3 (Visage Imaging Inc.) software. Immunohistochemistry results were acquired with an Olympus BX60 microscope coupled to an Olympus DP50 digital camera and posteriorly analysed using the previously mentioned software, Fiji version 1.49.

## **Statistical analysis**

Statistical analyses were performed using GraphPad Prism 5, R software and Excel.

## **Data analysis of $dy^W$ muscle masses**

Synaptic size and distribution play an important role in the functional properties of synapses. (Tarusawa et al., 2009). The distribution of synapses within the muscle can be described as a spatial point pattern which consists in a spatial arrangement of events in a study area generated by a multi-dimensional stochastic process which can be analyzed with mathematical methods (Baddeley et al., 1993; Illian et al. 2008). Spatial point patterns might be classified in three main classes, namely clustering, regularity and randomness (Diggle, 2003).

A stochastic process is a process that randomly generates points in space and can be characterized by first-order and second-order effects. First-order effects are the global or large-scale effects which correspond to the variation of the mean value of the process, the value referring to the intensity ( $\lambda$ ), the number of events per area unit. Second-order effects are the local or small-scale effects and they represent the spatial dependency of the process, that is, the covariance.

Quadrat analysis explores the first-order properties while distance-based methods such as G-Function or Ripley's K-Function explore the second-order properties. Although both functions explore the same effects, Ripley's K-Function considers several spatial scales. To understand the pattern of distribution of synapses, all these spatial point pattern analyses were performed with R version 3.4.1 statistical computing platform (R Development Core Team, 2017) and spatstat package for R (Baddeley and Turner, 2005; Baddeley, 2010) in R Studio 1.0.153, an integrated development environment for R.

### **a. Coordinate acquisition**

Fluorescence microscopy images showed the spatial distribution of the synapses. The images were scaled to  $\mu m$  in Fiji, the fluorescent spots corresponding to the synapses locations were pin-pointed and

the point coordinates were exported as a text file. The perimeter of longissimus muscle was traced using the polygon selection tool and the coordinates of the perimeter vertices were also exported as a text file. It is important that the polygon vertices are navigated in anticlockwise order since this is a requirement to a further step.

### ***b. Data visualization***

To start, it is necessary to open R Studio and load the spatstat package using the command `library(spatstat)`. We also used lattice package to plot data and it may be necessary to load it as well. Since spatstat is not a standard package in R, it may be necessary to download and install it first which can simply be done by running the command `install.packages("spatstat")`. Alternatively, spatstat is available at <https://CRAN.R-project.org/package=spatstat>.

We set the working directory, which is the place where our files are and to where our result files are going to be exported, using the function `setwd`, and imported the coordinate files using the function `read.delim` since we worked with text files. One should type carefully both the path to working directory and file names since R is case sensitive. Also, if the path to working directory has any graphic accents R may not be able to read it correctly. Before creating the actual spatial point pattern, it is necessary to create a window object that will delimit the study area using the coordinates of the muscle perimeter that were exported from Fiji in anticlockwise order. To create the window object, here called `muscle_limits`, we used the function `owin` like in the following example

```
muscle_limits <- owin(poly = list(x = c(x1, x2, x3,.....,xn), y = c(y1, y2, y3,.....,yn)))
```

where the x and y correspond to the coordinates of the polygon vertices defining the muscle perimeter. After this we creates a point pattern object, here designated `synapses_pattern`, by running the command `ppp`, in the form

```
synapses_pattern <- ppp(x = c(x1, x2, x3,.....,xn), y = c(y1, y2, y3,.....,yn), window = muscle_limits)
```

where the x and y are the coordinates of the synapses centroids. To finally visualize the created spatial point pattern, we ran the command `plot(synapses_pattern)`. The visualized point pattern orientation is mirrored to the original image due to differences in the origin location between R and Fiji.

Data visualization allows us to have a first visual perception of the synapses distribution and to simply describe it by its frequency (number of synapses) or density (number of synapses per muscle area unit), but further data exploration is necessary.

### ***c. Quadrat analysis and Variance-to-Mean Ratio***

To perform a quadrat analysis, we divided the study area in small homogenous sub-regions by placing a quadrat grid over the study area and counting the number of synapses within each grid cell, also called quadrat (Câmara & Carvalho, 2004). The cells can have any size or regular shape and its position is arbitrary, which is one of the weaknesses of this kind of analysis, so the quadrat choice should be meaningful. We used squared cells with an area of  $113\mu\text{m}^2$ . The optimal quadrat size was calculated by applying the formula:

$$\text{Quadrat size} = \frac{2A}{n} \quad (1)$$

where  $A$  is the average of the muscle area and  $n$  is the mean number of synapses, both for all embryo sections.

Having the frequency of synapses per quadrat, we can calculate its mean and variance and, with that, the Variance-to-Mean Ratio, hereafter referred as VMR, as a preliminary approach to understand

the distribution pattern of our data. VMR is an index of dispersion that indicates us if the observed events are more clustered or dispersed according to its value and can be calculated as followed

$$VMR = \frac{s^2}{\bar{x}} \quad (2)$$

where  $s^2$  and  $\bar{x}$  are respectively the variance of and the mean frequency of synapses per cell.

In a complete random pattern, the frequency of most cells is close to the mean frequency, a few cells have no counts and a few have large counts. In such pattern the variance equals the mean and VMR equals to 1. In a regularly dispersed pattern, most cells have about the average frequency, therefore, a small spatial variance of points per cell. A clustered pattern has many cells with high frequencies and many empty cells, translating into a large variance of points per cell. So, a VMR smaller than 1 indicates uniformity and a VMR above 1 indicates clustering.

After calculating the VMR value for the observed point pattern, we must statistically test if the observed pattern is different from the expected pattern for a random process. The standard model used to make that comparison is the Complete Spatial Randomness (CSR) because it serves as a dividing hypothesis between a regular and a clustered pattern (Sanchez et al., 2014). This theoretical model has two assumptions which are met by a homogeneous/ stationary Poisson process and those are that the spatial process is both first- and second-order stationary.

First-order stationarity is the assumption that there is an equal probability of an event to occur in any part of the study area, i.e. the intensity of the process remains constant in the study area (Câmara & Carvalho, 2004). Basically, this implies that if one would look to a small part of the spatial point pattern with a fixed observation window and determined the intensity of points inside that window, the intensity would remain the same no matter the chosen location for the window in the study area. If rotating that same observation window also does not affect the intensity of the process, the process is also isotropic. This means that the events are uniformly distributed in all directions.

On the other side, second-order stationarity is the assumption that there is no interaction between events, in other words that the locations of the points have no influence on each other. If the data presents significant deviation from the expected Poisson distribution, that is an evidence for a spatial distribution different from the spatial randomness (Câmara & Carvalho, 2004).

To statistically compare the observed VMR with the expected VMR for a random distribution generated by a Poisson process with the same intensity as the observed pattern, we applied a two-tailed chi-square test (Smith, Goodchild, Longley, 2015). If the data are generated by a Poisson distribution, the VMR should be equal to 1 because variance equals the mean for this kind of distribution. Our test hypotheses are defined as  $H_0: VMR = 1$  vs  $H_1: VMR \neq 1$  and the test statistic ( $\chi^2_{test}$ ) is defined as

$$\chi^2_{test} = \frac{(m-1)s^2}{\bar{x}} \quad (3)$$

where  $m$  is the number of quadrats and  $s^2$  and  $\bar{x}$  are respectively the variance of and the mean number of synapses per cell. Looking at equation 2, we can simplify the formulation of the test statistic as

$$\chi^2_{test} = (m-1) \times VMR \quad (4)$$

The test statistic follows a chi-square distribution with  $m-1$  degrees of freedom and we worked with a significance level  $\alpha = 0.05$ . Since we are dealing with a two-tailed test we must compare the test statistic with the lower critical value ( $\chi^2_{crit (lower)} = \chi^2_{(1-\alpha/2, m-1)} = \chi^2_{(0.975, m-1)}$ ) and the upper critical value ( $\chi^2_{crit (upper)} = \chi^2_{(\alpha/2, m-1)} = \chi^2_{(0.025, m-1)}$ ). If the test statistic lays between the lower and upper critical values we do not reject the null hypothesis of a random distribution of points.

#### d. G function

The G function, also called the nearest-neighbour distance cumulative distribution function is, for a distance  $d$ , the probability that a point separates from its nearest-neighbour a distance of at most  $d$  (Merchán-Pérez et al., 2014). The nearest neighbour cumulative distribution,  $G(d)$ , at a distance  $d$  is defined as

$$G(d) = P(\text{distance from a point to the nearest point of process} \leq d) \quad (5)$$

where  $P()$  indicates probability. In a practical manner, this function goes to a point, looks for the closer point (its nearest neighbour), calculates the distance between that pair of points and repeats the process for all points of the distribution. Then, the ratio between the number of points that are separated from their nearest neighbours by a distance equal or less than  $d$  and the total number of points of the distribution is plotted in function of distance  $d$ .

The slope of  $G(d)$  provides information about the observed spatial point pattern in comparison to the expected G function for a random spatial point pattern resulting from a stationary Poisson point process. The G function for such process,  $G_{\text{Poisson}}(d)$ , is given by the expression

$$G_{\text{Poisson}}(d) = 1 - e^{-\lambda \pi d^2} \quad (6)$$

where  $\lambda$  is the process intensity and  $d$  is the distance. If the curve of  $G(d)$  is above the curve of  $G_{\text{Poisson}}(d)$ , there are lots of nearest neighbour pair points at short distances and we have evidence of clustering. If  $G(d)$  only starts growing at higher distances and is below  $G_{\text{Poisson}}(d)$ , it shows a tendency for dispersion in the data. These functions were created in R software with the command *Gest*. Having these two functions, we can calculate the nearest neighbour index ( $R$ ) which is the ratio between the observed mean distance between nearest neighbours ( $R_O$ ) and the expected mean value for the same distance ( $R_E$ ) according to a homogeneous Poisson distribution as follows

$$R = \frac{R_O}{R_E} \quad (7)$$

The observed mean distance between nearest neighbours ( $R_O$ ) is calculated as in

$$R_O = \frac{\sum_{i=1}^n d_{\min}(x_i)}{n} \quad (8)$$

where  $d_{\min}(x_i)$  is the distance between the pair of nearest neighbours  $x_i$  and  $n$  is the number of points in the distribution (Smith, 2016). The expected mean distance between nearest neighbours from a stationary Poisson process of intensity  $\lambda$  is given by

$$R_E = \frac{1}{2\sqrt{\lambda}} \quad (9)$$

Just as VMR,  $R$  value gives an idea of the pattern of the distribution. The ratio  $R_O$  and  $R_E$  can be equal, less than or greater than 1. If we have a completely random pattern,  $R_O$  is equal to  $R_E$  and  $R$  will be equal to 1. If we have clustering,  $R_O$  should be smaller than  $R_E$  and  $R$  less than 1. In the limit, the maximum degree of clustering would correspond to all the points being located at the same place. If this happened,  $R_O$  would be equal to 0 such as  $R$ . Thus, the closer  $R$  is from 0, the greater the tendency for clustering, because it indicates that there are several points very close to each other. At last, if  $R$  is higher than 1, it indicates tendency for dispersion.

Just as in the previous analysis we compared the observed spatial distribution of our data with the theoretical distribution according to CSR. This comparison was done in two different ways: by

means of a statistical test and by random simulations of G function with construction of confidence envelopes.

A Z-test is a two-tailed statistical test that compares the mean of a set of measurements to a given constant. Since we want to compare the mean of the distances between nearest neighbours ( $R_O$ ) to the expected mean distance ( $R_E$ ) according to a Poisson process which is a constant, we applied a Z-test to our data. Our test hypotheses are defined as  $H_0: R_O - R_E = 0$  vs  $H_1: R_O - R_E \neq 0$ . We can use  $R_O - R_E$  as a test statistic, but since the probabilities for any normal distribution are hard to calculate, we used a standardized test statistic ( $Z_{test}$ ) described as

$$Z_{test} = \frac{R_O - R_E}{V[R_E]} \quad (10)$$

where  $V[R_E]$  is the variance of  $R_E$  (Smith, 2016). The variance of the mean distance between nearest neighbours can be calculated as

$$V[R_E] = \frac{4 - \pi}{4\pi\lambda n} \quad (11)$$

where  $\lambda$  is the intensity of the process and  $n$  is the number of points from the distribution (Smith, 2016). The standardized test statistic has standard normal distribution with a mean of 0 and a standard deviation of 1 and we worked with a significance level  $\alpha = 0.05$ . Since the null hypothesis is equality, we are dealing with a two-tailed test and we must compare the test statistic with the lower critical value ( $Z_{crit(lower)}$ ) and the upper critical value ( $Z_{crit(upper)}$ ). If the  $Z_{test}$  lays between  $Z_{crit(lower)}$  and  $Z_{crit(upper)}$ , we do not reject the null hypothesis of a random distribution of points.

Other form to evaluate if  $G(d)$  is statistically different from  $G_{Poisson}(d)$  is by simulating a certain number of random spatial point patterns and calculating the respective empirical G functions for each of those patterns and then plotting the maximum and minimum values of the empirical G functions. The higher the number of simulations, the higher the confidence we have in the results. In this study we simulated 999 random distributions of points and their empirical G functions and plotted the confidence envelopes for them. Those permutations were computed in R using the command:

*envelope(synapses\_pattern, fun = Gest, nsim = 999).*

### ***e. Ripley's K function***

The Ripley's K function estimates the mean number of points within a sphere of increasing radius centred on each sample point (Ripley and Kelly, 1977). Ripley's K function,  $K(d)$ , can be defined as follows

$$K(d) = \frac{E((\text{Number of points within } d \text{ of point}) - 1)}{\lambda} \quad (12)$$

where  $E()$  is the expected value,  $d$  is the search radius distance and  $\lambda$  is the density of points in the study area (Dixon, 2002). To simply explain how this function works, for a certain event  $x_i$  it is defined a circle of radius  $d$  centred in the event  $x_i$  itself and then it is counted the number of events that occur inside that circle. This is repeated for all events. Then, it is calculated the mean number of points counted in all circles of radius  $d$  and that value is divided by the density of events in the study area. All this process is repeated for several  $d$ , allowing to construct  $K(d)$ . As always, we must compare the observed  $K(d)$  with the expected K function according to CSR,  $K_{Poisson}(d)$ , which is given by

$$K_{Poisson}(d) = \pi d^2. \quad (13)$$



If  $K(d)$  is above  $K_{\text{Poisson}}(d)$ , there is evidence of clustering. If  $K(d)$  is lower  $K_{\text{Poisson}}(d)$ , there is tendency for dispersion. These functions were created in R software with the command *Kest*.

Some great advantages of Ripley's K function in comparison to G function are the accounting of the distance between a point to all points, instead of only the nearest neighbour distance, and possibility of analysis at several scales, since it considers several increasing search radiuses. This implies that we can see if the pattern changes with scale of analysis. A spatial pattern can be clustered at small scales and dispersed at larger scales or vice-versa (**Figure 9**). If the first case happens, we can get an idea about the average size of the clusters by looking at the distance where  $K(d)$  intersects  $K_{\text{Poisson}}(d)$ .

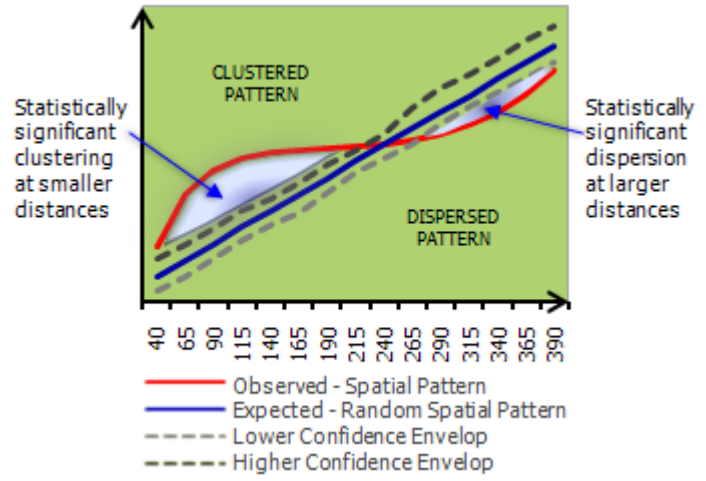


**Figure 9 - Schematic representation of Ripley's K function results.** From Boots, B. and A. Getis. "Point Pattern Analysis". Sage University Paper Series on Quantitative Applications in the Social Sciences, series no. 07-001. Sage Publications. 1988.

In previous analyses it was possible to determine a statistical test with an associated known probability distribution. This is not the case for K function and that is the reason why we statistically compared  $K(d)$  with  $K_{\text{Poisson}}(d)$  by performing random simulations and constructing confidence envelopes in the same way we explained for G function. We ran 999 random permutations in R using the command

*envelope(synapses\_pattern, fun = Kest, nsim = 999).*

K-Ripley's function is often transformed into a linear function called L function,  $L(d)$ . Since  $K_{\text{Poisson}}(d)$  is transformed into a straight line,  $L_{\text{Poisson}}(d) = d$ , the plots are much easier to visualize. For this reason, we also plotted this function. The linearization of  $K(d)$  into  $L(d)$  is given by

$$L(d) = \sqrt{\frac{K(d)}{\pi}} \quad (14)$$

For the L function, a regular pattern curve will be below the diagonal and a clustered pattern will be plotted above (Sánchez et al., 2014). The command *Lest* generates the  $L(d)$  for a spatial point pattern.



# **Chapter 3**

## **Results**

## Results

### Both myofibers and mononucleated cells contribute to the production of *Lama2*, *Lama4* and *Lama5* mRNA

Our group has recently shown that laminin 211 seems to play a critical role in muscle growth during late fetal stages, more specifically between E17.5 and E18.5 (Nunes et al., 2017). In *dy<sup>W/-</sup>* muscle, growth is impaired at those stages, in spite of the presence of laminins 411 and 511, and correlates with a failure to fully expand the Pax7-positive cell population (Nunes et al., 2017). These results indicated a specific role for laminin 211 in fetal muscle growth.

To gain further insight into the dynamics of laminin deposition during fetal development, we first sought to determine which cell types in the fetal muscle masses express *Lama2*, *Lama4* and *Lama5* genes. We chose two stages, E15.5 and E17.5, corresponding to the fetal stage preceding and following, respectively, the migration of Pax7-positive cells to their niche between the muscle fiber and its basement membrane (Ontell and Kozeka, 1984; Kassar-Duchossoy et al., 2004), as these stages are likely to catch key moments of laminin assembly with relevance for the Pax7-positive cells. For this purpose, we performed *in situ* hybridization for *Lama2*, *Lama4* and *Lama5* on transverse cryostat sections of E15.5 and E17.5 fetuses.

At E15.5, both mononucleated cells (yellow arrows) and muscle fibers (red arrows) seem to transcribe all three genes, but *Lama2* and *Lama5* gene expression appears higher in the mononucleated cells (insert in **Figure 10A** and **C**). *Lama2* and *Lama5* have practically undistinguishable expression patterns (**Figure 10A** and **C**), but *Lama4* expression, appears to be proportionately more strongly expressed in the myofibers than in the mononucleated cells (**Figure 10B**). Regardless, *Lama4* mRNA is also produced by the mononucleated cells, but with less intensity.

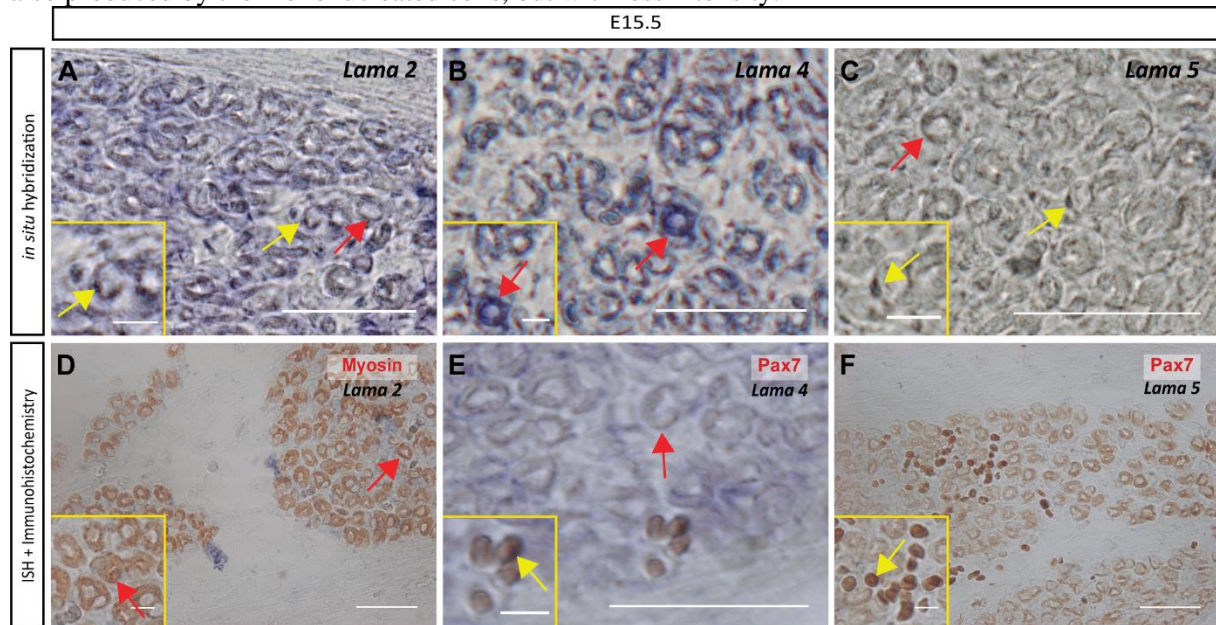


**Figure 10 - Both myofibers and mononucleated cells express *Lama2*, *Lama4* and *Lama5* genes at E15.5, but expression in mononucleated cells appears stronger.** *In situ* hybridization for *Lama2* (A), *Lama4* (B), *Lama5* (C) on transverse sections of E15.5 fetuses at forelimb level showing the epaxial muscle. *Lama2* and *Lama5* genes appear to be more strongly expressed by the mononucleated cells (A and C, yellow arrows). In contrast, the *Lama4* gene appears more strongly expressed in the myofibers (B, red arrows), than in mononucleated cells. However, both cell types appear to contribute to the expression of all three genes (A, B, C, yellow and red arrows). Immunohistochemistry assay with peroxidase, over the *in situ* hybridization staining, reveals the co-localization of MHC and *Lama2* mRNA (D) displaying evidence that the myofibers are involved in the expression of the *Lama2* gene. The same assay shows that Pax7-positive cells lie in the interstitial space at this stage (E and F). Staining for Pax7 is strong so it is difficult to determine whether the cells co-express mRNA for *Lama* genes. Scale bars: 50  $\mu$ m in A, C, D-F; 25  $\mu$ m in B; 10  $\mu$ m in inserts (A-F).



We then stained the sections hybridized with laminin gene probes with anti-myosin heavy chain (MHC) and anti-Pax7 antibodies in order to identify myofibers and muscle stem cells, respectively. We applied a secondary antibody with peroxidase activity and used a precipitating substrate for the localization of these proteins on top of the *in situ* hybridization results. This assay aims to compare the mRNA and the protein location, to verify whether a certain mRNA and MHC or Pax7 are localized in the same cells.

Immunohistochemistry revealed that MHC protein expression coincides with the *in situ* hybridization staining for *Lama2* gene (**Figure 10D**). Immunohistochemistry for Pax7 at E15.5 showed the presence of muscle stem cells in the muscle interstitial space (**Figure 10E and F**), which is in agreement with previous studies (Ontell and Kozeka, 1984; Kassam-Duchossoy et al., 2004). Expression of *Lama* genes appears to be detected in at least some Pax7-positive cells, but they may also be expressed in other mononucleated cells (**Figure 10E and F**, *Lama2* data not shown).

At E17.5, we can observe that the expression pattern for all three *Lama* genes has not changed significantly as development proceeds. *Lama2* expression is maintained in mononucleated cells (**Figure 11 A-A''**), but the expression levels in myofibers increases (**Figure 11A'**, red arrows). *Lama4* and *Lama5* expression becomes more equally expressed by both cell types. Both mononucleated cells and myofibers stain positively for these two genes. Strikingly, we also find that some interstitial muscle cells express *Lama2*, *Lama4* and *Lama5* (compare **Figure 10E-F** with Fig. 11B, B' and C and C'). This pattern is highly similar to the distribution pattern of Pax7-positive cells at E15.5, suggesting that these cells may play a role in laminin gene expression as well.

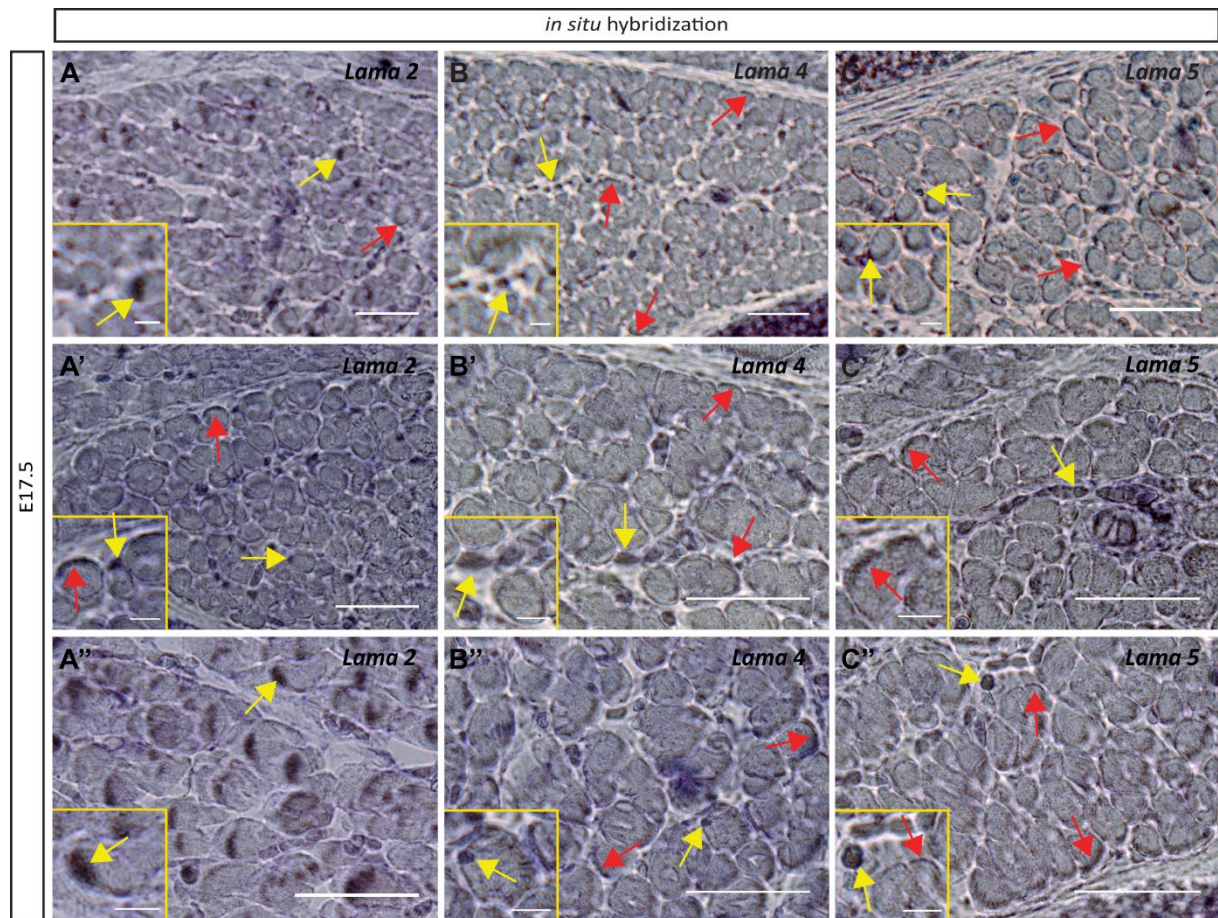


**Figure 11 - Both myofibers and mononucleated cells still express *Lama2*, *Lama4* and *Lama5* genes at E17.5.** *In situ* hybridization for *Lama2* (A, A', A''), *Lama4* (B, B', B'') and *Lama5* (C, C', C'') on transverse sections of E17.5 fetuses at forelimb level showing epaxial muscles. (Continues next page)

(Continued from previous page) *Lama2* expression continues to be strongest in mononucleated cells (A, A' and A'', yellow arrows) but positive staining can also be seen in myofibers (A and A' [insert], red arrows). *Lama4* (B-B'') and *Lama5* (C-C'') gene expression signal now seems more similar in intensity in mononucleated cells and myofibers than at E15.5 (yellow and red arrows). Scale bars: 50  $\mu$ m (A – C''), 10  $\mu$ m in all inserts.

---

Together, our data indicate that there are three distinct cell types expressing *Lama* genes: the Pax7-positive mononucleated cells, the Pax7-negative mononucleated cells and the myofibers. Both mononucleated cells and myofibers play a role in the synthesis of *Lama2*, *Lama4* and *Lama5* genes. Interestingly our results indicate that mononucleated cells may be the main source of laminin gene expression in muscle during the stages studied (E15.5 and E17.5). However, our results demonstrate that the myofibers synthesize laminin as well.

### A stage-dependent role for mononucleated cells in the synthesis of laminin

Given that both Pax7-positive cells and myofibers express *Lama* genes, and knowing that the basement membrane is assembled around the fibers, it would be interesting to understand if the Pax7-positive cells produce laminins (and if so which ones) in the absence of communication with the myofibers. For that purpose, we used E14.5 and E17.5 *Myf5<sup>Cre</sup>*-NICD fetuses, which have Pax7-positive muscle stem cells, but produce very few and small muscle fibers (Mourikis et al., 2012). In these fetuses the transcription of notch intracellular domain (NICD) is under the control of the *Myf5* promoter (Mourikis et al., 2012). The overexpression of NICD results in its translocation to the nucleus where it will block myogenic differentiation (Mourikis et al., 2012). Since most muscle stem cells express or have expressed *Myf5* at some point of their lives (Kuang et al., 2007), the constitutive overexpression of NICD under the control of the *Myf5* promoter will block differentiation in the great majority of muscle stem cells and prevent myotube formation (Mourikis et al., 2012). Therefore, these conditional transgenic fetuses make it possible to assess what laminin isoforms are produced by muscle stem cells in the absence of myotubes, and whether they are being assembled.

Immunostaining for distinct laminin chains revealed that, at E14.5,  $\alpha 2$ ,  $\alpha 4$ ,  $\alpha 5$ ,  $\beta 1$ ,  $\beta 2$  and  $\gamma 1$  chains are produced in the presumptive epaxial “muscle” areas, i.e. the areas which did not form myofibers, but contain Pax7-positive muscle stem cells (**Figure 12**). Double staining for  $\alpha 2$  and  $\alpha 5$  (**Figure 12B** and B'', orange arrows), as well as, for  $\alpha 2$  with  $\alpha 4$  (**Figure 12F-F''**, orange arrows), shows that these chains co-localize around the same cells, although not all  $\alpha 2$ -positive cells have the  $\alpha 4$  chain (**Figure 12F**). Laminin  $\beta 1$  and  $\gamma 1$  are present on most cells at this stage (**Figure 12G'** and H) and the laminin  $\beta 2$  chain co-localizes with  $\beta 1$  in some of the cells (**Figure 12G-G''**, orange arrows). Thus most cells in E14.5 *Myf5<sup>Cre</sup>*-NICD muscle areas have laminins 211 and 511 around them, while some also have 411. The presence of the  $\beta 2$  chain raises the possibility that laminins 221, 521 and/or 421 are also found around a subset of cells.

Interestingly, double staining for Pax7 and  $\alpha 5$  laminin chain at E14.5 (**Figure 12D**), shows that the Pax7-positive cells with high immunofluorescence intensity for Pax7 (**Figure 12D'** and D'', orange arrows) do not have laminin  $\alpha 5$  around them. However, Pax7-positive cells with lower immunofluorescence intensity for Pax7 (**Figure 12D'** and D'', red arrows), have laminin  $\alpha 5$  assembled around them. Since all laminin  $\alpha 5$ -positive cells also have laminin  $\alpha 2$ , and some of those also have laminin  $\alpha 4$ , we can tentatively conclude that Pax7-positive cells with low immunofluorescence intensity for Pax7 are likely to also have at least  $\alpha 2$ - and  $\alpha 5$ -containing laminins around them. Our results thus raise the possibility that the described heterogeneity within the population of muscle stem cells (Kuang et al., 2007; Rocheteau et al., 2012) also involves a heterogeneity in the capacity to produce and assemble laminins.



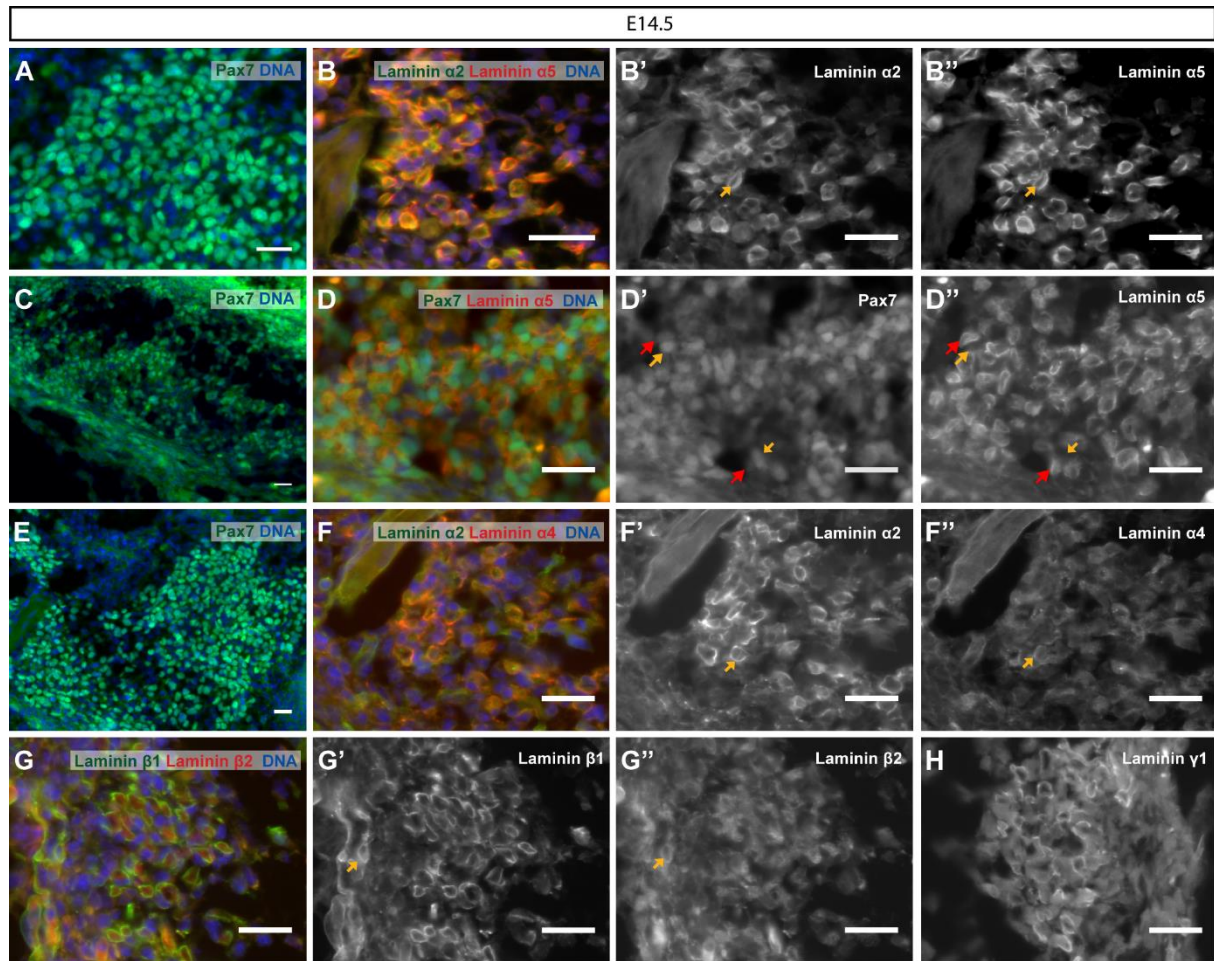


**Figure 12 - Characterization of laminin assembly in the presumptive epaxial muscle area in the absence of myofibers at E14.5.** Transverse sections of E14.5 *Myf5<sup>Cre</sup>*-NICD fetuses processed for immunofluorescence, at forelimb level showing the presumptive epaxial muscles. Immunostaining for Pax7 (A, C, D, E; green), laminin α2 (B and F, green; B' and F', grayscale), laminin α5 (B and D, red; B'' and D'', grayscale), laminin α4 (F, red; F'', grayscale), laminin β1 (G, green; G', grayscale), laminin β2 (G, red; G'', grayscale), laminin γ1 (H, grayscale), and DNA (A, B, C, D, E, F, G, blue). A, C and E reveals that the Pax7-positive cell population is widespread in the presumptive epaxial muscle masses. A and B, E and F, are pairs of adjacent sections immunostained to analyze Pax7-positive cells in relation to staining for laminin α2, α5 and α4 chains. Double labeling for laminin α2 and α5 shows that these two chains are co-localized in most of the cells (B, B' and B'', orange arrows). Laminin α2 and α4 are also co-localization around some, but not all, cells. Double labeling for Pax7 (green) and laminin α5 (red) (D, D', D'') shows that the Pax7-positive cells do not all have laminin around them (D' and D''; orange arrows). It appears that cells with high levels of immunofluorescence for Pax7 do not have laminin α5 around them (D' and D''; orange arrow), while Pax7 cells with low immunofluorescence assemble that α chain (D' and D'', red arrow). Laminin β1 appears to be the predominant β chain at E14.5 (G and G'), with almost no β2 present (G and G''), but where it appears, it co-localizes with β1 (G', G'', orange arrow). Laminin γ1 is ubiquitously expressed around cells at E14.5 (H). Scale bars: 25 μm.

At E17.5, our results show a dramatic decrease in assembled laminins within the *Myf5<sup>Cre</sup>*-NICD muscle masses. More specifically, positive immunostaining is only obtained for α5-, β1- and γ1-laminin chains (Figure 13D'', F' and H', orange arrows). All other chains revealed diminished presence compared to E14.5. This result suggests that at E17.5, laminin 511 is the only laminin produced and assembled by Pax7-positive cells. Double staining for laminin (polyclonal antibody; for more detail see Material and Methods) and Pax7 (Figure 13B-B'') reveal a pattern resembling the one described for E14.5, in which Pax7-positive cells with lower immunofluorescence levels for Pax7 are the only ones that display assembled laminin in their basement membrane (Figure 13B-B''; red arrows). In contrast, the Pax7 cells with high immunofluorescence intensity for Pax7 do not have any laminin around them (Figure 13B-B''; orange arrows).

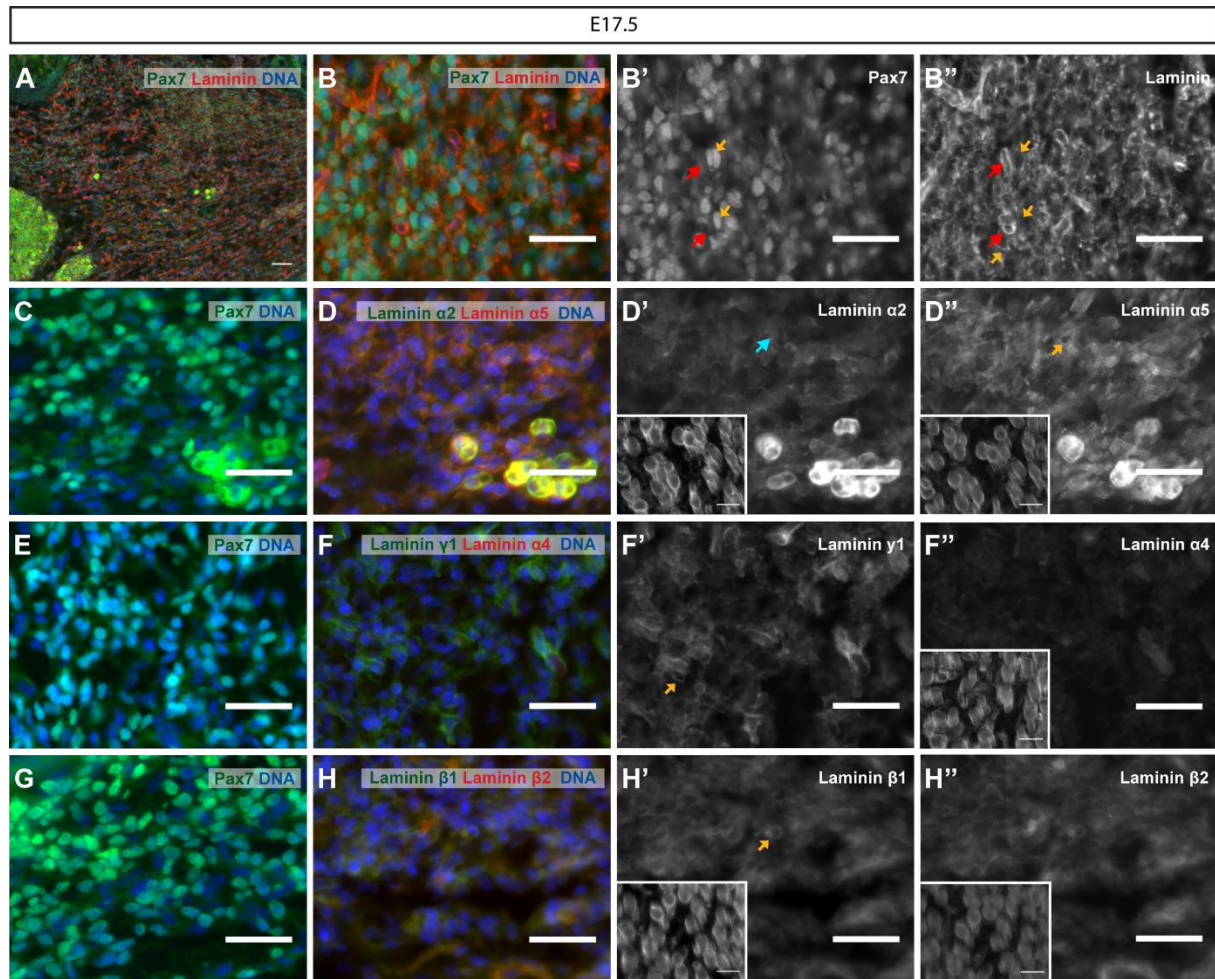


**Figure 13 - Laminin assembly in the presumptive epaxial muscle area decreases as development proceeds.** Transverse sections at forelimb level shows the laminin matrix in the presumptive epaxial muscle masses of E17.5 *Myf5<sup>Cre</sup>*-NICD fetuses. Immunostaining for polyclonal laminin (A and B, red; B'', grayscale), Pax7 (A, B, C, E and G, green; B', grayscale), laminin α2 (D, green; D', grayscale), laminin α5 (D, red; D'' grayscale), laminin α4 (F, red; F'', grayscale), laminin β1 (H, green; H', grayscale), laminin β2 (H, red; H'', grayscale), laminin γ1 (H, green; H', grayscale), and staining for DNA (A, B, C, D, E, F, G and H, blue). Double labeling of polyclonal laminin and Pax7 (A-B') reveals concordant results regarding the immunostaining at E14.5. In B the Pax7-positive cells with higher levels of immunofluorescence intensity do not have assembled laminin around them, whereas the cells with lower immunofluorescence intensity Pax7 expression appear to have laminin around them. B' orange arrow points to a Pax7-high cell, and B'' red arrow points to laminin around cells with low Pax7. C and D, E and F, G and H are pairs of adjacent sections to analyze the expression of Pax7 in relation to laminin α (C-D), β (G-H), and γ (E-F) chains. Laminins α2 (D), α4 (F) and β2 (H') expression decreases between E14.5 and E17.5 in *Myf5<sup>Cre</sup>*-NICD fetuses, in the absence of myofibers. Laminin β1 (H') staining also decreases, but is present, even if faint. Laminins α5 (D and D''), and γ1 (F and F'') chains appear in a similar pattern in E17.5 *Myf5<sup>Cre</sup>*-NICD fetuses compared to E14.5, suggesting that laminin 511 is the only isoform that is maintained in the muscle areas in the absence of myofibers. D', D'', F'', H' and H'' inserts represent the positive controls for the immunostaining of each chain. Scale bars: 25 μm in A-G; 10 μm in inserts.

Together, these data indicate that Pax7-positive cells with low immunofluorescence intensity for Pax7 produce laminins 211 and 511 (and some also laminin 411 and β2-containing laminins) at early stages of fetal myogenesis, but later on, at E17.5, these cells only produce laminin 511. Thus their laminin-producing capacity diminishes from early to late fetal myogenesis.

### Number of synapses increases in neuromuscular junctions lacking laminin 211 and 221

Interestingly, some studies have shown that the presence of nerves (Hurren et al., 2015) and innervation per se (Ross et al., 1987; Duxson et al., 1989; Cachaço et al., 2003) influences the population of mononucleated myogenic cells within the muscle masses. Proper contact between the muscle fiber and the motor nerve is an essential step to a correct organization of the muscle endplate (Patton et al.,



1997; Patton, 2000). There is strong evidence to suggest, that although the AChR have a prepatterned distribution, this initial organization is later remodelled by contact with the nerve (Witzemann, 2006). Laminins have been shown to be crucial in the differentiation of the pre- and postsynaptic structure (Nishimune et al., 2008). Nevertheless, it is currently unknown if the absence of  $\alpha 2$ -laminin has consequences at the level of the development of neuromuscular junctions.

Nunes et al. (2017) demonstrated that  $\alpha 2$ -laminin chain deficiency in  $dy^{W/-}$  fetal muscles leads to an impaired expansion of the pool of Pax7-positive cells, when compared to same stage wildtype fetal muscles. Given the described role of nerves and innervation in regulating the population of mononucleated cells (Ross et al., 1987; Duxson 1989; Hurren et al., 2015), it is conceivable that the impaired expansion of Pax7-positive cells could be due to defects in innervation. Thus, we sought to determine whether innervation proceeds normally in  $dy^{W/-}$  fetuses and, if not, in what way innervation is perturbed in these animals.

In this context, we are interested in understanding if the potential disruption in the basement membrane, either of the muscle or of the pre-synaptic area, caused by  $\alpha 2$ -laminin chain deficiency would result in a defective phenotype at the nerve level. To this end we investigated if the number of synapses and their organization in the muscle, i.e., if the AChR clustering occurs is perturbed or not.

Immunostaining for  $\alpha$ -bungarotoxin, synaptophysin and neurofilament on consecutive longitudinal sections of *longissimus* muscles, made it possible to pinpoint all the synapses within an extensive area of these muscles. Hence, we counted all the muscle synapses in a defined area at E15.5 in both wildtype and  $dy^{W/-}$  fetuses. Our data suggest that the number of synapses may be increased in the  $dy^{W/-}$  muscles, although the difference was not statistically significant with our low n number (n=2) (**Figure 14A**).

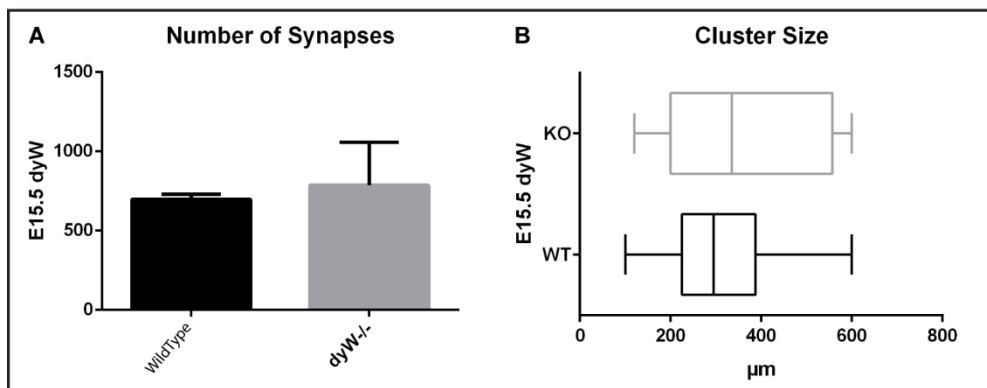


**Figure 14 – E15.5  $dy^{W/-}$  fetuses display differences concerning the synaptic number and size.** Quantification of the number of synapses in wildtype and  $dy^{W/-}$ -*longissimus* muscles reveals an increase in the  $dy^{W/-}$  (A). K-Ripley's function analysis shows a tendency for clusters with larger size (B) in the  $dy^{W/-}$  indicating a potential dispersion of the synapses throughout the muscle masses, which is suggestive of a disorganization in NMJ development.

To investigate this issue further, we asked whether the absence of the laminin  $\alpha 2$  chain results in more defects than this observed trend of an increase in synaptic number. We were interested in understanding if the synaptic plate organization was altered. For that purpose we performed a spatial distribution analysis.

We first analysed the variance-to-mean ratio (VMR) results in wildtype versus  $dy^{W/-}$  *longissimus* muscle (**See Materials and Methods for details**) and found that, like the case of the wildtype,  $dy^{W/-}$  *longissimus* muscle has a coefficient larger than 1, indicating that the synapses are invariably arranged in a clustered distribution (Table S2).

We next asked whether the degree of clustering is similar between wildtype and  $dy^{w/-}$  longissimus muscle. To answer this question, we performed a more thorough analysis by applying two distinct mathematical models to our data, namely the G-function and K-Ripley's functions. Analysing our data with the G-function, demonstrated that the R score associated with the G-function of the wildtype is closer to zero than the R score of the  $dy^{w/-}$  (n=2). Following this mathematical model, the closer the values are to zero, the greater the tendency for clustering. Based on this second result, we can hypothesize that in the  $dy^{w/-}$  there is a deviation from the initial clustered pattern, i.e., the trend towards clusters seems to be fading (Table S3). We next subjected our data to analysis with the K-Ripley's function and tested our experimental hypothesis by comparing our data distribution with a reference model for homogeneous patterning. In other words, we tested whether the synaptic organization throughout the muscle presents a clustered pattern, against the null hypothesis that argues that the spatial distribution follows a random pattern (Jafari et al., 2010). Our results showed that both wildtype and  $dy^{w/-}$  muscles present a clustered distribution of the synaptic structures (**Figure 15** and **16**). Next, we sought to understand if there are some differences in the organization of the clusters themselves using the K-Ripley's function which allow us to know the average size of the clusters. We found that there is a clear tendency for the existence of bigger clusters in  $dy^{w/-}$ , in a sense that their diameter is larger indicating a dispersion of points (**Figure 14B**). In summary, together, these results strongly suggest that the absence of  $\alpha 2$ -laminins in the neuromuscular junctions leads to a disorganization of the AChR patterning, possibly affecting the normal competitive elimination of a subset of AChRs. This defect is illustrated by a trend towards an increase in number of synapses in the  $dy^{w/-}$  muscles and a disorder in the arrangement and alignment of the synaptic structure, influencing both pre- and post-synaptic area.

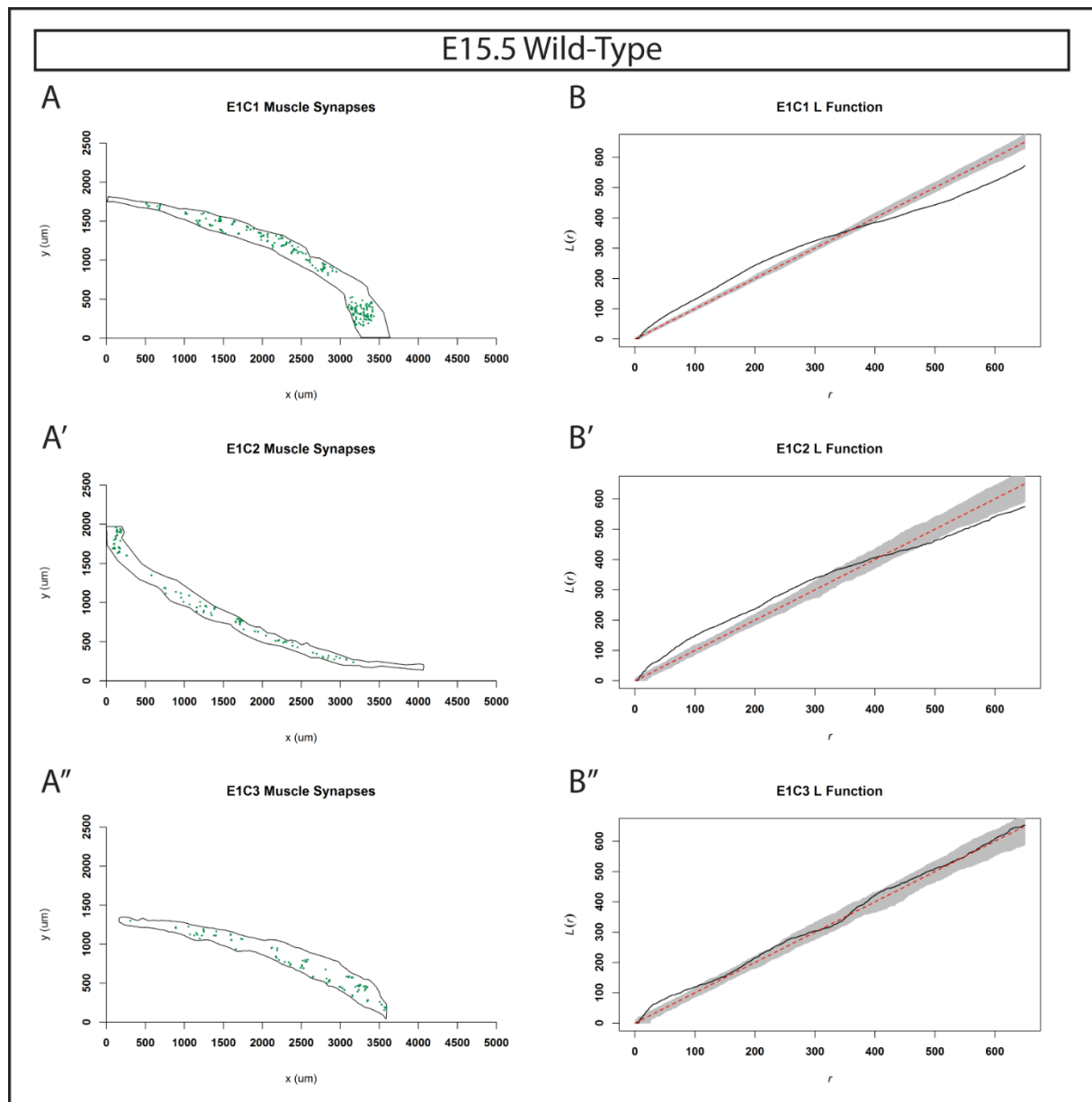


**Figure 15 - Spatial analysis of the distribution of synapses in wildtype E15.5 longissimus muscle.** The distribution and clustering of synapses in wildtype longissimus muscle was analyzed by assigning geographic coordinates to the points marked by the immunofluorescence assay (**A-A''**). Synaptic structures were marked by staining simultaneously with  $\alpha$ -bungarotoxin that marks the AChRs, and with antibodies against neurofilament and synaptophysin (green points). Column (**B – B''**) is a graphical representation of the L-Function, which is a K-Ripley's function transformation. The functions obtained from the experimentally observed data (**L obs**, dark line) are compared with a homogenous and theoretical Poisson process (**L theo**, red dash line). The shaded area represents the envelopes of values calculated from a set of 999 simulations. The experimental line (dark) above the theoretical dashed line (red) reveals the propensity for clustering with a set of points at small distances. The interception point, where the experimental line crosses over the theoretical one, shows a value representing the approximate average cluster size. Six consecutive muscle sections were analysed to ensure maximum standardization. Graphs are only representative of three muscle sections (remaining muscle sections not shown).

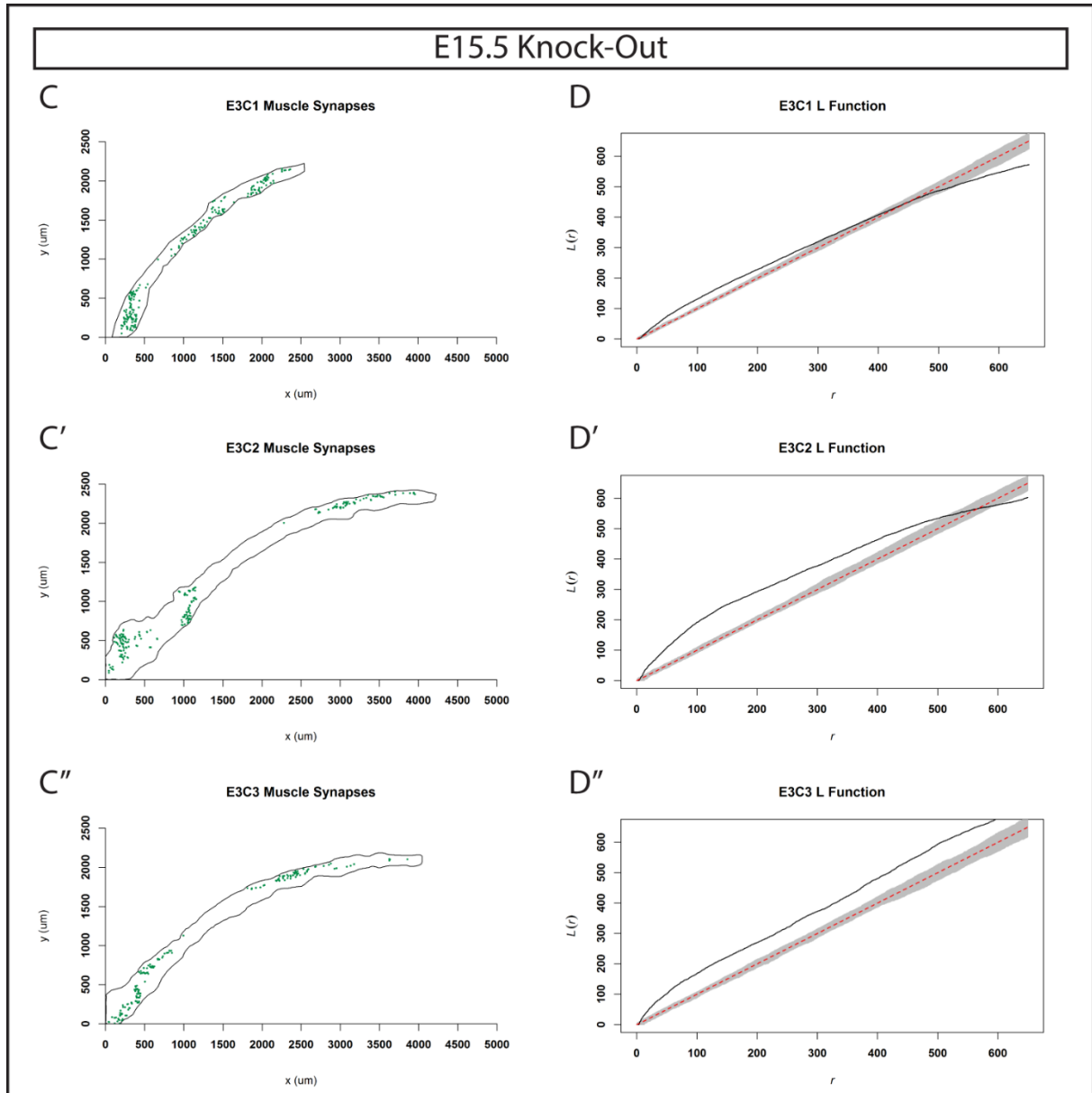


**Figure 16 – Spatial analysis of the distribution of synapses in  $dy^{W/-}$  E15.5 longissimus muscle.** The distribution and clustering of synapses in  $dy^{W/-}$  longissimus muscle was analyzed by assigning geographic coordinates to the points marked by the immunofluorescence assay (A-A’’’). Synaptic structures were marked by staining simultaneously with  $\alpha$ -bungarotoxin that marks the AChR, and with antibodies against neurofilament and synaptophysin (green points). Column (B – B’’’) is a graphical representation of the L-Function, which is a K-Ripley’s function transformation. The functions obtained from the experimentally observed data (**L obs**, dark line) are compared with a homogenous and theoretical Poisson process (**L theo**, red dash line). The shaded area represents the envelopes of values calculated from a set of 999 simulations. The experimental line (dark) above the theoretical dashed line (red) reveals the propensity for clustering with a set of points at small distances. The interception point, where the experimental line crossover the theoretical one, shows a value representing the approximate average cluster size. Six consecutive muscle sections were analysed to ensure maximum standardization. Graphs are only representative of three muscle sections (remaining muscle sections not shown).

### The absence of $\alpha 2$ laminin does not interfere with the distribution of $\alpha 4$ and $\alpha 5$ laminin in the synapse

Lastly, we were interested in finding out whether the absence of laminin  $\alpha 2$ -chain at the level of the neuromuscular junctions has any detrimental effect on the assembly of  $\alpha 4$ - and  $\alpha 5$ -containing laminins in the synaptic basement membranes. To address this issue, we used 3D reconstructions of the

synaptic complex to study its morphology and to assess the distribution pattern of laminins in the wildtype and  $dy^{W/-}$  synapses at E15.5.

At E15.5, the 3D reconstruction results present no significant differences regarding the morphology and laminin interaction with the synaptic structure between the wildtype and  $dy^{W/-}$  fetuses, with exception for the  $\alpha 2$  laminin which, as expected, it is not present in the  $dy^{W/-}$  fetuses. Through this preliminary observation it is possible to assess that in the wildtype, both  $\alpha 2$  and  $\alpha 4$  laminins display similar interactions with the synaptic structure. In contrast  $\alpha 4$ -laminin and  $\alpha 5$ -laminin seem to differ in terms of how they interact with the synaptic structure.  $\alpha 2$ - and  $\alpha 4$ -laminins do not appear to touch the synaptic structure (**Figure 17A** and **B**, yellow and red arrows). In contrast,  $\alpha 5$ -laminins display a distribution which appears more “intermingled” with the synaptic structure (**Figure 17C** and **F**, blue arrows), indicating a closer interaction.

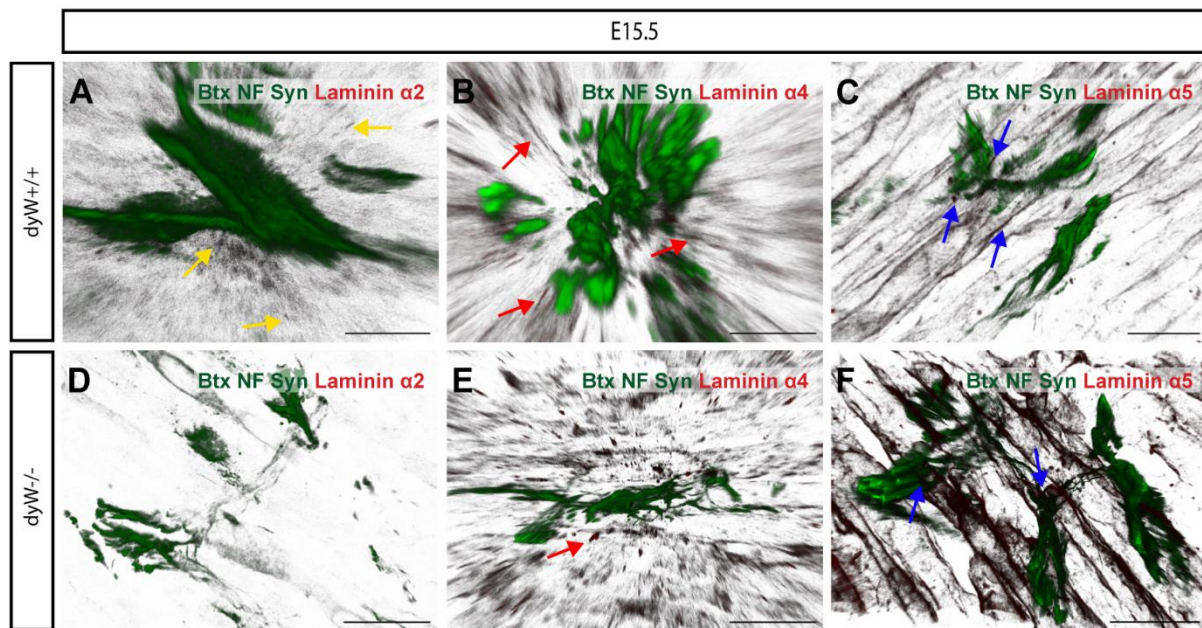


**Figure 17 - Laminin distribution in the NMJ at E15.5.** Immunostaining of E15.5 wildtype and  $dy^{W/-}$  muscle masses with a cocktail of  $\alpha$ -bungarotoxin, anti-neurofilament and anti-synaptophysin (all green) which together stain the full synaptic structure including the pre- and post-synaptic area (**A-F**, green) and laminin  $\alpha 2$  (**A** and **D**, red),  $\alpha 4$  (**B** and **E**, red) or  $\alpha 5$  (**C** and **F**, red). 3D reconstructions of 63x zoomed in synaptic structures, performed using the Amira software, reveal no obvious morphological differences regarding the pattern of laminin  $\alpha 4$  and  $\alpha 5$  in the synaptic structures, when comparing the wild-type and fetuses lacking laminin- $\alpha 2$ . In the wildtype, laminin  $\alpha 4$  (**B**) appears to have a similar interaction with the synaptic structure as laminin- $\alpha 2$  (**A**), with almost no physical contact between the two at E15.5 and laminin  $\alpha 4$  has the same distribution pattern in the  $dy^{W/-}$  (**A**, yellow arrow; **B** and **E**, red arrows). In comparison, laminin  $\alpha 5$  matrix distribution appears more intermingled with the motor neuron area in both wildtype (**C**) and  $dy^{W/-}$  (**F**) muscle (blue arrows). Scale bars: 50  $\mu$ m.

To summarize, confocal 3D reconstruction results reveal that among the three laminin  $\alpha$ -chains, both  $\alpha 2$  and  $\alpha 4$  present similar distribution patterns around the synaptic structure with apparently little or no contact. In contrast, at E15.5,  $\alpha 5$ -laminins seem to be in close contact with the synapse (**Figure 18**), raising the possibility that this isoform (521) might be the first to be assembled in the NMJ. In addition, our results show that  $dy^{W/-}$  fetuses appear to display a normal distribution pattern of  $\alpha 4$ - and  $\alpha 5$ -laminins in their synapses (**Figure 17E** and **F**) when compared to wildtype (**Figure 17B** and **C**). Thus, the defects in synapse formation found in  $dy^{W/-}$  fetuses do not appear to be due to any detectable changes in the organization of laminins 421 and 521. Rather they appear to be caused by a mechanism that specifically requires the presence of the laminin  $\alpha 2$  chain.

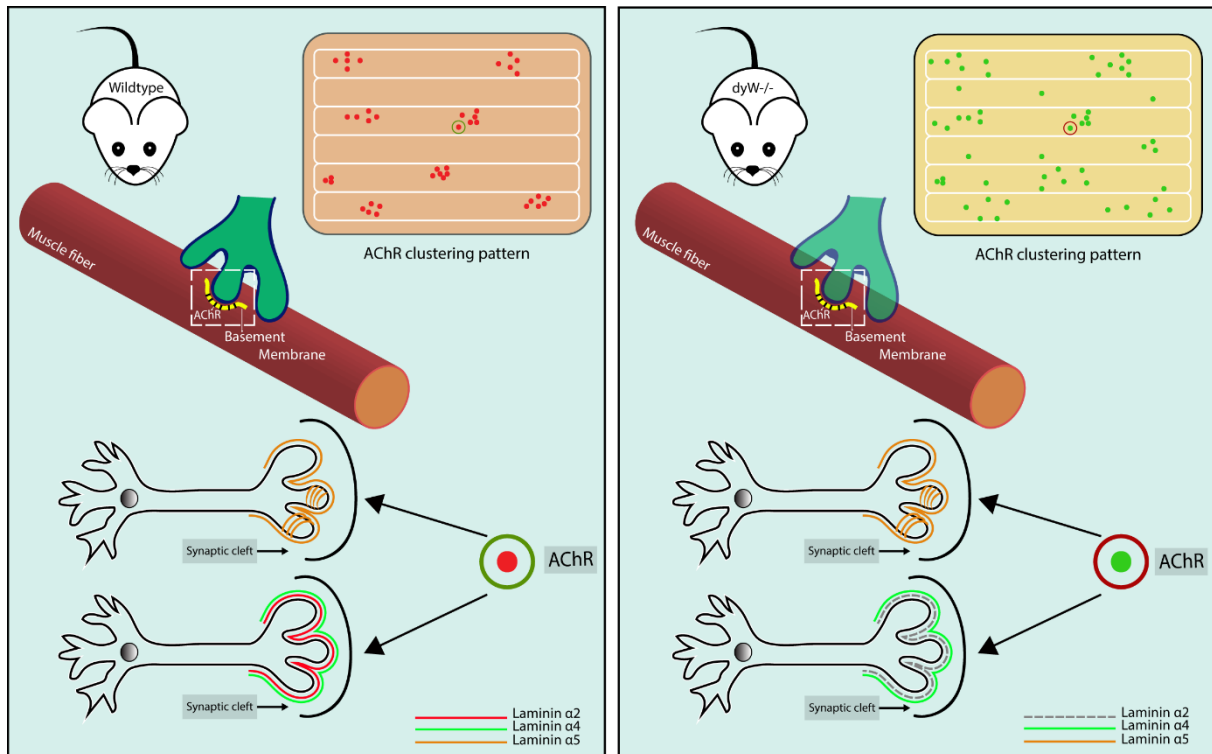


**Figure 18 – Schematic representation depicting the main alteration in neuromuscular junction development in  $\alpha 2$ -laminin-deficient muscles at E15.5.** In the absence of  $\alpha 2$ -laminins, the patterning of AChR (red and green dots, in wildtype and  $dy^{W-/-}$ , respectively) is disorganized. The number of synapses is increased in the  $dy^{W-/-}$  compared to the wildtype. Synaptic cluster size is also increased and presents a scattered distribution in the  $dy^{W-/-}$  muscles. Laminin assembly in the synaptic basal laminar does not present any obvious differences when comparing wildtype and  $dy^{W-/-}$  fetuses. Moreover, in the wildtype, both  $\alpha 2$  and  $\alpha 4$  are assembled in similar pattern around the motor neuron. It did not appear to be any physical contact between these two laminins (i.e. 221 and 421) and the synaptic structure (red and green lines). However, in both wildtype and  $dy^{W-/-}$ , laminin  $\alpha 5$  chain distribution suggests an intermingled interaction with the motor neuron (orange lines), in a pattern distinct from the other two laminins. The two motor neuron diagrams represent equivalent structures.

# **Chapter 4**

## **Discussion**

## Discussion

### Laminin assembly dynamics in fetal muscles: mononucleated cells and myofibers working together

Skeletal muscle development is a process that runs throughout the entire period of organogenesis and encompasses several phases with distinct requirements. Studies from our lab have shown that laminin-containing basement membranes play key roles during dermomyotome and myotome development (Bajanca et al., 2006), but primary myogenesis proceeds without laminins (Deries et al., 2012; Nunes et al., 2017). However, during secondary myogenesis, laminins build up around myofibers, and muscle stem cells enter their niche under this basement membrane at around E16.5 (Kassar-Duchossoy et al., 2005; Nunes et al., 2017), suggesting a role for laminins during these stages.

The stem cell niche is a dynamic microenvironment in which a number of inputs regulate stem cell behavior. These signals come from different structures like blood vessels, immune cells, myofibers and nerves (Gattazzo et al., 2014). There is growing evidence for a key role of the basement membrane in the niche of muscle stem cells (Boonen & Post, 2008; Jones & Wagner 2008; Gattazzo et al., 2014). For example, while undergoing an asymmetric cell division, one of the Pax7-positive daughter cells generated by cell division maintains its Myf5-negative status (Pax7<sup>+</sup>/Myf5<sup>-</sup>) and contacts with the basement membrane, whereas the other starts expressing Myf5 (Pax7<sup>+</sup>/Myf5<sup>+</sup>) and preferentially differentiates while facing the myofiber (Kuang et al., 2007). Moreover, it has been shown that after injury, the basement membrane of damaged fibers functions as “ghost fibers” that regulate muscle stem cell behavior (Webster et al., 2016). Additionally, the muscle stem cells stimulated by Notch signaling induce the expression of several ECM proteins that will help them regulate their behavior and reshape their microenvironment (Bröhl et al., 2012). Such remodeling occurs both during development as well as in postnatal life (Tierney et al., 2016), revealing a dynamic niche. Laminin 211, was shown to be important for myofiber survival (Vachon et al., 1996) and recently it was demonstrated that the absence of laminins 211/221 results in changes in the stem cell population because Pax7- and Myogenin-positive cell population fail to expand normally (Nunes et al., 2017), raising the question whether laminins 211/221 play a role in the niche of muscle stem cells.

Considering the influence of the niche in fetal muscle stem cell behavior, we aimed to determine the dynamics of laminin production and assembly during fetal myogenesis. Our results showed that during normal fetal muscle development, the mononucleated cells and the myofibers are both involved in building the laminin matrix. However, interestingly, their contribution to laminin matrix assembly is stage-dependent. At E15.5, myofibers express laminin genes, but mononucleated cells, including Pax7-positive cells, strongly express laminin genes and seem to be the main contributors to laminin matrix production at this stage. We demonstrate that the majority of mononucleated cells express both *Lama2* and *Lama5* genes. Strikingly, in the absence of myofibers, at E14.5, Pax7-positive cells produce both  $\alpha$ 2- and  $\alpha$ 5- laminins, and assemble both on their cell surface. These findings suggest that: (1) Pax7-positive cells appear to express and assemble a laminin matrix; and (2) Pax7-positive muscle stem cells can activate a laminin production and assembly program in a myofiber-independent manner.

At E15.5, the expression of *Lama4* appears weaker than that of *Lama2* and *Lama5* genes. Although it is not possible to draw quantitative conclusions from *in situ* hybridization, these findings are nevertheless in accordance with previous studies suggesting that blood vessels are the initial source of laminin 411 for the myofiber basement membrane (Yousif et al., 2003), and only later in myogenesis, fetal myoblasts start expressing *Lama4* (Biressi et al., 2007).

As development proceeds, at E17.5, the intensity of laminin gene expression signal in myofibers compared to mononucleated cells becomes very similar. Myofibers appear to express high levels of



laminin genes at E17.5 when compared to E15.5, while mononucleated cells maintain high expression levels. This suggests that myofibers only activate the laminin gene expression program once they reach a certain maturity. Remarkably, at E17.5, we can observe a significant number of cells away from myofibers, expressing laminin genes. Our data cannot clarify the identity of these cells, but further studies at E17.5 should determine whether these mononucleated cells are myogenic cells or another cell type.

Our hypothesis that myofibers assume a crucial role in laminin synthesis as fetal myogenesis proceeds is strengthened by our immunostaining results in *Myf5<sup>Cre</sup>*-NICD fetuses which uncovered the dynamics of laminin assembly around Pax7-positive cells in the absence of myofibers. Our results demonstrate that, in the beginning of secondary myogenesis, at E14.5, Pax7-positive cells build a laminin matrix around themselves, since the major laminin isoforms of fetal muscle, laminins 211 and 511, as well as (although to a lesser extent) laminin 411 are present in the basement membrane surrounding Pax7-positive cell. This result points to a more significant role of mononucleated muscle cells (including Pax7-positive cells) in the assembly of the laminin matrix, when compared to the myofiber, in early stages of secondary myogenesis and raises the interesting possibility that mononucleated cells produce a significant proportion of the laminin matrix surrounding the myofibers at those early stages of secondary myogenesis (see 3D reconstruction of laminin matrix in Fig. 3M; Nunes et al., 2017). However, the myofibers seem to gain a prominent role in the laminin synthesis program, during later stages (E17.5) of fetal myogenesis.

In early phases of normal fetal muscle development, Pax7-positive cells have a predominant role in the production of laminins and the same is observed in *Myf5<sup>Cre</sup>*-NICD fetuses. However, as myogenesis proceeds in *Myf5<sup>Cre</sup>*-NICD fetuses, laminin expression in Pax7-positive cells is reduced. This decrease suggests that the mechanism regulating laminin production in Pax7-positive cells is complex and stage-specific. In fact, a recent study has shown that the muscle stem cell microenvironment is actively modulated during fetal, postnatal and adult muscle development (Tierney et al., 2016). We propose two non-mutually exclusive scenarios to explain these results. In one scenario, the myofibers (which are absent in *Myf5<sup>Cre</sup>*-NICD fetuses) might normally produce the laminins that are assembled around Pax7-positive cells at E17.5. In this scenario, myofiber-derived laminins would provide important environmental cues to Pax7-positive muscle stem cells. These myofiber-derived laminins may also be important to promote laminin synthesis by the Pax7-positive cells themselves. Indeed, laminin and laminin-binding integrins are known to mutually downregulate each other's expression, through a negative feedback loop, either at the mRNA and protein level (Vachon et al., 1997; Aumailley et al., 2000; Cao et al., 2007). For example, in  $\alpha$ 2-laminin deficient mice, the loss of laminin 211 results in the reduction of  $\alpha$ 7 $\beta$ 1 integrin levels (Vachon et al., 1997). It is possible that in *Myf5<sup>Cre</sup>*-NICD fetuses, the absence of myofiber-derived laminins, and a subsequent absence of laminin-integrin signaling in Pax7-positive cells, results in decreased laminin expression in these cells. In another scenario, the absence of the myofibers in *Myf5<sup>Cre</sup>*-NICD fetuses may result in the loss of other myofiber-derived signaling factors such as paracrine factors and/or cell adhesion molecules involved in muscle stem cell-myofiber communication (Bentzinger et al., 2010). The lack of these signals might have a negative impact on the capacity of Pax7-positive muscle stem to express and assemble their own laminin matrix.

In summary, we show that mononucleated muscle cells play an active role in laminin synthesis during all stages of fetal muscle development, while the myofibers appear to start their laminin-synthesis program later during fetal muscle development. Furthermore, we show that at the later stages of fetal muscle development, Pax7-positive cells need the presence of myofibers to synthesize laminins.

## The muscle stem cell population: a diverse population with different niches

Previous studies have demonstrated that the Pax7-positive muscle stem cell population is heterogeneous. For example, while 90% of the Pax7-positive cells have at one point in their lives expressed Myf5, 10% of this population has never expressed Myf5 (Kuang et al., 2007). Furthermore, the Pax7-positive population can be divided into different subsets of cells expressing different levels of Pax7 (Rocheteau et al., 2012). Our results are in agreement with these studies, as they show that during fetal myogenesis, some cells appear to express high levels of Pax7 protein, while others express low levels of Pax7 protein. Interestingly, in addition our results indicate that the Pax7-positive population might be heterogeneous also in their capacity to produce and assemble laminins. Double-labelling for Pax7 and laminins revealed that laminins tend to be assembled around the cells with low immunofluorescence intensity for Pax7. We further demonstrate that the laminin niche surrounding these Pax7-positive cells stains positively for  $\alpha 5$ -laminins. Since we also showed that  $\alpha 2$ - and  $\alpha 5$ -laminin co-localize around the same cells (see schematic representation in **Figure 19**), it is reasonable to suggest that  $\alpha 2$ -laminin also assembles around the Pax7-positive cells with low immunofluorescence intensity for Pax7. Currently, it is not clear whether the populations described by Kuang et al. and Rocheteau et al. are the same populations. However, if the 10% of Pax7-positive cells that never expressed Myf5 is the same population that expresses high levels of Pax7, these would be the muscle stem cells that have the most “stem identity”. We propose that the Pax7-positive cells with high immunofluorescence intensity in our experiments correspond to the most “stem” population, and our results show that these do not assemble laminins. In contrast, the cells with low immunofluorescence intensity for Pax7, and thus “less stem”, display a basement membrane containing both  $\alpha 5$ - and  $\alpha 2$ -laminins (see schematic model in **Figure 20**).

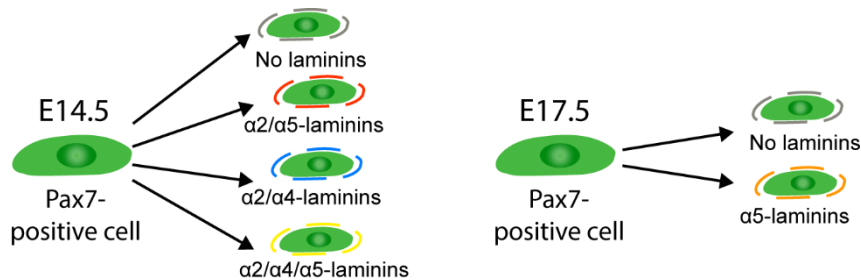


**Figure 19 – Schematic representation of Pax7-positive cells possible laminin niches at E14.5 and E17.5.** Adapted from Nunes, 2017.

Recently, Nunes et al. showed a correlation between the reduction of Pax7-positive cells and impaired fetal muscle growth in the absence of laminin 211 (Nunes et al., 2017). Our results raise the possibility that the described defect might be related to a possible role of laminin 211 in promoting the proliferation of committed cells, and restraining their precocious differentiation. If this is correct, then the Pax7-low cells in *dy<sup>W/-</sup>* muscles, would, in the absence of laminin 211, differentiate faster without significant proliferation and thus originate fewer myoblasts. This could provoke an imbalance between the proliferation and differentiation ratio that ultimately leads to reduction of Pax7-positive cells as observed previously (Nunes et al., 2017). Future studies will be necessary to address this issue further. These include the study of Pax7-positive cell population and the assessment of the differentiation status of the presumptive Pax7-high and Pax7-low populations. With this we aim to confirm if indeed this heterogeneity regarding Pax7 expression is associated with a different commitment towards differentiation and different laminin microenvironments.

## Absence of $\alpha 2$ -laminins appears to lead to alterations in acetylcholine receptor clustering

Neuromuscular junctions are formed upon nerve arrival to the muscle, when the acetylcholine receptors (AChRs) start to cluster in the area of the muscle where the NMJ will later become established (Smirnov et al., 2005).  $\alpha 4$  and  $\alpha 5$ -laminins are mainly responsible for organizing presynaptic active zones and endplate structures in the NMJs (Rogers and Nishimune, 2017).  $\alpha 4$ -laminins are particularly important for the alignment of presynaptic active zones and postsynaptic endplate structures, because in *Lama4* mutants this alignment is disrupted (Patton et al., 2001). *Lama5* null mice present delayed post-synaptic differentiation (Nishimune et al., 2008). The  $\beta 2$ -chain is specifically enriched in the basement membrane of NMJs, and the absence of this chain results in abnormal formation of pre- and post-synaptic structures, reduced number of active zones and Schwann cell infiltration in the synaptic cleft (Patton et al., 1998; Nishimune et al., 2004). Laminins 211 and 221 are known to associate into a multimeric structure, promoting the clustering of AChR and leading to the accumulation of pro-neuromuscular development factors such as agrin at the innervation points (Montanaro et al., 1998; Burkin et al., 2000; Yurchenco et al., 2004; Smirnov et al., 2005; Vilmont et al., 2016). These studies suggest that these laminins may stimulate the formation of NMJ and therefore, promote the development of denser clusters. Here we used the *dy<sup>W</sup>* model to elucidate whether  $\alpha 2$ -laminins play a role in NMJ formation and, if so, whether NMJ related defects could be a feature of MDC1A onset. Our results, although preliminary, suggest that the clustered arrangement of AChRs is diminished in the absence of  $\alpha 2$ -laminins, suggesting a role for  $\alpha 2$ -laminins in the aggregation of AChRs near the synaptic cleft. Furthermore, they show that in the *dy<sup>W/-</sup>* *longissimus* muscles, clusters with a larger size than in the wildtype tend to form. Our findings can be explained in two ways. One is that the absence of  $\alpha 2$ -laminin leads to a dispersion of synapses and thus the clusters tend to be bigger in the *dy<sup>W/-</sup>* muscles. Alternatively, *dy<sup>W/-</sup>* fetuses could have more synapses (indeed we observed such a trend), which would lead to larger clusters simply because more synapses were present. This increase in the number of synapses in the *dy<sup>W/-</sup>* fetuses could in turn be the consequence of a deficiency in synapse elimination (Purves & Lichtman, 1980). Synapse elimination is dependent on the signals that mediate synaptic competition (Sanes & Lichtman, 1999). Although there are currently no evidence for an involvement of laminin 221 in synaptic elimination, their restricted and characteristic location at the NMJ may function as a potential signal, which would be lost in *dy<sup>W/-</sup>* muscles. Further studies are necessary to cast light on this issue. Considering that motor neuron-derived agrin, “neural agrin”, promotes clustering in a laminin-dependent way (Smirnov et al., 2005; Qiao et al., 2005) and laminins induce AChR clustering in a  $\alpha 7\beta 1$  integrin-dependent process (Burkin et al., 2000), one way to address whether the disruption in cluster formation is somehow associated with the loss of  $\alpha 2$  laminins, is to analyze whether AChR and the  $\alpha 7\beta 1$  integrin co-localize. In addition, it would also be insightful to ascertain the levels of agrin in  $\alpha 2$ -laminin-deficient mice through Western blot analysis. It is known that  $\alpha 2$ -laminins regulate the threshold of agrin production (Burkin et al., 2000) priming the myofibers to respond to lower agrin concentrations (Burkin et al., 2000). Thus it would be expected that more agrin was produced when these laminins are absent. In addition, further assessment of agrin assembly through 3D imaging might provide further insights about its potential role in  $\alpha 2$ -laminin-deficient mice. Detailed studies concerning the laminin-dependent role of agrin in the neuromuscular junctions may represent a new direction in the research of possible therapies concerning MDC1A.

## Does innervation influence muscle stem cell dynamics?

Our preliminary results reveal a difference in the NMJ clustering arrangement and distribution of the AChR in  $\alpha 2$ -laminin-deficient mice. This defect in the overall organization of the synaptic endplate, if confirmed, could possibly affect the muscle innervation process and mislead axon guidance towards the synaptic cleft.

It is well known that nerves promote secondary myogenesis (Ross et al., 1987) and muscle stem cell proliferation (Ross et al., 1987; Kuschel et al., 1999). In denervated embryos, the number of mononucleated muscle cells and, in particular, the number of muscle stem cells are decreased (Ross et al., 1987; Kuschel et al., 1999). The moment in which the nerve contacts the muscle coincides with the expression of Pax7 in a subset of muscle stem cells that will give rise to secondary myoblasts and satellite cells (Hurren et al., 2015). The differentiation and survival of Pax7-positive myogenic progenitors was shown to be critically dependent on developmental interactions between the muscle and the nerve (Hurren, 2013). Accordingly, the increased susceptibility to apoptosis of Pax7-positive cells in denervated muscles (Jejurikar et al., 2002) and the role of nerves in the maintenance of satellite cells (Montarras et al., 2013) points to an influence of innervation in skeletal muscle growth and Pax7-positive cell population behavior.

Our results suggest that the myofibers are preponderant laminin producers during the stages that precede the onset of MDC1A in the *dy<sup>w</sup>* mouse model (Nunes et al., 2017). We suggest that the lack of laminin 211 production by the myofibers might deregulate the muscle stem cell identity in these mice. This deregulation may result from a direct effect of the absence of laminin 211 in the muscle stem cell niche or an indirect effect due to abnormal myofiber-derived signaling in the absence of laminin 211. In a third scenario, the abnormal NMJ development might have an impact on Pax7-positive cell population. In light of the current literature regarding the dynamics between innervation and the behavior of the Pax7-positive cell population, it is tempting to hypothesize that the reduction in the number of Pax7-positive cells associated with the onset of MDC1A (Nunes et al., 2017) may be correlated with an improper innervation, starting at E15.5. We suggest that laminin 211/221 deficiency may cause a disruption in the NMJ maturation, resulting in impaired innervation, which together with the lack of  $\alpha$ 2-laminins in the myofibers would culminate in the phenotype described at E17.5/18.5. Future studies addressing what happens to the NMJs at later stages of fetal development in the *dy<sup>w</sup>* mouse while monitoring the behavior of the Pax7-positive cell population in the vicinity of NMJs are needed to provide further insight into this hypothesis.

## Final considerations

The lack of laminin 211 and 221 in the myofiber and NMJ, respectively, is likely to change the way several skeletal muscle elements respond to the surrounding environment. Altered signaling in the muscle fibers caused by the absence of  $\alpha$ 2-laminins could affect the Pax7-positive cells lying in their niche next to the myofibers, and could possibly lead to a change in their identity, compromising their ability to contribute to muscle growth in the long-term. The results from this thesis also raise the possibility that  $\alpha$ 2-laminins may play a role in the correct clustering of AChR. A well accomplished clustering is crucial for a correct organization of the endplate, leading to a functional innervation of the muscle. In addition, a proper muscle innervation is critical for the maintenance of muscle stem cell population. Therefore, if further studies confirm that NMJ development is impaired in absence of  $\alpha$ 2-laminins, we can conclude that  $\alpha$ 4- and  $\alpha$ 5-laminins appear to be unable to make up for the lack of  $\alpha$ 2-laminin in the NMJs, in analogy to what was shown during fetal myogenesis (Nunes et al., 2017). Additional studies aimed at understanding the specific roles of  $\alpha$ 2-laminins in (1) the muscle stem cell niche, (2) the communication between the myofibers and Pax7-positive cells and (3) in the interaction between NMJs and the Pax7-positive cells are needed to understand the detailed mechanism underlying MDC1A onset, and, consequently, to design targeted therapies for this disease.

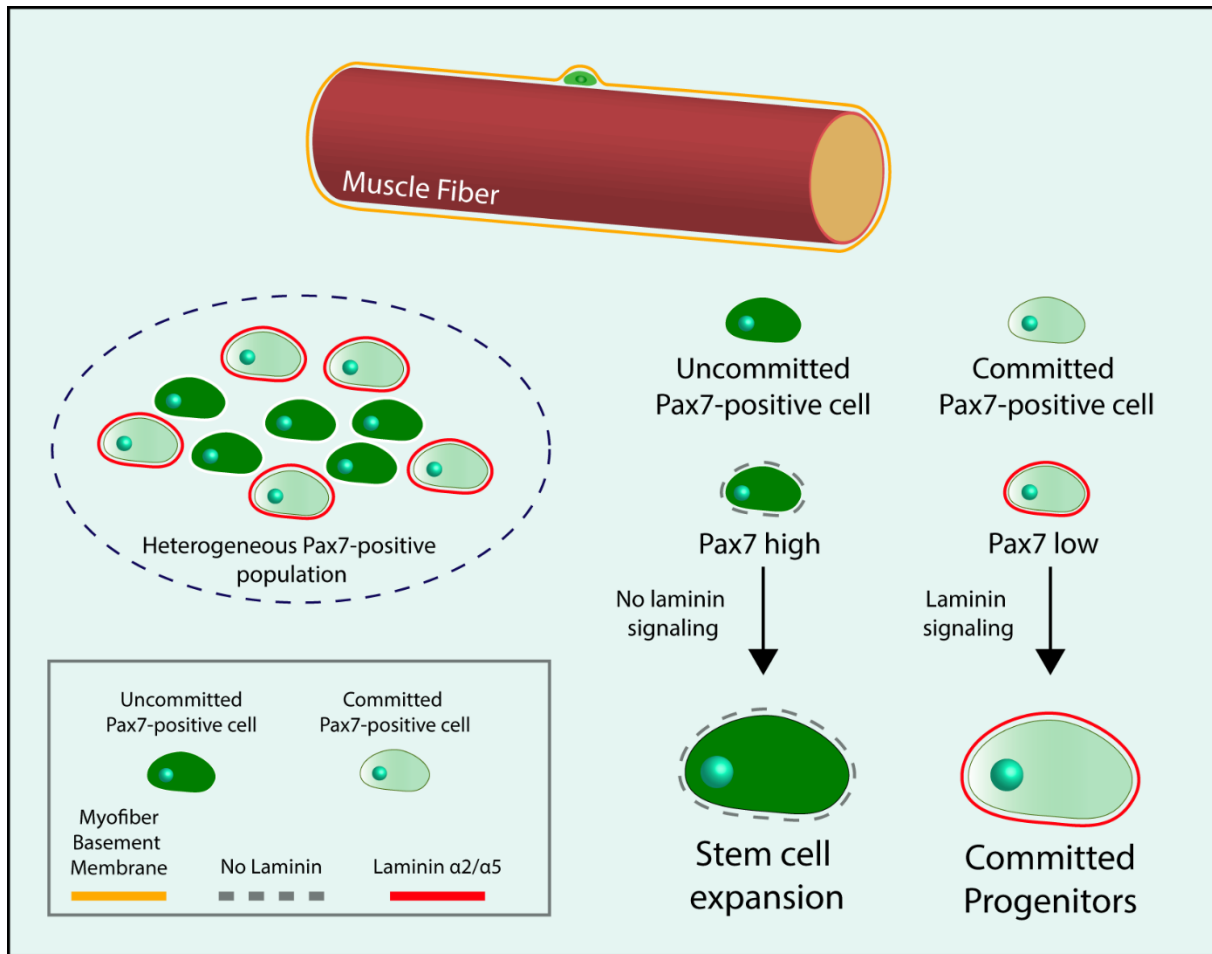


**Figure 20 – The diversity of laminin niches in the heterogeneous population of Pax7-positive cell.** During fetal myogenesis, the Pax7-positive cell population seems to be diverse regarding the levels of Pax7 protein per cell. Whereas a certain proportion of the muscle stem cell pool express high levels of Pax7 (dark green) and another proportion expresses low levels of Pax7 (light green). Our results indicate that the fraction of cells with lower Pax7 expression assemble  $\alpha 2/\alpha 5$ - laminins (red line). It is worth noticing that, given that our results showed that laminin  $\alpha 2$  co-localizes with laminin  $\alpha 4$  in some cells, it is possible that laminin  $\alpha 4$  is also present around these same Pax7-positive cells. In contrast, the fraction of cells with higher Pax7 expression apparently does not assemble laminins. This scenario leads to the proposition of a model, where the high Pax7-positive cells are in an uncommitted state, with a stronger stem cell identity, and therefore are more prone to proliferate and contribute to stem cell pool expansion. In contrast, the cells with lower Pax7 expression are believed to be in a committed state, and would differentiate after a few cell divisions. This model proposes that  $\alpha 2/\alpha 5$ -laminins play a role in the mechanism regulating the balance between proliferation and differentiation, restraining an unbridled and precocious differentiation of the cells with low levels of Pax7.



# **Chapter 5**

## **References**

## References

- Allamand, V. and Guicheney, P.** (2002) Merosin-deficient muscular dystrophy, autosomal recessive (MDC1A, MIM#156225, LAMA2 gene coding for  $\alpha 2$  chain of laminin). *Eur. J. Hum. Genet.* **10**, 91-94.
- Anderson, C., Thorsteinsdóttir, S. and Borycki, A.** (2009) Sonic hedgehog-dependent synthesis of laminin  $\alpha 1$  controls basement membrane assembly in the myotome. *Development* **136**, 3495-3504.
- Andrade, R.P., Pascoal, S. and Palmeirim, I.** (2005) Thinking clockwise. *Brain Res. Brain Res. Rev.* **49**, 114-119.
- Aumailley, M.** (2013) The laminin family. *Cell Adh Migr.* **7**, 48-55.
- Aumailley, M., Bruckner-Tuderman, L., Carter, W.G., Deutzmann, R., Edgar, D., Ekblom, P., Engel, J., Engvall, E., Hohenester, E., Jones, J. C. R. et al.** (2005) A simplified laminin nomenclature. *Matrix Biol.* **24**, 326-332.
- Aumailley, M., Pesch, M., Tunggal, L., Gaill, F. and Fässler, R.** (2000) Altered synthesis of laminin 1 and absence of basement membrane component deposition in  $\beta 1$ -integrin-deficient embryoid bodies. *J. Cell Sci.* **113**, 259-268.
- Baddeley A, Turner R.** (2005) Spatstat: An R package for analyzing spatial point patterns. *J Stat Softw.* **12**, 1-42.
- Baddeley AJ, Moyeed RA, Howard CV, Boyde A.** (1993) Analysis of a three-dimensional point pattern with replication. *Appl Stats.* **42**, 641-668.
- Bajanca, F., Luz, M., Duxson, M.J. and Thorsteinsdóttir, S.** (2004) Integrins in the mouse myotome: developmental changes and differences between the epaxial and hypaxial lineage. *Dev. Dyn.* **231**, 402-415.
- Bajanca, F., Luz, M., Raymond, K., Martins, G. G., Sonnenberg, A., Tajbakhsh, S., Buckingham, M. and Thorsteinsdóttir, S.** (2006) Integrin  $\alpha 6 \beta 1$ -laminin interactions regulate early myotome formation in the mouse embryo. *Development* **133**, 1635-1644.
- Barczyk, M., Carracedo, S. and Gullberg, D.** (2010) Integrins. *Cell Tissue Res.* **339**, 269-280.
- Bentzinger, C.F., von Maltzahn, J. and Rudnicki, M.A.** (2010) Extrinsic regulation of satellite cell specification. *Stem Cell Res. Ther.* **1**, 27.
- Biressi, S., Molinaro, M. and Cossu, G.** (2007) Cellular heterogeneity during vertebrate skeletal muscle development. *Dev. Biol.* **308**, 281-293.
- Boonen, K.J. and Post, M.J.** (2008) The muscle stem cell niche: regulation of satellite cells during regeneration. *Tissue Eng. Part B Rev.* **14**, 419-431.
- Bowman, W.** (1840) On the minute structure and movements of voluntary muscle. *Phil. Trans. R. Soc. Lond.* **130**, 457-501.
- Brent, A.E. and Tabin, C.J.** (2002) Developmental regulation of somites derivatives: muscle, cartilage and tendon. *Curr. Opin. Genet. Dev.* **12**, 548-557.
- Bröhl, D., Vasyutina, E., Czajkowski, M.T., Griger, J., Rassek, C., Rahn, H.P., Purfürst, B., Wende, H. and Birchmeier, C.** (2012) Colonization of the satellite cell niche by skeletal muscle progenitor cells depends on Notch signals. *Dev. Cell* **23**, 469-481.
- Buckingham, M. and Rigby, P.W.J.** (2014) Gene regulatory networks and transcriptional mechanisms that control myogenesis. *Dev. Cell* **28**, 225-238.
- Burkin, D.J. and Kaufman, S.J.** (1999) The  $\alpha 7 \beta 1$  integrin in muscle development and disease. *Cell Tissue Res.* **296**, 183-190.
- Burkin, D.J., Kim, J.E., Gu, M. and Kaufman, S.J.** (2000) Laminin and  $\alpha 7 \beta 1$  integrin regulate agrin-induced clustering of acetylcholine receptors. *J. Cell Sci.* **113**, 2877-2886.



- Cachaço, A.S., Pereira, C.S., Pardal, R.G., Bajanca, F. and Thorsteinsdóttir, S.** (2005) Integrin repertoire on myogenic cells changes during the course of primary myogenesis in the mouse. *Dev. Dyn.* **232**, 1069-1078.
- Cao, X., Pfaff, S.L. and Gage, F.H.** (2007) A functional study of miR-124 in the developing neural tube. *Genes Dev.* **21**, 531-536.
- Chakkalakal, J.V., Jones, K.M., Basson, M.A. and Brack, A.S.** (2012) The aged niche disrupts muscle stem cell quiescence. *Nature* **490**, 355-360.
- Chal, J. and Pourquié, O.** (2017) Making muscle: skeletal myogenesis in vivo and in vitro. *Development* **144**, 2104-2122.
- Chargé, S. B. P. and Rudnicki, M. A.** (2004) Cellular and molecular regulation of muscle regeneration. *Physiol. Rev.* **84**, 209-238.
- Cheng, Y.S., Champlaud, M.F., Burgeson, R.E., Marinkovich, M.P. and Yurchenco, P.D.** (1997) Self-assembly of laminin isoforms. *J. Biol. Chem.* **272**, 31525-31532.
- Cinnamon, Y., Kahane, N. and Kalcheim, C.** (1999) Characterization of the early development of specific hypaxial muscles from the ventrolateral myotome. *Development* **126**, 4305-4315.
- Conboy, I.M. and Rando, T.A.** (2002) The regulation of Notch signaling controls satellite cell activation and cell fate determination in postnatal myogenesis. *Dev. Cell* **3**, 397-409.
- Deries, M. and Thorsteinsdóttir, S.** (2016) Axial and limb muscle development: dialogue with the neighbourhood. *Cell. Mol. Life Sci.* **73**, 4415-4431.
- Deries, M., Gonçalves, A.B., Vaz, R., Martins, G.G., Rodrigues, G. and Thorsteinsdóttir, S.** (2012) Extracellular matrix remodeling accompanies axial muscle development and morphogenesis in the mouse. *Dev. Dyn.* **241**, 350-264.
- Deries, M., Schweitzer, R. and Duxson, M.J.** (2010) Developmental fate of the mammalian myotome. *Dev. Dyn.* **239**, 2898-2910.
- Domogatskaya, A., Rodin, S. and Tryggvason, K.** (2012) Functional diversity of laminins. *Annu. Rev. Cell Dev. Biol.* **28**, 523-553.
- Duband, J.L. and Thiery, J.P.** (1987) Distribution of laminin and collagens during avian neural crest development. *Development* **101**, 461-478.
- Dumont, N. A., Wang, Y. X. and Rudnicki, M. A.** (2015a) Intrinsic and extrinsic mechanisms regulating satellite cell function. *Development* **142**, 1572-1581.
- Dumont, N.A., Bentzinger, C.F., Sincennes, M.C. and Rudnicki, M.A.** (2015b) Satellite Cells and Skeletal Muscle Regeneration. *Compr. Physiol.* **5**, 1027-1059.
- Durbeej, M.** (2010) Laminins. *Cell Tissue Res.* **339**, 259-268.
- Eloy-Trinquet, S. and Nicolas, J.F.** (2002) Clonal separation and regionalization during formation of the medial and lateral myotomes in the mouse embryo. *Development*, **129**, 111-122.
- Frantz, C., Stewart, K. M. and Weaver, V. M.** (2010) The extracellular matrix at a glance. *J. Cell Sci.* **123**, 4195-4200.
- Gattazzo, F., Urciuolo, A. and Bonaldo, P.** (2014) Extracellular matrix: A dynamic microenvironment for stem cell niche. *Biochim. Biophys. Acta*, **1840**, 2506-2519.
- Gawlik, K.I. and Durbeej, M.** (2011) Skeletal muscle laminin and MDC1A: pathogenesis and treatment strategies. *Skelet. Muscle* **1**, 9.
- Gonçalves, A.B., Thorsteinsdóttir, S. and Deries, M.** (2016) Rapid and simple method for *in vivo* ex utero development of mouse embryo explants. *Differentiation* **91**, 57-67.

- Grady, R.M., Starr, D.A., Ackerman, G.L., Sanes, J.R. and Han, M.** (2005) Syne proteins anchor muscle nuclei at the neuromuscular junction. *Proc. Natl. Acad. Sci. U.S.A.* **102**, 4359-4364.
- Gros, J., Scaal, M. and Marcelle, C.** (2004) A two-step mechanism for myotome formation in chick. *Dev. Cell* **6**, 875-882.
- Hohenester, E. and Yurchenco, P.D.** (2013) Laminins in basement membrane assembly. *Cell Adh. Migr.* **7**, 56-63.
- Holmberg, J. and Durbeej, M.** (2013) Laminin-211 in skeletal muscle function. *Cell Adh Migr.* **7**, 111-121.
- Hurren, B.** (2013). Myogenic Progenitors in the Rat Hindlimb: Role of Innervation (*PhD thesis*), University of Otago, New Zealand.
- Hurren, B., Collin, J.J.P., Duxson, M.J. and Deries, M.** (2015) First neuromuscular contact correlates with onset of primary myogenesis in rat and mouse limb muscles. *Plos ONE* **10**, e0133811.
- Hutcheson, D.A., Zhao, J., Merrel, A., Haldar, M. and Kardon, G.** (2009) Embryonic and fetal limb myogenic cells are derived from developmentally distinct progenitors and have different requirements for  $\beta$ -catenin. *Genes Dev.* **23**, 997-1013.
- Jafari-Mamaghani, M., Andersson, M. and Krieger, P.** (2010) Spatial point pattern analysis of neurons using ripley's K-function in 3D. *Front. Neuroinform.* **4**, 9.
- Jejurikar, S.S., Marcelo, C.L. and Kuzon, W.M. Jr.** (2002) Skeletal muscle denervation increases satellite cell susceptibility to apoptosis. *Plast. Reconstr. Surg.* **110**, 160-168.
- Jones, D.L. and Wagers, A.J.** (2008) No place like home: anatomy and function of the stem cell niche. *Nat. Rev. Mol. Cell Bio.* **9**, 11-21.
- Kablar, B. and Rudnicki, M.A.** (2000) Skeletal muscle development in the mouse embryo. *Histol. Histopathol.* **15**, 649-656.
- Kablar, B., Krastel, K., Tajbakhsh, S. and Rudnicki, M.A.** (2003) Myf5 and MyoD activation define independent myogenic compartments during embryonic development. *Dev. Biol.* **258**, 307-318.
- Kassar-Duchossoy, L., Gayraud-Morel, B., Gomès, D., Rocancourt, D., Buckingham, M., Shinin, V. and Tajbakhsh, S.** (2004) Mrf4 determines skeletal muscle identity in Myf5:MyoD double-mutant mice. *Nature* **431**, 466-471.
- Kassar-Duchossoy, L., Giacone, E., Gayraud-Morel, B., Jory, A., Gomès, D. and Tajbakhsh, S.** (2005) Pax3/Pax7 mark a novel population of primitive myogenic cells during development. *Genes Dev.* **19**, 1426-1431.
- Kuang, S., Kuroda, K., Le Grand, F. and Rudnicki, M. A.** (2007) Asymmetric self-renewal and commitment of satellite stem cells in muscle. *Cell* **129**, 999-1010.
- Kuschel, R., Yablonka-Reuveni, Z. and Bornemann, A.** (1999) Satellite cells on isolated myofibers from normal and denervated adult rat muscle. *J. Histochem. Cytochem.* **47**, 1375-1384.
- Laurila, P. and Leivo, I.** (1993) Basement membrane and interstitial matrix components form separate matrices in heterokaryons of PYS-2 cells and fibroblasts. *J. Cell Sci.* **104**, 59-68.
- Le Grand, E. and Rudnicki, M.** (2007) Satellite and stem cells in muscle growth and repair. *Development* **134**, 3953-3957.
- LeBleu, V.S., Macdonald, B. and Kalluri, R.** (2007) Structure and function of basement membranes. *Exp. Biol. Med.* **232**, 1121-1129.
- Martins, G.G., Rifes, P., Amândio, R., Rodrigues, G., Palmeirim, I. and Thorsteinsdóttir, S.** (2009) Dynamic 3D cell rearrangements guided by a fibronectin matrix underlie somitogenesis. *Plos ONE* **4**, e7429.
- Mauro, A.** (1961) Satellite cell of skeletal muscle fibers. *J. Biophys. Biochem. Cytol.* **9**, 493-495.

- Merchán-Pérez, A., Rodríguez, J.R., González, S., Robles, V., DeFilipe, J., Larrañaga, P. and Bielza, C.** (2014) Three-dimensional spatial distribution of synapses in the neocortex: a dual-beam electron microscopy study. *Cereb. Cortex* **24**, 1579-1588.
- Messina, G., Biressi, S., Monteverde, S., Magli, A., Cassano, M., Perani, L., Roncaglia, E., Tagliafico, E., Starnes, L., Campbell, C.E., Grossi, M., Goldhamer, D.J., Gronostajski, R.M. and Cossu, G.** (2010) Nfix regulates fetal-specific transcription in developing skeletal muscle. *Cell*, **140**, 554-566.
- Miner, J.H., Li, C., Mudd, J.L., Go, G. and Sutherland, A.E.** (2004a). Compositional and structural requirements for laminin and basement membranes during mouse embryo implantation and gastrulation. *Development* **131**, 2247-56.
- Montanaro, F., Gee, S.H., Jacobson, C., Lindenbaum, M.H., Froehner, S.C. and Carnonetto, S.** (1998) Laminin and  $\alpha$ -Dystroglycan mediate acetylcholine receptor aggregation via MuSK-independent pathway. *J. Neurosci.* **18**, 1250-1260.
- Montarras, D., L'honoré, A. and Buckingham, M.** (2013) Lying low but ready for action: the quiescent muscle satellite cell. *FEBS J.* **280**, 4036-4050.
- Mourikis, P., Gopalakrishnan, S., Sambasivan, R. and Tajbakhsh, S.** (2012) Cell-autonomous Notch activity maintains the temporal specification potential of skeletal muscle stem cells. *Development* **139**, 4536-4548.
- Murray, P. and Edgar, D.** (2000) Regulation of programmed cell death by basement membranes in embryonic development. *J. Cell Biol.* **150**, 1215-1221.
- Nishimune, H., Sanes, J.R. and Carlson, S.S.** (2004) A synaptic laminin-calcium channel interaction organizes active zones in motor nerve terminals. *Nature* **432**, 580-587.
- Nishimune, H., Valdez, G., Jarad, G., Moulson, C.L., Müller, U., Miner, J.H. and Sanes, J.R.** (2008) Laminins promote postsynaptic maturation by an autocrine mechanism at the neuromuscular junction. *J. Cell Biol.* **182**, 1201-1215.
- Nishiuchi, R., Takagi, J., Hayashi, M., Ido, H., Yagi, Y., Sanzen, N., Tsuji, T., Yamada, M. and Sekiguchi, K.** (2006) Ligand-binding specificities of laminin-binding integrins: a comprehensive survey of laminin-integrin interactions using recombinant  $\alpha 3\beta 1$ ,  $\alpha 6\beta 1$ ,  $\alpha 7\beta 1$  and  $\alpha 6\beta 4$  integrins. *Matrix Biol.* **25**, 189-197.
- Noakes, P.G., Gautam, M., Mudd, J., Sanes, J.R. and Merlie, J.P.** (1995) Aberrant differentiation of neuromuscular junctions in mice lacking s-laminin/laminin  $\beta 2$ . *Nature* **374**, 258-262.
- Nunes, A. M., Wuebbles R. D., Sarathy A., Fontelonga T. M., Deries M., Burkin D.J. and Thorsteinsdóttir S.** (2017) Impaired fetal muscle development and JAK-STAT activation mark disease onset and progression in a mouse model for merosin-deficient congenital muscular dystrophy. *Hum. Mol. Genet.* **26**, 2018-2033.
- Nunes, A.M.** (2017) Dynamics of laminin niches during muscle development and disease. *PhD thesis*, University of Lisbon, Lisbon.
- Ostrovsky, D., Sanger, J.W. and Lash, J.W.** (1988) Somitogenesis in the mouse embryo. *Cell Differ.* **23**, 17-25.
- Patton, B. L., Cunningham, J. M., Thyboll, J., Kortessmaa, J., Westerblad, H., Edström, L., Tryggvason, K. and Sanes, J. R.** (2001) Properly formed but improperly localized synaptic specializations in the absence of laminin  $\alpha 4$ . *Nat. Neurosci.* **4**, 597-604.
- Patton, B.L.** (2000) Laminins of the neuromuscular system. *Microsc. Res. Tech.* **51**, 247-261.
- Patton, B.L.** (2003) Basal lamina and the organization of neuromuscular synapses. *J. Neurocytol.* **32**, 883-903.
- Patton, B.L., Miner, J.H., Chiu, A.Y. and Sanes, J.R.** (1997) Distribution and function of laminins in the neuromuscular system of developing, adult and mutant mice. *J. Cell Biol.* **139**, 1507-1521.
- Picard, B., Lefaucher, L., Berri, C. and Duclos, M.J.** (2002) Muscle fibre ontogenesis in farm animal species. *Reprod. Nutr. Dev.* **42**, 415-431.

- Preibisch, S., Saalfeld, S. and Tomancak, P.** (2009) Global optimal stitching of tiled 3D microscopic image acquisitions. *Bioinformatics* **25**, 1462-1465.
- Pöschl, E., Schlötzer-Schrehardt, U., Brachvogel, B., Saito, K., Ninomya, Y. and Mayer, U.** (2004) Collagen IV is essential for basement membrane stability but dispensable for initiation of its assembly during early development. *Development* **131**, 1619-1628.
- Pownall, M.E. and Emerson, C.P. Jr.** (1992) Sequential activation of three myogenic regulatory genes during somite morphogenesis in quail embryos. *Dev. Biol.* **151**, 67-79.
- Pu, Q., Patel, K. and Huang, R.** (2015) The lateral plate mesoderm: a novel source of skeletal muscle. *Results Probl. Cell Differ.* **56**, 143-163.
- Purves, D. and Lichtman, J.W.** (1980) Elimination of synapses in the developing nervous system. *Science* **210**, 153-157.
- Qiao, C., Li, J., Zhu, T., Draviam, R., Watkins, S., Ye, X., Chen, C., Li, J. and Xiao, X.** (2005) Amelioration of laminin- $\alpha$ 2-deficient congenital muscular dystrophy by somatic gene transfer of miniagrin. *Proc. Natl. Acad. Sci. U.S.A.* **102**, 11999-12004.
- Relaix, F., Rocancourt, D., Mansouri, A. and Buckingham, M.** (2005) A Pax3/Pax7-dependent population of skeletal muscle progenitor cells. *Nature*, **435**, 948-953.
- Ripley, B.D. and Kelly, F.P.** (1977) Markov point processes. *London Math. Soc.* **15**, 188-192.
- Rocheteau, P., Gayraud-Morel, B., Siegl-Cachedenier, I., Blasco, M.A. and Tajbakhsh, S.** (2012) A subpopulation of adult skeletal muscle stem cells retains all template DNA strands after cell division. *Cell* **148**, 112-125.
- Rogers, R.S. and Nishimune, H.** (2017) The role of laminins in the organization and function of neuromuscular junctions. *Matrix Biol.* **58**, 86-105.
- Ross, J.J., Duxson, M.J. and Harris, A.J.** (1987) Neural determination of muscle fiber numbers in embryonic rat lumbrical muscles. *Development* **100**, 395-409.
- Rozario, T. and DeSimone, D.W.** (2010) The extracellular matrix in development and morphogenesis: a dynamic view. *Dev. Biol.* **341**, 126-140.
- Sambasivan, R., Yao, R., Kissenpfenning, A., Van Wittenberghe, L., Paldi, A., Gayraud-Morel, B., Guenou, H., Malissen, B., Tajbakhsh, S. and Galy, A.** (2011) Pax7-expressing satellite cells are indispensable for adult skeletal muscle regeneration. *Development* **138**, 3647-3656.
- Sanes, J.R.** (2003) The basement membrane/basal lamina of skeletal muscle. *J. Biol. Chem.* **278**, 12601-12604.
- Sanes, J.R. and Lichtman, J.W.** (1999) Development of the vertebrate neuromuscular junction. *Annu. Rev. Neurosci.* **22**, 389-442.
- Scaal, M. and Christ, B.** (2004) Formation and differentiation of the avian dermomyotome. *Anat. Embryol.* **208**, 411-424.
- Schéele, S., Nyström, A., Durbeej, M., Talts, J.F., Ekblom, M. and Ekblom, P.** (2007) Laminin isoforms in development and disease. *J. Mol. Med.* **85**, 825-836.
- Schultz, E. and Jaryszak, D.L.** (1985) Effects of skeletal muscle regeneration on the proliferation potential of satellite cells. *Mech. Ageing Dev.* **30**, 63-72.
- Shea, K. L., Xiang, W., LaPorta, V. S., Licht, J. D., Keller, C., Basson, M. A. and Brack, A. S.** (2010) Sprouty1 regulates reversible quiescence of a self-renewing adult muscle stem cell pool during regeneration. *Cell Stem Cell* **6**, 117-129.
- Smirnov, S.P., Barzaghi, P., McKee, K.K., Ruegg, M.A. and Yurchenco, P.D.** (2005) Conjugation of LG domains of agrins and perlecan to polymerizing laminin-2 promotes acetylcholine receptor clustering. *J. Biol. Chem.* **280**, 41449-41457.

- Tajbakhsh, S.** (2009) Skeletal muscle stem cells in developmental versus regenerative myogenesis. *J. Intern. Med.* **266**, 372-389.
- Tajbakhsh, S. and Buckingham, M.** (2000) The birth of muscle progenitor cells in the mouse: spatiotemporal considerations. *Curr. Top. Dev. Biol.* **48**, 225-268.
- Tarusawa, E., Matsui, K., Budisantoso, T., Molnár, E., Watanabe, M., Matsui, M., Fukazawa, Y. and Shigemoto, R.** (2009) Input-specific intrasynaptic arrangements of ionotropic glutamate receptors and their impact on postsynaptic responses. *J. Neurosci.* **29**, 12896-12908.
- Thorsteinsdóttir, S.** (1992) Basement membrane and fibronectin matrix are distinct entities in the developing mouse blastocyst. *Anat. Rec.* **232**, 141-149.
- Thorsteinsdóttir, S., Deries, M., Cachaço, A.S. and Bajanca, F.** (2011) The extracellular matrix dimension of skeletal muscle development. *Dev. Biol.* **354**, 191-207.
- Tierney, M.T., Gromova, A., Sesillo, F.B., Sala, D., Spenlé, C., Orend, G. and Sacco, A.** (2016) Autonomous extracellular matrix remodeling controls a progressive adaptation in muscle stem cell regenerative capacity during development. *Cell Rep.* **14**, 1940-1952.
- Tomé, F. M., Evangelista, T., Leclerc, A., Sunada, Y., Manole, E., Estournet, B., Barois, A., Campbell, K. P. and Fardeau, M.** (1994). Congenital muscular dystrophy with merosin deficiency. *Sciences de la Vie* **317**, 351-357.
- Tosney, K.W., Dehnbostel, D.B. and Erickson, C.A.** (1994) Neural crest cells prefer the myotome's basal lamina over the sclerotome as a substratum. *Dev. Biol.* **163**, 389-406.
- Vachon, P. H., Loechel, F., Xu, H., Wewer, U. M. and Engvall, E.** (1996) Merosin and laminin in myogenesis; specific requirement for merosin in myotube stability and survival. *J. Cell Biol.* **134**, 1483-1497.
- Vachon, P.H., Xu, H., Liu, L., Loechel, F., Hayashi, Y., Arahata, K., Reed, J.C., Wewer, U.M. and Engvall, E.** (1997) Integrins ( $\alpha\beta1$ ) in muscle function and survival. Disrupted expression in merosin-deficient congenital muscular dystrophy. *J. Clin. Invest.* **100**, 1870-1881.
- Vasyutina, E., Lenhard, D.C., Wende, H., Erdmann, B., Epstein, J.A. and Birchmeier, C.** (2007) RBP-J (Rbpsi) is essential to maintain muscle progenitor cells and to generate satellite cells. *Proc. Natl. Acad. Sci. U.S.A* **104**, 4443-4448.
- Vilmont, V., Cadot, B., Ouanounou, G. and Gomes, E.R.** (2016) A system for studying mechanisms of neuromuscular junction development and maintenance. *Development* **143**, 2464-2477.
- Wigmore, P.M. and Evans, D.J.** (2002) Molecular and cellular mechanisms involved in the generation of fiber diversity during myogenesis. *Int. Rev. Cytol.* **216**, 175-232.
- Williams, B.A. and Ordahl, C.P.** (1994) Pax-3 expression in segmental mesoderm marks early stages in myogenic cell specification. *Development* **120**, 785-796.
- Witzemann, V.** (2006) Development of the neuromuscular junction. *Cell Tissue Res.* **326**, 263-271.
- Yousif, L. F., Di Russo, J. and Sorokin, L.** (2013) Laminin isoforms in endothelial and perivascular basement membranes. *Cell Adh. Migr.* **7**, 101-110.
- Yurchenco, P. D.** (2015) Integrating activities of laminins that drive basement membrane assembly and function. *Curr. Top. Membr.* **76**, 1-30.
- Yurchenco, P.D.** (2011) Basement membranes: cell scaffoldings and signaling platforms. *Cold Spring Harb. Perspect. Biol.* **3**, a004911.
- Yurchenco, P.D., Amenta, P.S. and Patton, B.L.** (2004) Basement membrane assembly, stability and activities observed through a developmental lens. *Matrix Biol.* **22**, 521-538.
- Zammit, P. and Beauchamp, J.** (2001) The skeletal muscle satellite cell: stem cell or son of stem cell? *Differentiation* **68**, 193-204.

**Books:**

**Baddeley, A.** (2010) *Analysing Spatial Point Patterns in 'R'*. Clayton South: CSIRO.

**Carvalho, M.S. and Câmara, G.** (2004) *Análise espacial de eventos. Análise espacial de dados geográficos*, pp. 2-15. Brasília.

**Diggle, P.J.** (2003) *Statistical Analysis of Spatial Point Patterns*, Hodder Education Publishers; 2 edition.

**Illian, J., Penttinen, A., Stoyan, H. and Stoyan, D.** (2008) *Statistical Analysis and Modelling of Spatial Point Patterns*. Hoboken, NJ: Wiley.

**Smith, T.E.** (2016) *Notebook on Spatial Data Analysis* [online]

**Smith, M.J., Goodchild, M.F. and Longley, P.A.** (2015) *Geospatial analysis: A comprehensive guide to principles, techniques and Software tools*. United Kingdom, Troubador Publishing Ltd, 5<sup>th</sup> Edition.

# **Annexes**

## Annex I – Protocols

### P1 – Genotyping

Extract genomic DNA from tail snips, and proceed for the digestion.

1. Add proteinase K 20mg/mL to the lysis buffer in a proportion of 25µL pk per 250mL buffer and leave it overnight at 55°C.
2. Centrifuge for 60min at 14000rpm
3. Remove the supernatant to a new microcentrifuge tube and add 250µL of isopropanol.
4. Keep it 2h at -20°C to precipitate.
5. Centrifuge 25min at 13000rpm. Remove the supernatant by inversion.
6. Wash the pellet subsequently with 1mL of 100% EtOH (30 to 40min), 1mL of 70% EtOH (30 to 40min), and 700µL of 70% EtOH (30min).
7. Dry the pellet at room temperature.
8. Dilute in 20µL of TE.

#### PCR Genotyping for *dy<sup>w</sup>*

For PCR run a positive control, the unknown samples and a negative control. Set up 25µL PCR reactions as follows:

- a) Positive control and unknowns: 2µL DNA+ 23µL Master Mix
- Negative control: 2µL H<sub>2</sub>O + 23µL Master Mix
- Laminin allele wildtype band: 250bp
- Laminin allele LacZ Mutant band: 480bp

Master Mix 1x	
<b>GoTaq:</b>	12.5µL
<b>dyWF1:</b>	0.5µL
<b>dyWR2:</b>	0.5µL
<b>LacZ:</b>	0.5µL
<b>H<sub>2</sub>O:</b>	9.0µL
	23

PCR Program:	
<b>95°C</b>	<b>5'</b>
<b>95°C</b>	<b>30''</b>
<b>60.6°C</b>	<b>30''</b> } 35 cycles
<b>72°C</b>	<b>45''</b>
<b>72°C</b>	<b>10''</b>
<b>4°C</b>	-



## **P2: Mini-Prep**

1. Centrifuge 1mL of the primary culture for 2min, full speed, at room temperature.
2. Discard the supernatant and re-suspend the pellet in 100µL TE + Rnase (10ug/mL).
3. Add 300µL of TENS and vortex.
4. Add 150µL of KAc 3M pH 5.2 and vortex
5. Centrifuge at room temperature for 3min, full speed, and pass the supernatant to a new tube.
6. Add to the new tube 900µL EtOH 100%.
7. Centrifuge 3min at room temperature, full speed, to precipitate the pellet.
8. Discard the supernatant and let it dry.
9. Re-suspend the pellet in 50µL of TE.
10. Run the samples in a 1% agarose gel for about 30min 100V.
11. The sample with the best band will be used to do a secondary culture.

## **P3 - JETSTAR KIT**

For the Midi-Prep, 500µL of primary culture were incubated in 100mL of new LB selective medium with ampicillin (100µg/mL) for 12 to 16h at 37°C, 300rpm. The protocol used to extract the DNA plasmid was the JETSTAR KIT, according to which we start by centrifuging the *E. coli* cells and remove all traces of the supernatant. After that, we add the solution E1 (4mL) to the pellet and re-suspend the cells until the suspension is homogeneous. Following that, the solution E2 (4mL) is added and mix gently but thoroughly by inverting until the lysate appear to be homogeneous, without vortex and always at room temperature for 5min. After that, we proceed for the neutralization adding solution E3 (4mL) and mix immediately by multiple inverting until a homogeneous suspension is obtained, without any remainders of the results of cell lysis. Once again, it is important that we do not vortex. Centrifuge the mixture at room temperature at 12000xg for 10min and discard the supernatant from the previous step to the equilibrated JETSTAR column, allowing the lysate to run by gravity flow. Subsequently, the column must be washed twice with solution E5 (10mL), allowing the column to empty by gravity flow. Finally, in order to elude the DNA we use the solution E6 (5mL). The DNA is precipitated with 3.5mL of isopropanol, centrifuged at 4°C, 12 000xg for 30min and washed with 70% ethanol before one last centrifugation. The pellet is air dried for 10min and re-dissolved in a suitable volume of **TE** buffer.

## **P4 – cDNA production**

To perform a reverse transcription producing cDNA from RNA, 500ng of RNA were mixed with 1µL of random primers, 1µL of DNTP's and molecular grade water until 13µL of final volume. Then we incubated at 65°C for 5min and put it on ice for 2min. After that, we added 2µL of Buffer 10x FS, 1µL of DTT, 1µL of RNase out, 1µL of Super Script III and 2µL of molecular grade water. The mix is left for 10min at room temperature and then incubated at 55°C for about 50min. Afterwards, we dissolve it in 15µL of water

## Annex II – Solutions and Reagents

### General Solutions

1% agarose gel		TBE 10x:	
–	TBE 0.5x: 50mL	–	Tris: 53.91g
–	Agarose RNase free: 0.5g	–	Boric Acid: 27.52g
–	Green Safe: 1µL	–	EDTA: 0.5M: 20mL
		–	ddH <sub>2</sub> O until 500mL
TE buffer:		Tris 1M pH = 7.5 200mL:	EDTA 0.5M pH = 8.0
–	ddH <sub>2</sub> O: 100mL	–	Tris: 24.22g
–	Tris 1M pH = 8.0: 1mL	–	HCL: 10mL
–	EDTA 0.5M pH = 8.0: 0.2mL	ddH <sub>2</sub> O until final volume	EDTA: 9.30g
			– NaOH: 1.10g
			ddH <sub>2</sub> O: until final volume
PFA 4%		FISH 2% 50mL	
–	Paraformaldehyde 4g	–	Sucrose: 2g
–	PBS 1x: 100mL	–	CaCl <sub>2</sub> : 6µL
–	NaOH 10N to adjust pH to 7.3	–	Na <sub>2</sub> HPO <sub>4</sub> : 19.25mL
		–	NaH <sub>2</sub> PO <sub>4</sub> : 5.75mL
		–	PFA: 5mL
		–	ddH <sub>2</sub> O: until 25mL
PBS 10x:		PBS with Ca <sup>2+</sup> and Mg <sup>2+</sup> (Complete) 1L	
–	NaCl: 137mM	–	PBS 10x: 100mL
–	KCl: 2.68mM	–	ddH <sub>2</sub> O: ~ 600mL
–	Na <sub>2</sub> HPO <sub>4</sub> : 8.1mM	–	CaCl <sub>2</sub> 10x: 100mL
–	KH <sub>2</sub> PO <sub>4</sub> : 1.47mM	–	MgCl <sub>2</sub> 10x: 100mL
–	ddH <sub>2</sub> O until final volume		
–	adjust to pH 6.8		
Lysis buffer			
–	Tris 1M pH = 9.5: 25mL		
–	EDTA 0.5 pH = 8.0: 2mL		
–	NaCl 5M: 0.1mL		
–	SDS 10%: 2.5mL		
–	H <sub>2</sub> O: 19.15mL		

## Bacterial Growth

LB medium (Lysogeny Broth)	Selective medium:
<ul style="list-style-type: none"><li>– Bactotrypsin: 1%</li><li>– Yeast Extract: 0.5%</li><li>– NaCl: 1%</li><li>– ddH<sub>2</sub>O until final volume</li></ul>	<ul style="list-style-type: none"><li>– LB medium until final volume</li><li>– Ampicillin 100μL/mL</li><li>– For selective plates add 7.5g of agar</li></ul>

## Mini-Prep Solutions:

TENS	KAc 3M pH = 5.2 (1L)
<ul style="list-style-type: none"><li>– Tris pH = 7.5: 10Mm</li><li>– EDTA pH8: 1mM</li><li>– NaOH 0.1mM</li><li>– SDS: 0.5%</li></ul>	<ul style="list-style-type: none"><li>– KAC 3M: 408.24mL</li><li>– ddH<sub>2</sub>O: until 800mL</li><li>– Adjust pH with glacial acetic acid (100%)</li><li>– ddH<sub>2</sub>O until final volume</li></ul>

## Cryosection

Solution 1	Solution 2	Solution 3
<ul style="list-style-type: none"><li>– Sucrose: 4%</li><li>– CaCl<sub>2</sub>: 0.12mM</li><li>– Na<sub>2</sub>HPO<sub>4</sub>: 0.77mM</li><li>– NaH<sub>2</sub>PO<sub>4</sub></li><li>– ddH<sub>2</sub>O until final volume</li></ul>	<ul style="list-style-type: none"><li>– Sucrose: 15%</li><li>– Phosphate Buffer 0.12M</li><li>– ddH<sub>2</sub>O until final volume</li></ul>	<ul style="list-style-type: none"><li>– Sucrose: 15%</li><li>– Gelatine: 7.5%</li><li>– Phosphate Buffer 0.12M</li><li>– ddH<sub>2</sub>O until final volume</li></ul>

### Phosphate Buffer 0.24 M, pH7

- NaH<sub>2</sub>PO<sub>4</sub>.H<sub>2</sub>O
- Na<sub>2</sub>HPO<sub>4</sub>
- ddH<sub>2</sub>O until final volume

## In situ Hybridization

Hybmix:
<ul style="list-style-type: none"><li>– Formamide: 50%</li><li>– SSC (pH = 5): 1.3x</li><li>– EDTA pH8: 5mM</li><li>– tRNA: 0.05mg/mL</li><li>– Tween 20: 0.20%</li><li>– CHAPS: 5mg/mL</li><li>– Heparina: 0.1mg/mL</li><li>– ddH<sub>2</sub>O (depc) until final volume</li></ul>

<b>TBS 10x pH = 7.6 1L:</b>	<b>TBST:</b>	<b>TBST+BL+SS</b>
– NaCl: 80g	– TBS 1x: 99mL	– TBST: 30mL
– KCl: 2g	– Tween 20: 1mL	– Blocking solution 10%: 10mL
– Tris-HCl, pH = 7.5: 250mL		– Sheep Serum: 10mL

<b>PBT (PBS 0.1% Tween) 1000mL</b>	<b>Proteinase K solution: 50mL</b>
– PBS 10x: 100mL	– PBS: 50mL
– Tween: 1mL	– Proteinase K (20mg/mL): 25μL
– ddH <sub>2</sub> O: until final volume	

<b>NTMT: 100mL</b>
– NaCl 5M: 2mL
– Tris-HCL 2M pH = 9.5: 5mL
– MgCl <sub>2</sub> : 2.5mL
– Tween 20: 1mL
– ddH <sub>2</sub> O until final volume

### Immunohistochemistry

<b>ID</b>	<b>0.2% Triton X-100</b>
– Triton X 1%	– Triton X-100: 200μL
– Bovine Serum Albumen 1%	– PBS 1x: 100mL
– Add PBS 1x to final volume	

<b>Mouse-on-Mouse Kit (Catalog nr: BMK-2202)</b>	
<b>M.O.M.<sup>TM</sup> Mouse IgG Blocking Reagent:</b>	<b>M.O.M.<sup>TM</sup> Diluent:</b>
add 2 drops (90μL) of stock solution to 2.5mL of PBS or TBS.	add 600μL of Protein Concentrate stock solution to 7.5mL of PBS or TBS.

<b>Dent's fixative</b>	<b>Blocking solution</b>
– 1 part DMSO: 4 parts MeOH	– Normal goat serum: 5%
	– PBS 1x: 75%
	– DMSO: 20%

<b>Antigen Retrieval buffer:</b>	<b>Buffered glycerol with anti-fade</b>
– 10mM Tris Base	– N Propyl gallate: 100mg
– 1mM EDTA solution	– PBS 10x w/ 200 $\mu$ L azide: 2mL
– 0.05% Tween 20	– 18 mL glycerol
– pH9	

---

**DAPI (4',6-diamidino-2-phenylindole) 250mL**

---

- Stock solution (3.6mg/mL): 0.35mL
  - PBS 0.1% Triton: 250mL
-

# Supplementary Tables:

Table S1 – Laminin probes

Laminin chain	Direction	Linearize with	Polymerase	Vector	Size Insert (bp)
$\alpha 2$	5'3'	SacII	Sp6	pGEMT	587
$\alpha 4$	3'5'	SacI	T7	pGEMT	550
$\alpha 5$	5'3'	SacII	Sp6	pGEMT	563

Table S2 – Variance to mean ratio analysis.

		VMR						
		Variance	Mean	VMR	QuiTest	Qui_Inferior	Qui_Superior	p-value
Wildtype	E1C1	8.436213	1.848214	4.564521	506.6618	83.73503	142.0486	1.425339e-51
	E1C2	2.908625	0.8773585	3.315207	348.0968	78.5364	135.247	1.624004e-27
	E1C3	2.12987	0.8484848	2.510204	246.0000	72.50094	127.2821	2.068463e-14
	E1C4	4.305176	1.234694	3.486836	338.2231	71.64152	126.1414	3.843441e-28
	E1C5	2.496081	0.8421053	2.964096	278.625	69.06766	122.7151	7.131572e-20
	E1C6	2.736657	0.7672414	3.566878	410.191	87.21279	146.5711	1.839554e-34
dy <sup>w/-</sup>	E4C1	3.254938	1.08642	2.996023	239.6818	57.15317	106.6286	1.511043e-17
	E4C2	3.242449	1.114943	2.908175	250.1031	62.23863	113.5436	1.250519e-17
	E4C3	2.887525	1.049505	2.751321	275.1321	74.22193	129.5612	5.603155e-18
	E4C4	2.902516	1.04717	2.771772	291.036	78.5364	135.247	4.297636e-19
	E4C5	4.995286	1.490909	3.350497	180.9268	35.58634	76.19205	2.633339e-15
	E4C6	3.809002	0.9327731	4.083524	481.8559	89.82707	149.9569	3.668671e-45
Wildtype	E6C1	3.858396	0.887218	4.34887	574.0508	102.0888	165.6957	4.044993e-56
	E6C2	5.348713	1.346535	3.972206	397.2206	74.22193	129.5612	9.677501e-37
	E6C3	6.973141	1.649123	4.228394	477.8085	85.47275	144.311	4.731065e-46
	E6C4	5.862732	1.446809	4.052182	376.8529	68.21123	121.5715	2.988466e-38
	E6C5	3.373382	1.065934	3.164719	284.8247	65.64662	118.1359	8.754022e-22
	E6C6	1.192434	0.3629032	3.285818	404.1556	94.19496	155.5892	2.317016e-31
dy <sup>w/-</sup>	E3C1	10.53345	2.213483	4.758768	418.7716	63.94093	115.8414	3.052727e-44
	E3C2	6.971027	1.169697	5.959687	977.3886	130.4341	201.3512	1.552711e-115
	E3C3	7.013242	1.151079	6.092754	840.8	107.3722	172.4124	6.525693e-101
	E3C4	6.964444	1.326531	5.250119	509.2615	71.64152	126.1414	6.824848e-57
	E3C5	7.514813	1.372263	5.47622	744.766	105.6093	170.1753	2.276993e-84
	E3C6	2.887031	0.7801418	3.700649	518.0909	109.1369	174.6478	1.668611e-44

Table S3 – Nearest-neighbour distance analyses – G Function – R score and statistical significance, Z-test – associated.

		G Function							
		RO	RE	R	Variance	Z-test	Z_Inferior	Z_Superior	p-value
Wildtype	E1C1	20,70951	31,44882	0.6585146	1.305515	-8.226111	-1.959964	1.959964	1.933893e-16
	E1C2	30.29112	42.27788	0.7164769	5.251543	-2.28252	-1.959964	1.959964	0.02245865
	E1C3	32.55279	47.69192	0.682564	7.398674	-2.046195	-1.959964	1.959964	0.04073714
	E1C4	24.55393	37.2721	0.658775	3.137083	-4.05414	-1.959964	1.959964	5.031908e-05
	E1C5	29.67787	46.45064	0.6389119	7.2785	-2.304427	-1.959964	1.959964	0.02119869
	E1C6	34.19579	46.95468	0.7282721	6.768795	-1.884958	-1.959964	1.959964	0.05943545
dy <sup>w/-</sup>	E4C1	26.2415	39.18172	0.6697383	4.76681	-2.71465	-1.959964	1.959964	0.006634575
	E4C2	24.90519	36.43457	0.6835592	3.739376	-3.083238	-1.959964	1.959964	0.002047616
	E4C3	23.91159	40.49639	0.5904622	4.22737	-3.923196	-1.959964	1.959964	8.738216e-05
	E4C4	27.62514	41.26649	0.6694327	4.154517	-3.283499	-1.959964	1.959964	0.001025271
	E4C5	22.53266	35.09421	0.6420621	4.103935	-3.060854	-1.959964	1.959964	0.002207068
	E4C6	27.98177	44.37208	0.6306165	4.846633	-3.381794	-1.959964	1.959964	0.0007201412
Wildtype	E6C1	20.68457	48.10831	0.4299584	5.359222	-5.117111	-1.959964	1.959964	3.102504e-07
	E6C2	18.28116	37.44226	0.4882493	2.816623	-6.802864	-1.959964	1.959964	1.025597e-11
	E6C3	17.54719	34.69104	0.5058133	1.749123	-9.801396	-1.959964	1.959964	1.110398e-22
	E6C4	18.86282	36.67941	0.514262	2.70302	-6.591362	-1.959964	1.959964	4.358095e-11
	E6C5	22.64425	44.06395	0.5138951	5.469387	-3.916289	-1.959964	1.959964	8.992231e-05
	E6C6	30.55038	76.77734	0.3979089	35.79292	-1.291511	-1.959964	1.959964	0.1965265
dy <sup>w/-</sup>	E3C1	22.94058	27.60508	0.8310274	1.056952	-4.413161	-1.959964	1.959964	1.01872e-05
	E3C2	20.52492	41.7683	0.4913995	2.469903	-8.600897	-1.959964	1.959964	7.909528e-18
	E3C3	21.04081	40.30157	0.5220841	2.773752	-6.943939	-1.959964	1.959964	3.813159e-12
	E3C4	18.24872	36.91329	0.4943674	2.863951	-6.517067	-1.959964	1.959964	7.169535e-11
	E3C5	21.36592	36.73202	0.58167	1.96099	-7.835892	-1.959964	1.959964	4.655253e-15
	E3C6	29.91518	49.07259	0.6096108	5.981758	-3.202639	-1.959964	1.959964	0.001361747

### Annex III – Antibodies

Table C

Name	Clonality	Raised in	1°/2°	Source	Catalog Number	Dilution
Anti-Laminin	Polyclonal	<b>Rabbit</b>	1°	Sigma	L-9393	1:200
Anti-Laminin $\alpha$ 2	Monoclonal	<b>Rat</b>	1°	Sigma	L-0663	1:100
Anti-Laminin $\alpha$ 4	Polyclonal	<b>Rabbit</b>	1°	T.Sasaki (J.Miner)	1100	1:800
Anti-Laminin $\alpha$ 5	Polyclonal	<b>Rabbit</b>	1°	J.Miner	8948	1:800
Anti-Laminin $\beta$ 1	Monoclonal	<b>Rat</b>	1°	Abcam	Ab44941	1:100
Anti-Laminin $\beta$ 2		<b>Rabbit</b>		J.Miner		1:200
Anti-Laminin $\gamma$ 1	Monoclonal	<b>Rat</b>	1°	Milipore	Mab1914P	1:100
Anti-Pax7	Monoclonal	<b>Mouse</b>	1°	D.S.H.B.	Pax7	1:50
Anti-Myosin	Monoclonal	<b>Mouse</b>	1°	D.S.H.B	MF20	1:200
Neurofilament	Monoclonal	<b>Mouse</b>	1°	Sigma	N5264	1:100
Synaptophysin	Monoclonal	<b>Mouse</b>	1°	DAKO	M7315	1:50
$\alpha$ -bungarotoxin			1°	ThermoFisher	B13422	1:200
Anti-Mouse Alexa488	Polyclonal	<b>Goat</b>	2°	Molecular Probes	A-11017	1:1000
Anti-Mouse Alexa 568	Polyclonal	<b>Goat</b>	2°	Molecular Probes	A-11019	1:1000
Anti-Rabbit Alexa 488	Polyclonal	<b>Goat</b>	2°	Molecular Probes	A-11070	1:1000
Anti-Rabbit Alexa 568	Polyclonal	<b>Goat</b>	2°	Molecular Probes	A21069	1:1000
Anti-Rat Alexa488	Polyclonal	<b>Goat</b>	2°	Molecular Probes	A11006	1:1000
Anti-Rat Alexa 568	Polyclonal	<b>Goat</b>	2°	Molecular Probes	A11077	1:1000
Anti-Mouse HRP			2°			1:100



## Annex IV – R Script

```
#Installing needed packages
#install.packages("spatstat") #for spatial analysis
#install.packages("lattice") #for plotting
#Loading needed packages
library(spatstat)
library(lattice)

#Setting the working directory
#(this is the place where the data files are and where the exported files are going to be placed)
setwd("F:/ficheiros_txt/")

#Importing all muscle coordinate files
muscle_files <- list.files(pattern = "xy_muscle_")
muscle <- lapply(muscle_files, FUN = read.delim)

#Importing all synapses coordinate files
synapses_files <- list.files(pattern = "xy_synapsis_")
synapses <- lapply(synapses_files, FUN = read.delim)

#Creating a vector with embryo names
embryo <- c("E1C1", "E1C2", "E1C3", "E1C4", "E1C5", "E1C6", "E3C1", "E3C2", "E3C3", "E3C4", "E3C5", "E3C6",
"E4C1", "E4C2", "E4C3", "E4C4", "E4C5", "E4C6", "E6C1", "E6C2", "E6C3", "E6C4", "E6C5", "E6C6")

#Creating a looping function for the analysis
analysis <- function(muscle, synapses, embryo) { #Defining the function arguments
  for (m in muscle){
    for (s in synapses){
      for (e in embryo){
        #Creating the observation window which corresponds to muscle limits
        muscle_limits <- owin(poly = data.frame(x = m[,1], y = m[,2]))
        #Creating a point pattern object for the synapses locations within the observation window
        synapses_pattern <- ppp(s[,1],s[,2], window = muscle_limits)

#Ploting and exporting the synapses distribution plot
#Defining the exporting format and filename for the plot
png(filename = paste("Muscle_synapses_", e, ".png"), width = 750, height=526, units = "px", type = c("cairo"))
#Creating the actual plot of the synapses distribution within the muscle section
plot_syn_pat <- plot.ppp(synapses_pattern, cols = "springgreen4", pch = 20,
  cex = 0.5, main = "", ylim = c(0,2500), xlim = c(0,5000))
#Adding title and axis labels to the plot
title(main = substitute(paste("Muscle synopsis of ", e)),
  cex.main = 1.3, xlab = "x (um)", ylab = "y (um)")
#Defining x axis ticks and values positions
axis(side=1, pos=0, at=seq(0,5000, by=500), lwd=1, lty=1, font.axis=2)
#Defining y axis ticks and values positions
axis(side=2, pos=0, at=seq(0,2500, by=500), lwd=1, lty=1, font.axis=2)
dev.off()
#Creating G-function with confidence envelopes for 999 random simulations
g_fun <- envelope(synapses_pattern, fun = Gest, nsim = 999, correction = "none")
#Ploting and exporting the G-function plot
#Defining the exporting format and filename for the plot
png(filename = paste("G_function_", e, ".png"), width = 750, height=526, units = "px", type = c("cairo"))
#Creating the actual G_function plot
plot_g_fun <- plot(g_fun, main = substitute(paste("G function", e)), legend = FALSE, lwd = 2, font = 2)
dev.off()
#Creating K-function with confidence envelopes for 999 random simulations
```

```

k_fun <- envelope(synapses_pattern, fun = Kest, nsim = 999, correction = "isotropic", rmax = 600)
#Ploting and exporting the K-function plot
#Defining the exporting format and filename for the plot
png(filename = paste("K_function_", e, ".png"), width = 750, height=526, units = "px", type = c("cairo"))
#Creating the actual K-function plot
plot_k_fun <- plot(k_fun, main = substitute(paste("K function", e)), legend = FALSE,
                  xlim = c(0,600), ylim = c(0,1250000), lwd = 2, font = 2)
dev.off()

#Creating L-function with confidence envelopes for 999 random simulations
l_fun <- envelope(synapses_pattern, fun = Lest, nsim = 999, correction = "isotropic", rmax = 600)
#Ploting and exporting the L-function plot
#Defining the exporting format and filename for the plot
png(filename = paste("L_function_", e, ".png"), width = 750, height=526, units = "px", type = c("cairo"))
#Creating the actual L-function plot
plot_l_fun <- plot(l_fun, main = substitute(paste("L function", e)), legend = FALSE,
                  xlim = c(0,600), ylim = c(0,600), lwd = 2, font = 2)
dev.off()
}
}
}
}
analysis(muscle[1],synapses[1],embryo[1])
VMR - Script
#Quadrat Analysis
library(sp)
library(spatstat)
library(maptools)
library(lattice)
####E1C1####
#IMPORTING DATA TO R
Muscle_E1C1 <- read.delim("F:/dyW/Excel/ficheiros_txt/xy_muscle_E1C1.txt")
Synapsis_E1C1 = read.delim("F:/dyW/Excel/ficheiros_txt/xy_synapses_E1C1.txt")
#Defining study area and synopsis location as a point pattern
p_E1C1 <- Polygon(Muscle_E1C1)
ps_E1C1 <- Polygons(list(p_E1C1),1)
sp_E1C1 <- SpatialPolygons(list(ps_E1C1))
Muscle_Lim_E1C1 <- as(sp_E1C1, "owin")
#Creating point pattern
E1C1 <- ppp(Synapsis_E1C1$Xs_E1C1,Synapsis_E1C1$Ys_E1C1,Muscle_Lim_E1C1)
###Creating grid for quadrat analysis
XposE1C1 <- seq(0,5000,by=113) #113 number of square
YposE1C1 <- seq(0,2500, by=113)
grelhaE1C1 <- tess(xgrid=XposE1C1,ygrid=YposE1C1)
MuscleGridE1C1 <- intersect.tess(Muscle_Lim_E1C1, grelhaE1C1) #Grelha apenas no musculo
plot(MuscleGridE1C1)
#Counting
CountQuadE1C1 <- quadratcount.ppp(E1C1, tess=MuscleGridE1C1) #Contar o nr de sinapses por quadrante
plot(CountQuadE1C1)
#Export table to excel - VMR
write.table(CountQuadE1C1,"F:/dyW/Excel/ficheiros_txt/CountQuadE1C1.txt",sep="\t")
SFE1C1 <- read.delim("F:/dyW/Excel/ficheiros_txt/CountQuadE1C1.txt") #SF Synapse frequency

```

```

VarE1C1 <- var(SFE1C1$Freq)
meanE1C1 <- mean(SFE1C1$Freq)
VMR_E1C1 <- VarE1C1/meanE1C1
VMR_E1C1
nquad_E1C1 <- nrow(CountQuadE1C1) #nr de linhas da tabela que tem a contagem dos quadrantes
QuiTest_E1C1 <- VMR_E1C1*(nquad_E1C1-1) #Cálculo da Estatística de Teste
QuiTest_E1C1
qchisq(p=0.025,(nquad_E1C1-1)) -> QuiCri_Inf
QuiCri_Inf
qchisq(p=0.975,(nquad_E1C1-1)) -> QuiCri_Sup
QuiCri_Sup
P_value_E1C1 <- 2* (pchisq(QuiTest_E1C1, (nquad_E1C1-1), lower.tail = FALSE ))
P_value_E1C1
#G-Function R Score
#IMPORTING DATA TO R
Muscle_E1C1 <- read.delim("F:/dyW/Excel/ficheiros_txt/xy_muscle_E1C1.txt")
Synopsis_E1C1 = read.delim("F:/dyW/Excel/ficheiros_txt/xy_synapses_E1C1.txt")
#Defining study area and synopsis location as a point pattern
library(spatstat)
p_E1C1 <- Polygon(Muscle_E1C1)
ps_E1C1 <- Polygons(list(p_E1C1),1)
sp_E1C1 <- SpatialPolygons(list(ps_E1C1))
Muscle_Lim_E1C1 <- as(sp_E1C1, "owin")
#Calculation of observed minimum distance
RO_E1C1 <- mean(nndist(Synopsis_E1C1))
#Statistic
#Teste Z -> zscore
#Calculation expected minimum distance
Muscle_Area_E1C1 <- area.owin(Muscle_Lim_E1C1)
Nsyn_E1C1 <- nrow(Synopsis_E1C1)
dens_E1C1 <- Nsyn_E1C1/Muscle_Area_E1C1
RE_E1C1 <- 1/(2*sqrt(dens_E1C1))
RO_E1C1
RE_E1C1
# R<1 - Clustering
R_E1C1 <- RO_E1C1/RE_E1C1
#Values needed to statistic
1 Observed value
#2 Expected value
#3 Variance
#Variance Calculation
Var_RE_E1C1 <- (4-pi)/(4*pi*(dens_E1C1)*Nsyn_E1C1)
Var_RE_E1C1
Ztest <- (RO_E1C1-RE_E1C1)/Var_RE_E1C1
Ztest
Z_inf_E1C1 <- qnorm(p=0.025,mean=0,sd=1)
Z_inf_E1C1
Z_sup_E1C1 <- qnorm(p=0.975, mean=0, sd=1)
Z_sup_E1C1
pValue_E1C1 <- 2*(pnorm(Ztest, mean=0, sd=1))
pValue_E1C1

```